Electrical Properties of Rocks and Minerals

Short Course Notes

by Gary R. Olhoeft

Copyright 1980, 1981, 1982, 1983, 1985 by Gary R. Olhoeft.
Fair use of material herein is permitted, such as single copies for individuals, nonprofit institutions or libraries or multiple copies of small portions for school use as outlined in Sections 107 or 108 of the U.S. Copyright Law of 1976. All others wishing to copy all or portions of these notes for personal or internal use only, may do so, providing they pay the stated fee of $50.00 per copy to: Gary R. Olhoeft
P.O.Box 10870
Edgemont Branch
Golden, CO 80401-4498

Forward: These notes are the basis for an introductory short course held in Golden, Colorado on 23-25 September 1980, 22-24 September 1981, 6-8 April 1982, 27-29 September 1983, 19-21 November 1985 and in Brisbane, Australia on 28-30 October 1983. The notes are not intended to be as detailed as the lectures (which used over 1000 slides), but rather to be a source of review material and references for further study. Eventually, an expanded version of these notes and lectures will be published as a book.

ELECTRICAL PROPERTIES SHORT COURSE - Gary R. Olhoeft

TABLE OF CONTENTS

INTRODUCTION

Electrical properties describe the ability of charge to move inside matter. When an external electrical force is applied to matter, charges move in response. The movement of charge is called a current, and the ratio of the current density (current per unit area) to electric field strength (force per unit distance) is an electrical property of the material, called electrical conductivity. Conductivity is a measure of the ability of a material to transport charge.

Upon application of an electrical force, charges of opposite sign (positive or negative) respond by moving in opposite directions. Separation of opposite charges by a distance (or displacement from their equilibrium positions) creates another electric field which opposes the original external field. The charges stop moving when the two balance and cancel. This dynamic balance of electric fields and charge separation is called polarization. Non-electrical forces such as chemical, thermal, magnetic, and mechanical forces may also couple to charge, creating charge separation to produce polarization. Charge transport (conduction) and separation (polarization) are the two principal types of electrical properties.

The electrical properties of rocks and minerals are used for a wide variety of purposes. Passively, changes in

electrical properties within the earth cause warping of natural electric and magnetic fields. Actively, there are types of electrical properties that result in the generation of spontaneous voltages around flowing water or where two dissimilar materials meet. Active stimulation of the earth by natural or manmade forces can result in measurable electrical responses due to changes in electrical properties.

By measuring and mapping natural spontaneous polarization potentials, changes in natural magnetotelluric fields, electric field responses from actively induced currents, or variations in electromagnetic propagation, a picture is developed that describes variations in electrical properties. This picture may then be used to explore for oil, gas, geothermal, mineral, and other resources, to delineate faults and fractures in earthquake zones or near dams, power plants, and waste repositories, to locate leaks in dams or waste disposal sites, to map soil moisture variations for agricultural planning, or to acquire information for a host of other problems.

No geophysical technique works in all applications and none give unique answers. However, of the available geophysical tools, those exploiting electrical properties are the most sensitive to subtle changes within the earth and thus, often the most useful. Seismic velocity primarily responds linearly to changes in bulk density with a useful range of 1 order of magnitude. Magnetic properties primarily respond logarithmically to magnetite content (with a useful

range of 3 orders of magnitude). Radiometric properties similarly respond to uranium-thorium-potassium concentrations (3 orders of magnitude). Thermal properties primarily respond to bulk density and water content (2 orders of magnitude). High frequency electrical properties (above 1 MHz) primarily respond to bulk density and water content (2 orders of magnitude). However, at low frequencies, electrical properties respond to bulk density, water content, water salinity and chemistry, oxidation-reduction reactions, cation exchange processes, corrosion processes, water movement, chemical concentration gradients, clay-organic reactions, and other phenomena that involve the movement of charge over nearly 24 orders of magnitude.

Further, while viscosity has the widest dynamic range of any physical property (40 orders of magnitude), low frequency electrical properties have the widest dynamic range (24 orders of magnitude neglecting superconductors) of any readily-measured physical property (Table 1). Also, electrical properties are easily measured as a function of frequency, and the various processes which affect low frequency electrical responses are usually themselves strongly dependent upon frequency. This allows measurements as a function of frequency to yield useful information about physical and chemical activity in the earth.

Table 1 - The range of low frequency electrical properties.

Conductivity (mho/m)	Minerals	Rocks
10^{8}	copper	
10^{6}	iron sulfides	
10^{4}	tellurium	
10^{2}		anthracite
10^{0}	germanium	ocean water humic matter wet clay
10^{-2}		wet sandstone/fresh water
10^{-4}	silicon	wet basalt brown coal
10^{-6}	cryst.selenium	
10^{-8}	pure water	water ice
10^{-10}	iodine polyethylene	rock salt dry silicates
10^{-12}	amorph.selenium	
10^{-14}	teflon/paraffin	
10^{-16}	diamond	dry silicate powder alumina
10^{-18}	beryllium oxide	

The ranges of DC electrical conductivity shown in Table 1 are all typical values and are highly variable as environmental and other factors change. Sulfide minerals may range from 10^{-5} to 10^{6} mho/m depending upon the amount and kind of impurities, degree of crystallinity, and metal:sulfur stoichiometry. Most solid silicate rocks are around 10^{-11} mho/m when vacuum dry at room temperature, but

the addition of a single monolayer of adsorbed water (about 0.01 wt%) will increase the electrical conductivity by an order of magnitude. Similarly, the electrical conductivity may be increased by up to 9 orders of magnitude from the vacuum dry value by adding a few weight percent water, or by increasing the temperature from 20C to 900C, or by increasing the frequency of measurement from DC to 10^5 Hz, or by adding a few weight percent of a conductive mineral. This creates large ambiguity as to why a material has a given value of electrical conductivity.

Table 2 - Geophysical techniques and mechanisms of electrical properties versus frequencies.

Frequency (Hz)	Process	Technique
		Spontaneous Polarization
		DC Resistivity
10^{-5}	Ionic Conduction	Magnetic Sounding
10^{-3}		Magnetotellurics
	Cation Exchange	Complex Resistivity
10^{-1}	Clay/Organic Reactions	Induced Polarization
	Interfacial Processes	
10^{1}	Oxidation-Reduction	
	Diffusion/Migration	Audio-magnetotellurics
10^{3}		
	Ice Relaxation	Loop-Loop Electromagnetics
10^{5}	Bound Water Relaxation	
10^{7}		
		Radar Sounding
10^{9}	Electromagnetic scattering	
	Free Water Relaxation	Microwave Radiometry
10^{11}		IR Spectroscopy

Some of this ambiguity may be resolved by measuring the electrical properties as a function of frequency and

amplitude of stimulus in field applications and as a function of environmental parameters in the laboratory. Table 2 outlines some of the various field geophysical techniques and chemical mechanisms of electrical properties versus frequency.

Figure 1 illustrates the range of electrical resistivity (the reciprocal of conductivity) for basalt with 4.3% porosity from Thingvellir, Iceland as a function of

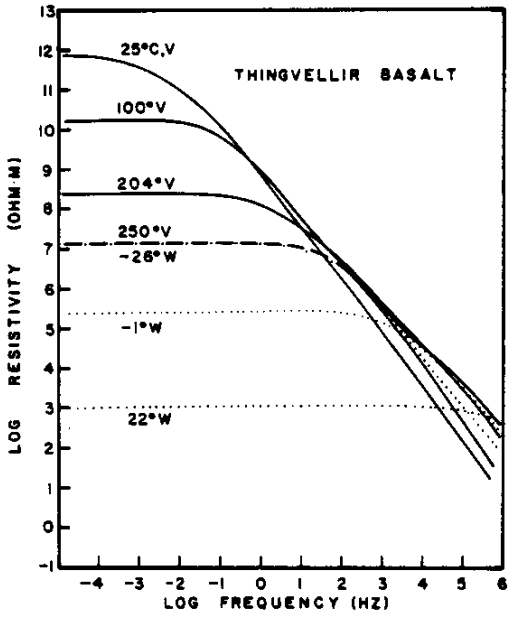

Figure 1 - Electrical resistivity of basalt as a function of frequency and temperature, wet and dry.

frequency. The solid lines are measured dry in ultra-high vacuum, and the dotted lines are measured saturated with distilled water. The portions of the curves that show resisitivity independent of frequency are where conduction

currents are dominant, and those with resistivity strongly varying with frequency are where displacement currents (polarization properties) are dominant. Note that the frequency of transition from conduction to displacement increases with increasing temperature and water content. Note also the ambiguity in that the sample vacuum dry at 250°C is identical with the water-saturated sample at -26°C.

By varying the frequency of measurement, field techniques also vary the depth of investigation. Records from magnetic observatories that stretch over periods of decades are used to obtain conductivity versus depth profiles to about 400km. DC resistivity and magnetotelluric tools measure as deep as 30 km. Induced polarization and low frequency electromagnetic induction tools penetrate to a few kilometers. These tools use induced fields to measure to depths of one or two skin depths (equation [46], primarily a function of conductivity and frequency) which will be less than 16% of an electromagnetic wavelength.

Radar and higher frequency electromagnetic tools may penetrate to several skin depths (many wavelengths) by using the propagation of electromagnetic energy. In these cases, the depth of penetration is determined by the amount of energy loss with distance due to conversion of electromagnetic energy to thermal energy (intrinsic conduction loss) and due to energy lost by scattering from the interaction of electromagnetic energy at a wavelength

about the same as the scale of electrical inhomogeneity in the material. This distance may range from a fraction of a meter in a clay soil (high intrinsic and high scattering loss) to tens of meters in granite to hundreds of meters in temperate glacier ice to two kilometers in dry salt domes.

In the 10^1 to 10^5 Hz range where induced electromagnetics and complex resistivity techniques are exploited, the frequency dependence of both the depth of investigation and of the electrical mechanism causes a complication. As the frequency is varied, the depth of investigation is varied and measurements will reflect changing electrical properties with depth. Changing frequency will also excite different mechanisms in the ground such as ionic conduction, cation exchange, and oxidation reduction reactions. In order to distinguish a change with frequency caused by depth variation in electrical properties versus a change with frequency caused by changing physical-chemical mechanisms, it is necessary to vary the geometry of the electrode array or induction loops (Keller and Frischknecht, 1966). The variable geometry also varies the depth of investigation. Thus, the effects of changing electrical properties with depth can be determined from the changing geometry of the electrode array and removed from the variable frequency data to leave the effects of physical chemical mechansims. Complications arise from the necessity of also removing inductive and capacitative coupling which change with frequency and electrode array, but these may be

handled mathematically (Millet, 1967; Dey and Morrison, 1973; Hohmann, 1973; Wynn and Zonge, 1975, 1977; Wynn, 1979; Pelton et al., 1978; Ramachandran and Sanyal, 1980; Coggon, 1984; Wang et al., 1985).

An alternative approach is to work at very low frequency (<1 Hz) and small electrode spacings, so the measured electrical properties are dominantly controlled in frequency by the physical-chemical processes in the earth, and the depth of investigation is dominantly controlled by the geometry of the electrode array. For a frequency of 1 Hz in 100 ohm-m material, the skin depth is 5033 m, requiring the electrode array to have a depth of investigation less than 5033 m in order to have the frequency dependence controlled by chemical process mechanisms instead of depth variation.

A different approach is to change the amplitude of the stimulus, and thus exploit the nonlinear electrical properties of some of the physical-chemical mechanisms as discussed later.

NOMENCLATURE

The electrical properties of all materials have two things in common: a low frequency limit at which conduction (charge transport) phenomena dominate and a high frequency limit at which dielectric polarization (charge separation) phenomena dominate. To introduce the nomenclature of electrical properties, start with the simplest electrical circuit (for an introduction to circuit theory, see Bose and Stevens, 1967) which includes these limits as in Figure 2.

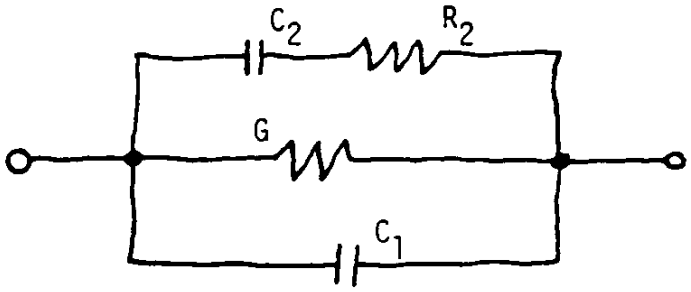

Figure 2 - Electrical circuit analog of simple rock.

where G = $1/R_1$ = low-frequency conduction limit

and C_1 = high-frequency polarization limit

represent the minimum circuit elements in all rocks and minerals. The R_2C_2 elements have been added to illustrate the simplest relaxation with

C_1+C_2 = low-frequency polarization limit

and $\tau = R_2C_2$ = time constant of relaxation. Such a relaxation feature does not necessarily appear in rocks, and is usually more complicated (as will be discussed below).

The simplest circuit elements of resistance, R, and capacitance, C, are defined as follows:

$$R = 1/G = V/I \qquad [1]$$

where V is the voltage (electrical force) in volts driving a current flow of I amperes through a resistance R (or equivalently a conductance G). The resistance describes an energy loss or dissipation of I^2R watts of power.

$$C = \frac{-I}{dV/dt} \qquad [2]$$

where t is time, and the capacitance describes the storage of charge in a system with a time-varying force.

The admittance (conductance) of the circuit in

Figure 2 is

$$Y = G + i\omega C_1 + \frac{1}{R_2 + (i\omega C_2)^{-1}} \qquad [3]$$

$$= G + i\omega C_1 + \frac{i\omega C_2}{1 + i\omega\tau}$$

To convert this expression into the properties of a material, divide the admittance of the material by the admittance of the same geometry of empty space. Since free space has no conductivity but always a minimum dielectric permittivity of 8.854185 picoFarads/meter, the admittance of the empty space is

$$Y_o = i\omega C_o \qquad [4]$$

where $C_o = \epsilon_o A/d$

and $\epsilon_o = 8.854185 \times 10^{-12}$ F/m = vacuum permittivity

A = cross-sectional area of the volume occupied by the material

d = thickness of the material volume.

Thus, the result becomes

$$\frac{Y}{Y_o} = \frac{C_1}{C_o} + \frac{C_2}{C_o}\frac{1}{1 + i\omega\tau} + \frac{G}{i\omega C_o} \qquad [5]$$

If the following definitions are made

$$K_\infty = C_1/C_o$$

$$K_o = (C_1 + C_2)/C_o$$

$$\sigma_{DC} = \epsilon_o G/C_o = G\ d/A$$

then [5] may be rewritten as

$$K' - iK'' - i\frac{\sigma_{DC}}{\omega\epsilon_o} = K_\infty + \frac{K_o - K_\infty}{1+i\omega\tau} - i\frac{\sigma_{DC}}{\omega\epsilon_o} \qquad [6]$$

where $K' - iK''$ = complex dielectric permittivity relative to free space

σ_{DC} = DC conductivity $[(ohm-m)^{-1}]$

$$K_o = \lim_{\omega\to 0} K'$$

and $$K_\infty = \lim_{\omega\to\infty} K'$$

The complex impedance of the circuit is

$$Z' - iZ'' = (Y' + iY'')^{-1} \qquad [7]$$

which is converted to a complex resistivity by

$$\rho' - i\rho'' = (Z' - iZ'')\ A/d. \qquad [8]$$

By defining a loss tangent and phase angle as

$$D = \tan(\pi/2 + \phi) = \frac{K''}{K'} + \frac{\sigma}{\omega\epsilon_0 K'} = \frac{\rho'}{\rho''} \qquad [9]$$

where D = loss tangent and ϕ = phase angle between voltage and current. This simple circuit model allows easy conversion from one parameter to another:

$$\rho' = \frac{1}{\omega\epsilon_0 K'} \frac{D}{1 + D^2} \qquad [10]$$

The following pages continue the discussion after: Olhoeft, G.R., C. Elliot, B. D. Fuller, G. V. Keller, W. J. Scott, and D. W. Strangway, 1978, Report of the Subcommittee on Electrical Standards, Mining Committee, Tulsa:Society of Exploration Geophysicists.

Proposed Standards for the Presentation of Electrical and Electromagnetic Data

INTRODUCTION

Unless otherwise specified, these standards are written for systems which are causal, linear, time-invariant, dynamic, and isotropic. The systems may be either lumped-parameter (ordinary differential equation) or distributed-parameter (partial differential equation) and they may be either discrete time (difference equation) or continuous time (differential equation). For definitions of these terms, see Cooper and McGillem (1967). If the system is non-causal, it is not physically realizable in geology. If the system is non-linear, the original raw data should be presented without any processing and with a complete description of the technique of measurement. If the system varies with time, that behavior should be completely described. If the system is not dynamic, it is a restricted subset of these standards and adequately represented by the terms defined here. If the system is anisotropic, the parameters of this standard must be made into tensor quantities (as is done in Sratton, 1941).

ELECTRICAL STANDARDS

Definitions in electrical properties logically begin with Ohm's law

$$J = \sigma E \qquad [11]$$

where J = free charge current density [amp/m^2]

E = electric field strength [volt/m]

and σ = electrical conductivity [siemens/m].

This is equivalently presented as

$$E = \rho J \qquad [12]$$

where $\rho = \sigma^{-1}$ = electrical resistivity [ohm-m]. Up to this point, resistivity and conductivity are defined including only free charge transport.

In the general case, the following linear relationship also applies

$$D = \epsilon E \qquad [13]$$

where ϵ = dielectric permittivity [farad/m]

and D = electric flux density [coulomb/m^2].

The real part of the relative permittivity, ϵ_r', is frequently used and defined:

$$\epsilon_r' = \epsilon'/\epsilon_o$$

where ϵ_o = free space permittivity = 8.854185 x 10^{-12} F/m. The real part of the relative permittivity is sometimes called the "dielectric constant", but this terminology is no longer preferred as the permittivity is not a "constant". The electric flux density is sometimes called the dielectric displacement (from displacement or separation of charge).

Combining this relationship with Ohm's Law through Maxwell's equation

$$\nabla \times H = J + \partial D/\partial t = J_T \qquad [14]$$

where H = magnetic field strength [amp-turn/m] yields a total current density, J_T, which includes both free carrier conduction and dielectric displacement terms

$$J_T = \sigma E + \epsilon \, \partial E/\partial t. \qquad [15]$$

Since, in the general case, both the conductivity and the dielectric permittivity may be complex, the total resistivity and the total conductivity may be defined through the relation

$$(\rho_T' - i\rho_T'')^{-1} = \sigma_T' + i\sigma_T'' = (\sigma' + i\sigma'') + i\omega\,(\epsilon' - i\epsilon'') \qquad [16]$$

with a loss tangent and phase angle defined

$$\tan \delta = -\cot \phi = \frac{\rho_T'}{\rho_T''} = \frac{\sigma_T'}{\sigma_T''} = \frac{\sigma' + \omega\epsilon''}{\sigma'' + \omega\epsilon'} \qquad [17]$$

where tanδ is the symbol to be used for the loss tangent,

ϕ = phase angle [radians]

and the unsubscripted σ and ϵ come from equation [16].

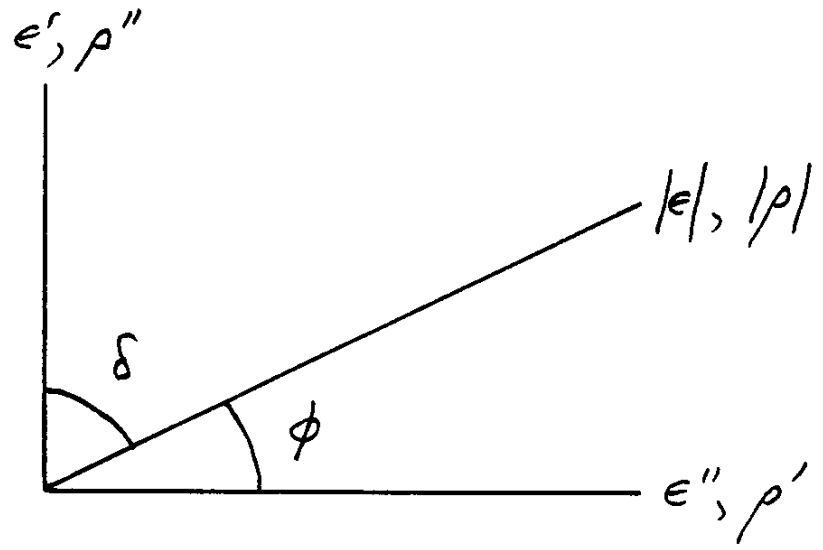

Figure 3 - Phasor diagram relating complex quantities.

Most instruments fall into two classes: they either measure volatage, V, and current, I, which are related to E and J by the geometry of the measurement system, or they measure equivalent series or parallel admittance or conductance by substitutional comparison against an internal standard or directly. In the latter case, the effective capacitance and conductance measured become effective dielectric permittivity, ($\epsilon' + \sigma''/\omega$) from equation [16] above, and the loss tangent as defined in equation [17].

Those instruments that measure voltage and current

usually measure the total current (hence the total current density), yielding a typical measurement of the form

$$E(t) = E_o \sin(\omega t + \phi_e)$$
$$J_T(t) = J_o \sin(\omega t + \phi_j) \qquad [18]$$

where E_o = amplitude of E

J_o = amplitude of J_T

t = time [sec]

ω = frequency [radians/sec] = $2\pi f$ (where f is frequency in Hz)

ϕ_e = arbitrary phase offset relative to some time zero for E

and ϕ_j = arbitrary phase offset for J_T relative to the same time as E.

In terms of these equations for E and J_T, the total resistivity is found to be given by

$$|\rho_T| = (\rho_T'^2 + \rho_T''^2)^{1/2} = E_o/J_o = \text{resistivity magnitude} \qquad [19]$$

$$\phi = \text{arccot}(\rho'/\rho'') = \phi_e - \phi_j = \text{phase angle} \qquad [20]$$

$$\rho_T' = (E_o/J_o)\cos\phi = \text{real resistivity} \qquad [21]$$

$$\rho_T'' = (E_o/J_o) \sin \phi = \text{imaginary resistivity.} \quad [22]$$

The complex total conductivity may be similarly derived or obtained through equation [16]. The loss tangent and phase angle of equation [17] are consistant with the phase angle of equation [20].

For measurements of induced polarization in the frequency domain, the following quantities are defined

$$FE(f_1,f_2) = \text{frequency effect} = \frac{|\rho_T(f_1)| - |\rho_T(f_2)|}{|\rho_T(f_1)|} \quad [23]$$

where f_1 and f_2 are the frequencies of measurement $f_1 < f_2$ and

$$NPFE(f_1,f_2) = \text{normalized percent frequency effect} = \frac{100\ FE(f_1,f_2)}{\log_{10}(f_2/f_1)}. \quad [24]$$

The definitions up to this point have been formulated for steady state, sinusoidal excitations. However, the definitions are equally valid whatever the form of excitation and response, provided that only the fundamental frequency is employed in determining the resistivity and phase angle at

that frequency from measured E and J. If harmonics are employed, their amplitude ratios still define a resistivity as in equation [19] only if the system is demonstratably linear. The problem is demonstrating that the system is linear. If the system is nonlinear, the fundamentals will still produce the same resistivity and phase as an equivalent linear system, but the harmonics will generate different values from those found using the fundamental at the same frequency as the harmonic. For this reason, all definitions in the literature are given for the fundamental frequency only.

Figure 4 illustrates and compares the complex dielectric permittivity and complex resistivity frequency spectra. The loss tangent and phase angle representations are very similar and mirror images of each other. The loss tangent shows dielectric relaxations better than the phase angle, whereas the phase angle shows lower frequency Faradaic relaxations better. The dielectric permittivity and real part of the complex resistivity are comparable (the log resistivity amplitude scale is twice that of the log permittivity). Note that after the initial frequency independent plateau in each, whenever the resistivity or permittivity has another frequency independent plateau, the other is strongly varying with frequency.

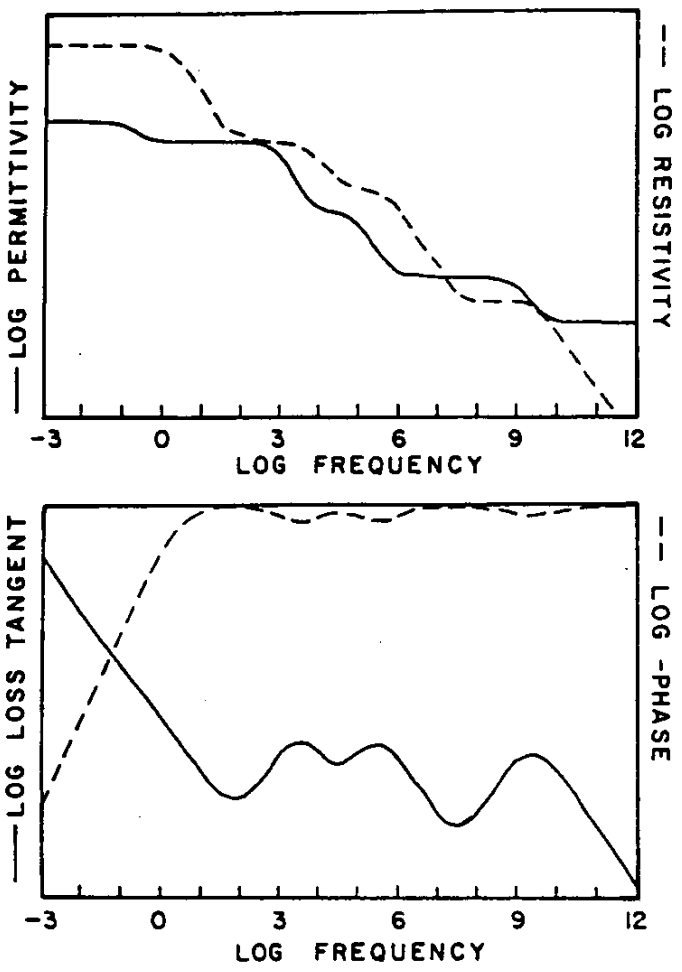

Figure 4 - Comparison of complex frequency spectra.

In the more general case, $\rho_T(\omega)$ and $\sigma_T(\omega)$ are the frequency dependent, complex transfer functions relating arbitrary transformable functions $E(\omega)$ to $J_T(\omega)$. The frequency dependence has the following general limit:

$$\sigma_{DC} = \rho_{DC}^{-1} = \lim_{\omega \to 0} [\sigma_T'(\omega) + i\sigma_T''(\omega)] = \lim_{\omega \to 0} [\rho_T'(\omega) - i\rho_T''(\omega)]^{-1} \quad [25]$$

In the time domain, the frequency domain parameters given above are transformed from transfer functions into impulse response functions through the Laplace transform. This causes Ohm's law to appear as a convolution of the form:

$$E(t) = \int_0^\infty r(\tau)\, J_T(t-\tau)\, d\tau$$

$$J_T(t) = \int_0^\infty s(\tau)\, E(t-\tau)\, d\tau \quad [26]$$

where r(t) and s(t) are the impulse response representations of resistivity and conductivity respectively. The impulse responses are given in terms of the transfer functions as

$$r(t) = \frac{1}{2\pi} \int_{-\infty}^{\infty} e^{+i\omega t}\, \rho_T(\omega)\, d\omega \quad [27]$$

and similarly for conductivity. Further introduction and discussion of these parameters may be found in Keller (1959), Fuller and Ward (1970), Shuey and Johnston (1973), Doetsch

(1971), and Cooper and McGillem (1967). With instruments capable of recording digitized waveforms of E(t) and J(t), the impulse response or the transfer function are the preferred forms for presenting the data.

Other acceptable parameters for induced polarization measurements in the time domain are the integral chargeability, M, for a full period symmetrical waveform (averaged over both halves of the period) where

$$M(T_1,T_2,T_3,T_4) = \frac{1}{V_p}\int_{t_a}^{t_b} V(t)\,dt \quad [\text{sec}] \qquad [28]$$

where common usage in terms of voltage instead of electric field has been followed, and

T_1 = "on" time for a symmetrical pulse

T_2 = "off" time interval between equal but opposite polarity "on" times,

T_3 = time interval from turn off time to first measurement of the response $V_s(t_a)$

T_4 = period of integration = $t_b - t_a$

V_p = amplitude of the "on" pulse = $\lim_{T_1 \to \infty} V(t)$

and $V_s(t)$ = the measured amplitude of the secondary voltage response.

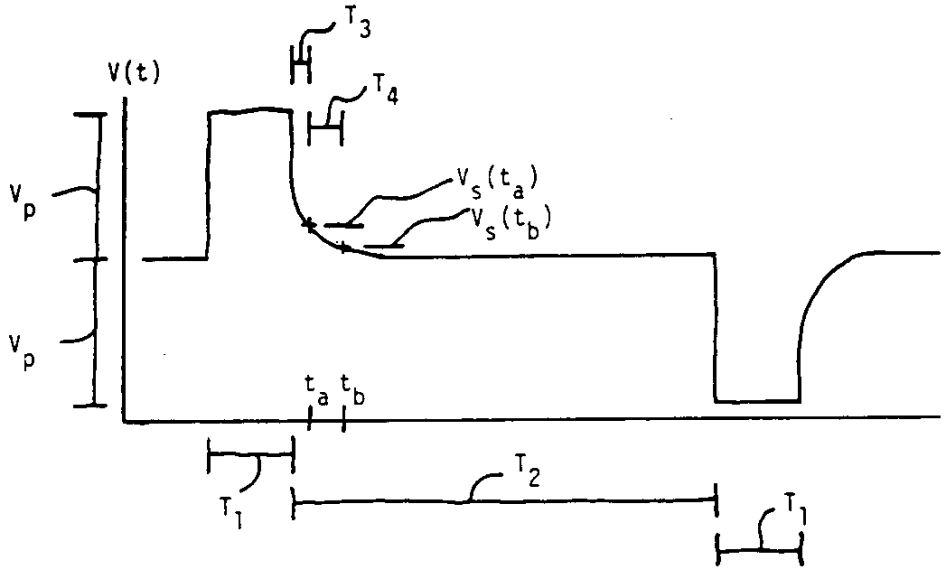

Figure 5 - Definitions for [28] through [32].

The instantaneous percent chargeability, Ch, is given by

$$Ch(T_1,T_2,T_3) = \frac{V(t_a)}{V_p} 100 \quad \text{[percent]} \qquad [29]$$

where T_1, T_2, and T_3 are as before. The general equation for V(t) with an arbitrary waveform is given by

$$V(t) = K \int_0^{\infty} r(\tau)\, I(t-\tau)\, d\tau \qquad [30]$$

similar to equation [26] but with the factor K to account for the geometry, where again

$$V_p = \lim_{T_1 \to \infty} V(t).$$

The volume chargeability, m, is given as (Siegel, 1959)

$$m = \frac{1}{V_p} \lim_{\substack{T_3 \to 0 \\ T_1 \to \infty \\ T_4 \to \infty}} V_s(t_a) \qquad [31]$$

The relation between the frequency and the time domain is expressed through the transforms [27] above and the limiting case

$$\lim_{\substack{T_1 \to \infty \\ T_2 \to \infty \\ T_3 \to 0 \\ T_4 \to \infty}} M = \lim_{\substack{f_1 \to 0 \\ f_2 \to \infty}} FE \qquad [32]$$

which represents a situation in the time domain of an infinitely long pulse, V_p, turned off and left off for an infinitely long time.

In field practice, the measured quantities are commonly termed "apparent" and are expressed in the same units as the

corresponding "true" quantities discussed here. No matter what the form of measurement, the data should be presented after correction for the geometric configuration of the system based upon an assumed homogeneous medium (converting V and I to E and J) and after correction for any known and stated instrument characteristics and inaccuracies, but before any corrections which are model dependent (including layering, three-dimensional effects, coupling, and others). After the data has been presented in this fashion, then interpretation and modelling may be presented.

If particular measurement systems yield data in another form than one of those presented here, that data should be presented with an explicit and detailed explanation of exactly what was measured and also with a derivation of the parameters in terms of those used here.

NONLINEARITY

Although many instances of nonlinear electrical properties exist (Shaub, 1965; Alvarez, 1973; Katsube et al., 1973; Parry-Jones, 1975; Devreese and Van Doren, 1976; Olhoeft, 1979, 1985; Klein and Shuey, 1979; Olhoeft and Scott, 1980; Anderson, 1981), none are sufficiently well understood or characterized as to allow parameter standardization. It is recommended that in situations where nonlinear behavior is suspected, both frequency and time

domain data should be recorded, the actual waveforms of E and J should be recorded, and a Lissajous plot of E versus J should be presented with the other forms of data. If these are not possible, a discussion of the probable consequences of using linear parameters should be provided.

ELECTROMAGNETIC STANDARDS

In electromagnetic systems, the linear relation

$$B = \mu H \qquad [33]$$

is added to the electrical systems discussed above, where

B = magnetic flux density [tesla]

H = magnetic field strength [amp-turn/m]

and μ = magnetic permeability [henry/m].

The relative magnetic permeability is also defined as

$$\mu_r = \mu/\mu_o \qquad [34]$$

where $\mu_o = 4\pi \times 10^{-7}$ Henry/m = free space or vacuum permeability.

The magnetic susceptibility is defined as

$$\chi_m = \mu_r^{-1} - 1 \qquad [35]$$

As discussed above for the electrical systems, μ has a

general form of a transfer function which may be complex and frequency dependent with the consequence that there is a magnetic loss tangent, defined as

$$\tan \delta_m = \mu''/\mu' \qquad [36]$$

with $\mu = \mu' - i\mu''$. The total electromagnetic loss tangent thus becomes

$$\tan \delta_{em} = \tan\left[\frac{\delta - \delta_m}{2}\right] = \cot \theta \qquad [37]$$

where δ and δ_{em} are loss angles from the electric (angle between E and J) and magnetic (between B and H) loss tangents respectively, and θ is the phase angle of E with respect to H. The phase angle is also given as

$$\tan \theta = \alpha/\beta \qquad [38]$$

where

$$(\alpha + i\beta)^2 = k^2 = -i\mu\omega\,(\sigma + i\omega\epsilon) = -i\mu\omega\sigma_T \qquad [39]$$

in which k = circular wave number

α = phase constant [radians/m]

$$= \omega \left\{ \frac{\mu\epsilon}{2} \left[\left(1 + \frac{\sigma^2}{\epsilon^2\omega^2}\right)^{1/2} + 1 \right] \right\}^{1/2} \qquad [40]$$

β = attenuation constant [nepers/m]

$$= \omega \left\{ \frac{\mu\epsilon}{2} \left[\left(1 + \frac{\sigma^2}{\epsilon^2\omega^2}\right)^{1/2} - 1 \right] \right\}^{1/2} \qquad [41]$$

and σ_T is the complex total electrical conductivity given in [16] above.

The attenuation (due to properties of the medium in the absence of scattering processes) is also commonly given as

$$N = -20\ \beta \log_{10} e = -8.686\ \beta \ [\mathrm{dB/m}]. \qquad [42]$$

The propagation constant in the medium is

$$\gamma = ik. \qquad [43]$$

Note that the older literature (e.g., Stratton, 1941) differs from the newer literature (IEEE Standard 211(1977); Lorrain and Corson, 1971) by a factor of i.

The phase velocity in the medium is

$$V_p = \omega/\alpha \quad [m/sec] \qquad [44]$$

The wavelength in the medium is

$$\lambda = 2\pi/\alpha \quad [m] \qquad [45]$$

and the skin depth or attenuation length is

$$\Delta = 1/\beta \quad [m] \qquad [46]$$

which is the distance an electromagnetic wave travels in the medium while being attenuated by 1/e.

The characteristic intrinsic impedance of the medium is

$$Z_o = \omega\mu/k \quad [ohms] \qquad [47]$$

The attenuation length or skin depth from [46] is frequently assumed to be a simple function that is dominantly controlled by frequency and electrical conductivity

$$\Delta = (2/\omega\mu\sigma)^{1/2} \qquad [48]$$

For most low-frequency electromagnetic induction problems, this is a valid approximation. However, in some materials, the dielectric contribution cannot be ignored and the original equation [46] must be applied. In Figure 6, the

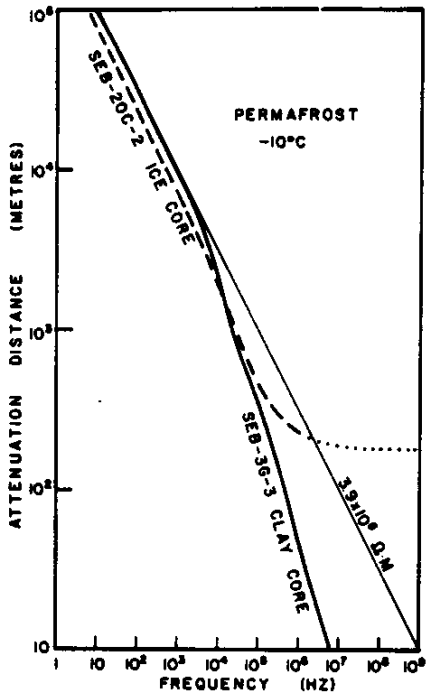

Figure 6 - The effect of displacement currents on skin depth.

light solid line labelled 3.9×10^5 ohm-m is equation [48] for a simple conductor without displacement currents (e.g., dielectric effects). The dashed-dotted line is for water ice including both dielectric and conduction effects per equation [46] and the heavy solid line is for clay permafrost including both effects (Olhoeft, 1977). Note that the dielectric effects are important only above 3×10^3 Hz.

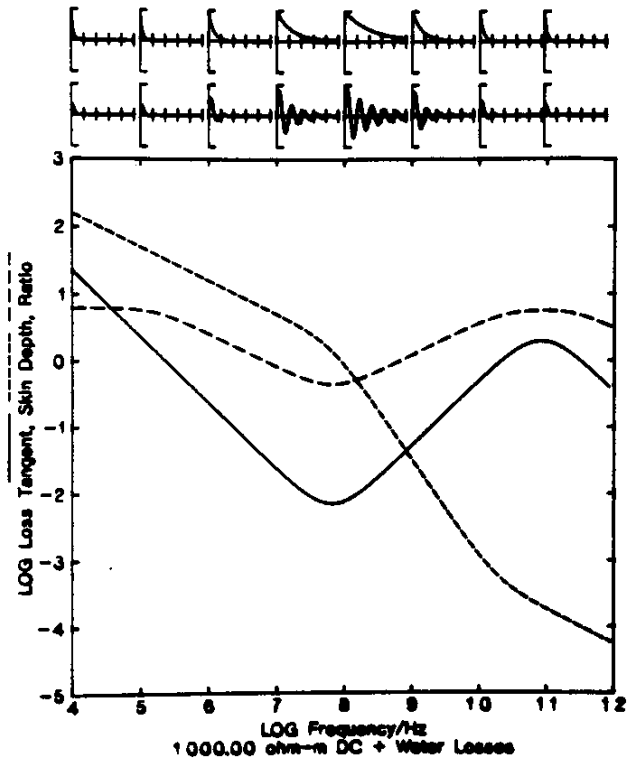

Figure 7 - The transition from induction to propagation.

Figure 7 illustrates the transition from inductive electromagnetic behavior described by the diffusion equation to electromagnetic propagation described by the wave equation (Stratton, 1941). The main plot shows the loss tangent (solid line), skin depth (fine dashed line), and the ratio of wavelength to skin depth (coarse dashed line). In the low-frequency inductive limit, the ratio is asymptotic to 2π, which results in electromagnetic energy that decays to 1/e in 16% of a wavelength and follows the diffusion equation. Across the top of the figure, the smaller plots show the decay of the electromagnetic energy versus distance in units of wavelength (the top row shows the envelope of decay; the bottom shows the actual waveform decaying). Figure 7 is drawn for the electrical properties of 1000 ohm-m water.

Note that there is an electromagnetic propagation window near 10^8 Hz, between the low frequency conduction loss mechanism and the high frequency orientational polarization relaxation near 10^{11} Hz.

The preceding discussion about nomenclature is not universally accepted. On page 32, it was noted that there is a factor of i between the older electromagnetic literature and that of the 1970's. Similarly, many of the symbols are themselves subject to dispute. Electrical engineers and physicists argue over the use of "i" versus "j" for $-1^{1/2}$, and several groups are using conflicting symbols for other parameters.

The most serious conflicts arise between the physics, electrical engineering, chemistry, and petroleum communities. Most of these conflicts can be resolved by careful attention to context. An example is the symbol used for electrical conductivity:

σ is commonly used by physicists and electrical engineers,

C is used by most well-loggers and petroleum engineers,

κ is used by chemists,

and γ or λ are sometimes used by physicists.

The problem compounds due to a limited number of symbols and the fact that nearly all symbols are used for something in each community. Thus, while C is electrical conductivity

to a petroleum engineer, C is capacitance to an electrical engineer. Similarly, σ is electrical conductivity in electrical engineering, is surface tension in chemistry, is strain in rock mechanics, and so on...

Part of the problem with symbols is being reduced by the journals that require tables of symbols in each article or reference to a standard such as the IUPAC, IUPAP, IEEE, SPE, ASTM, or other standards on terminology.

ELECTRICAL PROPERTIES SHORT COURSE - Gary R. Olhoeft

Charge Transport

Electrical properties are transport properties as they describe the motion and consequences of the motion of charged particles. The properties related to the actual motion of charge are various aspects of energy loss in a material. The five principle mechanisms of charge transport are:

1) diffusion: the random motion of matter through an ordered or random medium in response to a force,
2) percolation: the regular motion of matter through a random medium in response to a force,
3) migration: the diffusion or percolation of charge in response to an electric field (note that diffusion involves ions of opposite charge moving in similar directions while migration involves ions of opposite charge moving in opposite directions),
4) convection: the movement of matter in response to a thermal gradient,

and 5) tunnelling: the quantum statistical movement of charge through an energy barrier.

The two most important mechanisms are migration and tunnelling. The mathematics of diffusion and percolation in the migration mechanism fundamentally describe the DC electrical conduction of charge through bulk matter or along

surfaces. The tunnelling process primarily controls the movement of charge across interfaces between dissimilar materials. The best references to bulk conduction phenomena are Hladik (1972), Blatt (1968), Kofstad (1972), and the series Diffusion and Defect Data (1967-). In comparison, surface conduction is little studied, but has been recently reviewed by Henzler (1975), Bonzel (1975), and Binh (1983). Charge transport across interfaces will be discussed later.

Materials are also classified by the character and magnitude of their electrical conductance.

1) Metallic conductors: A material throughout which there is a uniform distribution of valence electrons that are not tightly bound or associated with any particular atom. Motions of electrons are constrained by electron-phonon scattering, electron-electron scattering, and scattering from stationary imperfections and impurities. Electrical conductivity increases with decreasing temperature (except near absolute zero). (Pratt and Sellors, 1973; Fish and Webb, 1981; Ho et al., 1981; Schroder, 1983.)

2) Nonconductor: Materials in which electrons are tightly trapped near atoms due to large energy barriers between atoms. Electrical conductivity increases with increasing temperature as thermal activity overcomes the energy barriers. Most rocks and minerals fall within this broad category, with further divisions of:

a) Insulators: Materials with very large energy barriers between atoms such that electrons rarely become

charge transport carriers. At elevated temperatures, charge is carried by ionic conduction through the movement of entire charged atoms within the material. At lower temperatures, charge transport is by tunnelling or defect diffusion. (Kofstad, 1972; Sorenson, 1981.)

b) Semiconductors: Materials with energy barriers that are slightly higher than the available energy from thermal activation at room temperature. At higher temperatures, electrons may be sufficiently activated to overcome the barriers. At lower temperatures, charge transport is by electrons or holes moving across barriers that are lowered by impurities within the material. (A "hole" in this context is the absence of an electron acting as an effective positive charge moving through matter.) (Harrison, 1970; Kittel, 1971; Shuey, 1975.)

c) Electrolytes: Materials which split (dissociate) into oppositely charged particles when treated appropriately (such as dissolving in a liquid solution or melting). The motion of the charged particles is hindered by interparticle interactions (scattering, viscous drag, etc.). Electrical conductivity increases with increasing temperature until near the critical point, above where it decreases with further temperature rise. (Hladik, 1972; Wooten, 1973; Archer and Armstrong, 1980; Yang and Isaacs, 1981; Anderson, 1981; Justice, 1983; Tischer, 1983.)

A very few natural materials are metallic conductors near

room temperature (such as native copper, silver, gold, etc. near 10^8 mho/m). Most geologic minerals are either semiconductors (most sulfides and oxides, ranging from 10^{-4} to 10^{+6} mho/m; Shuey, 1975; Vaughan and Craig, 1978) or insulators (most silicates, ranging from 10^{-9} to 10^{-17} mho/m; Olhoeft, 1980, 1981). Water ranges in conductivity from 5×10^{-6} (pure) to roughly 10^2 mho/m (saturated with salt in solution). Mixtures of these materials span the entire range of conductivity from 10^{-17} to 10^8 mho/m.

Although mixing laws will be discussed separately below, mixing water with other geological materials is the greatest cause of variation in the electrical behavior of rocks. A vacuum dry basalt with 4.3% porosity has an electrical resistivity of 10^{12} ohm/m. A fraction of a monolayer of water (about 0.002 wt%) can reduce that resistivity by an order of magnitude and full water saturation to 4.3% will reduce the resistivity by 9 orders of magnitude. Similarly, a pure sulfide mineral like pyrite will have a resistivity of 10^{-4} ohm/m that can be increased by four orders of magnitude if the current must cross a water/pyrite interface.

In the absence of water, the most significant impact on electrical conductivity is made by impurities and temperature. In pure materials with negative and positive free charged particles of density n_n and n_p respectively,

the application of an electric field will cause the acceleration and movement of the charged particles (in this discussion, neglect magnetic effects). The particles will also experience frictional forces that will dissipate some energy as heat and collisions with other particles that will scatter their direction of movement from that determined by the applied electrical field. The reciprocal of the time required for a given particle to be deflected or scattered through an angle of 90 degrees relative to the electric field is called the collision frequency which may have different values for negative and positive charged particles, ν_{cn} and ν_{cp}. Solving the equations of force and motion (Blatt, 1968; King and Smith, 1981) yields the complex conductivity of such a system:

$$\sigma = \sigma' - i\sigma''$$

where

$$\sigma' = \frac{e^2 Z_n^2 n_n \nu_{cn}}{m_n(\omega^2 + \nu_{cn}^2)} + \frac{e^2 Z_p^2 n_p \nu_{cp}}{m_p(\omega^2 + \nu_{cp}^2)}$$

$$\sigma'' = \frac{e^2 Z_n^2 n_n \omega}{m_n(\omega^2 + \nu_{cn}^2)} + \frac{e^2 Z_p^2 n_p \omega}{m_p(\omega^2 + \nu_{cp}^2)} \qquad [49]$$

with e = unit charge of electron = $1.6021892 \times 10^{-19}$ Coulombs

m_n = mass of negative particle with charge of Z_n

m_p = mass of positive particle with charge of Z_p.

In metals with electrons as charge carriers, $Z_n = 1$, $m_n << m_p$, and collisions are frequent due to the density of the material, $\omega^2 << \nu_n^2$, so these equations reduce to

$$\sigma = \sigma' = \frac{e^2 n_n}{m_n \nu_{cn}} \qquad [50]$$

with $\sigma'' << \sigma'$, and thus neglected. In metals, the addition of impurities causes an increase in scattering, increasing the collision frequency, and thus decreasing the electrical conductivity. In semiconductors and insulators, the addition of impurities lowers energy barriers, causing an increase in the free charge density which outweighs scattering effects, thus increasing the electrical conductivity.

The temperature dependence of the electrical conductivity of metals is very complicated, more easily written in the form of a resistivity such as (Blatt, 1968)

$$\rho(T) = \sigma^{-1} = 4R\left(\frac{T}{\theta_D}\right)^5 J_5\left(\frac{\theta_D}{T}\right) \qquad [51]$$

where R = intrinsic resistivity of the material (see Blatt, 1968)

θ_D = Debye temperature

T = temperature in degrees Kelvin

and

$$J_5(x) = \int_0^x \frac{z^5\,dz}{(e^z - 1)(1 - e^{-z})} .$$

Fortunately, this equation has two limiting cases which reduce the temperature dependence of the electrical conductivity to

$$\sigma = \frac{\theta_D}{RT} \quad \text{for} \quad T > \frac{2\theta_D}{3} \qquad [52]$$

$$\text{and} \quad \rho = 497.6\ R\ \left(\frac{T}{\theta_D}\right)^5 \quad \text{for} \quad T << \theta_D \qquad [53]$$

In this type of material, as the temperature rises from absolute zero the electrical conductivity decreases.

Insulators and semiconductors behave in an entirely different manner, following an equation of the form

$$\sigma = \frac{e^2 n}{kT} D_o\, e^{-E_o/kT} \qquad [54]$$

where e = electron charge

n = charge density

k = Boltzmann's constant = 8.61735×10^{-5} eV/K

D_o = diffusion coefficient

and only one term is shown for clarity (one is required for each type of charge carrier). This produces an electrical conductivity which increases with increasing temperature (the reverse of metals). In most practical situations, equation [54] is simplified to

$$\sigma = \sigma_o \, e^{-E_o/kT} \qquad [55]$$

where σ_o is simply an empirical parameter.

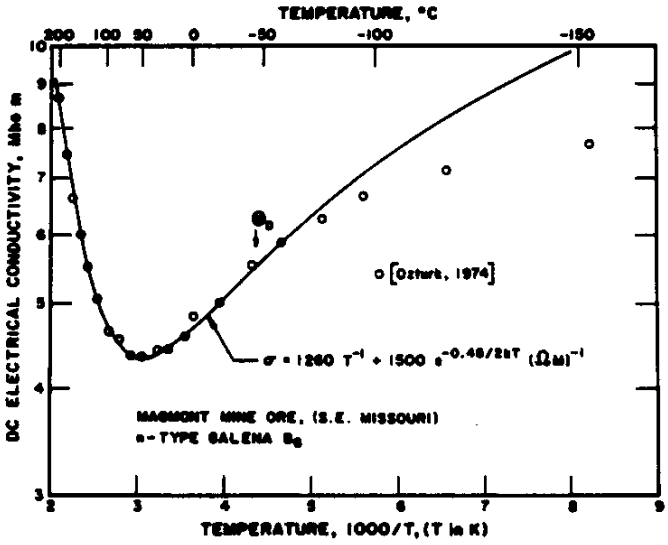

Figure 8 - Mixed metallic and semiconducting transport.

Many natural materials exhibit both metallic [51] and semiconducting [54] types of temperature dependence. Many sulfide minerals are metallic conductors at low temperatures, switching to semiconductors with increasing temperature. Figure 8 illustrates such a transition for a n-type galena from the Magmont Mine in Missouri. The circles are data points from Ozturk (1974) with a model fit according to the equation shown (solid line).

Figure 9 illustrates the electrical properties of granite, dry and wet, versus temperature. As discussed in Olhoeft (1980, 1981), most silicates including granites and basalts behave in a very similar fashion. Dry silicates have a strong temperature dependence, following a formula

$$\sigma = \sigma_0 e^{-E_0/kT} + \sigma_1 e^{-E_1/kT} + \sigma_2 e^{-E_2/kT} + \ldots \quad [56]$$

where several terms may be involved as different conduction mechanisms dominate different temperature regions. The activation energy increases from about 0.5 eV near room temperature to over 1.5 eV near melting.

The effects of other parameters are very slight in comparision to changes in electrical conductivity caused by changing water content amd temperature. To produce a one order of magnitude change in electrical conductivity in a dry silicate at 1000°C, the oxygen fugacity must be changed by more than 6 orders of magnitude, or the dry hydrostatic pressure by 13 kbars, or the temperature by 55 C, or the

water content by 0.3 wt%. At lower temperatures, the effects of water are even more pronounced.

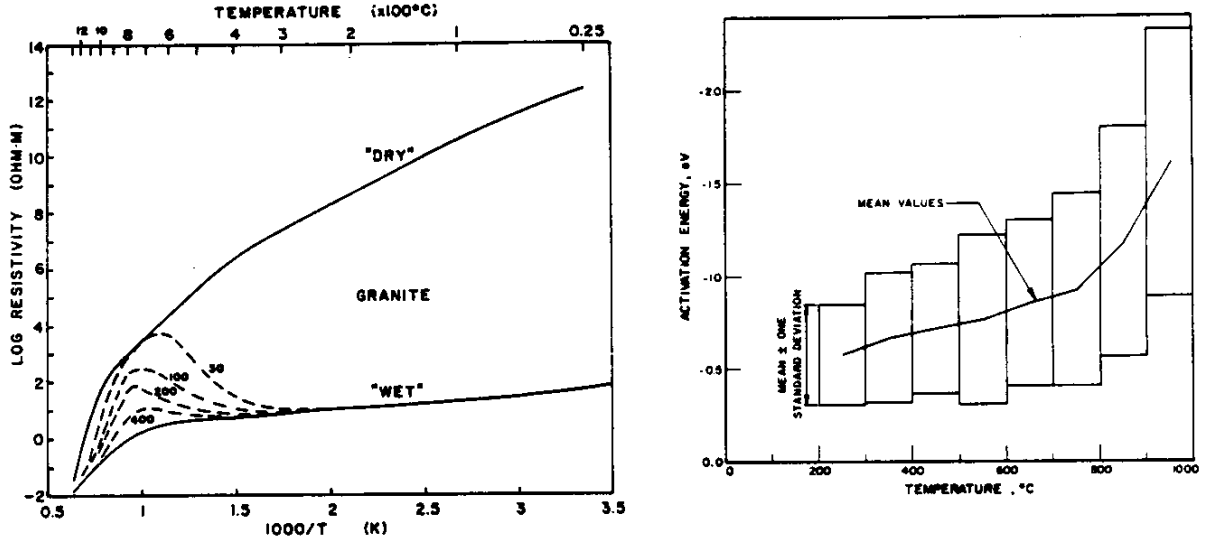

Figure 9 - Resistivity versus temperature of wet and dry granite.

Figure 9 summarizes the dependence of electrical resistivity upon temperature and water content after Olhoeft (1981). The "dry" curve is typical of nearly all silicates. The temperature dependence is characterized by the activation energies, E, from equation [55]. Olhoeft (1979) has reviewed the temperature dependence and E for 264 silicate rocks. Even hydrated minerals containing structural water such as hornblende do not deviate far from the "dry" dependence *unless* free water is present. As illustrated by the solid and dashed portions of the "wet" curve, the effects of free water are twofold -- first, there is a dramatic decrease in

the magnitude of the resistivity with water content, and second, there is a dramatic decrease in the temperature dependence. The effects shown for the solid line are typical of a few weight percent water. The solid line labelled "wet" is representative of water-saturated granite which has a resistivity that is independent of pressure from room temperature through melting if the saturating solution is more concentrated than 0.1 molar NaCl equivalent aqueous solution. For less concentrated solutions, the electrical resistivity becomes strongly pressure dependent above the critical point of the solution (illustrated by the dashed lines labelled in pressure in MPa). The electrical properties of these "wet" curves are essentially those of the volume conduction through the solution-filled pores in the rock. Olhoeft (1981) has a much more detailed discussion.

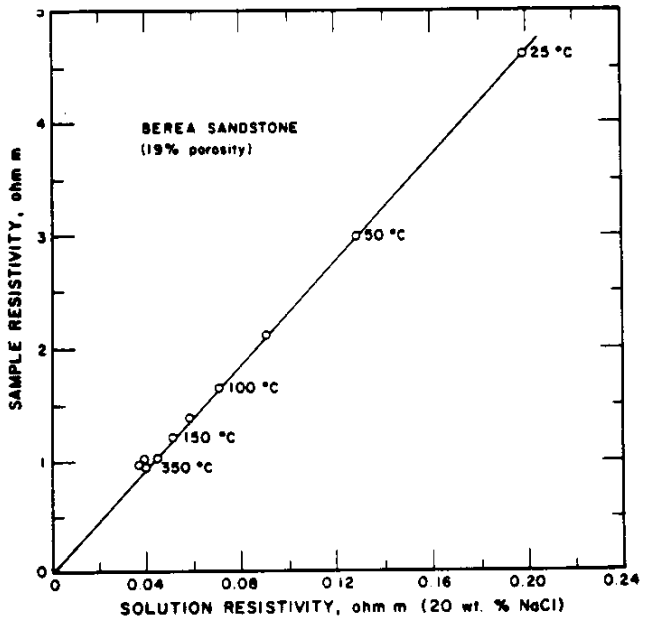

Figure 10 -

Figure 10 illustrates volume conduction through the pore solution by showing simultaneous measurements of the electrical resistivity of a brine-saturated Berea sandstone and of the saturating brine (from Ucok, 1979). The straight line is the path the electrical properties should follow with increasing temperature if the electrical resistivity of the rock is dominated by that of the solution through volume conduction in the pore system. This is the basis of many of the mixing formulas to be discussed later, including the classic Archie's Law (Archie, 1942).

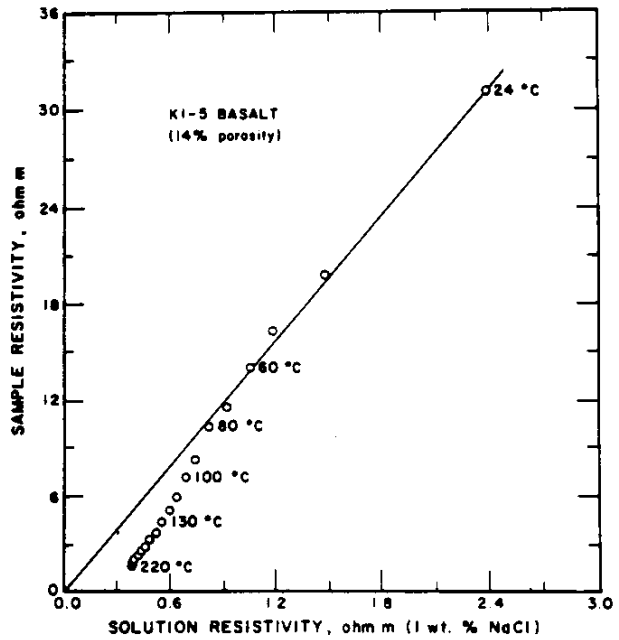

Figure 11 -

Unfortunately, as Figure 11 shows, the electrical properties of many water-saturated materials do not follow so simple a relationship. Figure 11 shows the data of Olhoeft

(1977) for water-saturated Hawaiian basalt. At the lower temperatures from 24 to 80°C, the sample obeys the volume conduction relationship dominated by the solution saturating the pores. Above 80°C, the resistivity of the rock sample decreases faster with increasing temperature than the resistivity of the solution alone. This may be attributed to increasing surface conduction along pore walls. Such surface conduction may be due to zeolitization as in this sample or to other types of alteration (Drury and Hyndman, 1979) including clay minerals. In many cases, the effects of surface conduction due to clays may be minimized by increasing the salinity of the saturating solution (Ucok, 1979).

The problems caused by surface conduction are also illustrated by the shaly sand problem in wireline log analysis. In that situation, a correction for surface conduction is applied to the normal volume mixing formula so as to allow the interpretation of formation porosity and water saturation from well logs (Waxman and Smits, 1968; Waxman and Thomas, 1974; Juhasz, 1979; Hill et al., 1979; Almon, 1979; Ruhovets and Fertl, 1982; Glanville, 1984; Vinegar and Waxman, 1984; Freedman and Ausburn, 1985; Silva and Bassiouni, 1985; Worthington, 1985; and others). Surface conduction is also important in electrokinetic phenomena such as streaming potential (Smits, 1968; Thomas, 1976; and discussions below). One of the best discussions of surface versus volume conduction for water on silicates may be found

in Clark et al.(1985). While surface conduction due to the presence of water is the dominant type in silicate rocks, other materials such as carbon lining grain boundaries (Duba and Shankland, 1982; Glassley, 1982) may also play a role.

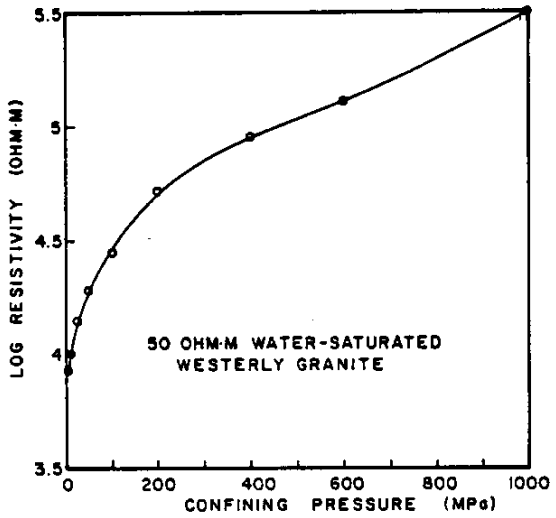

Figure 12 -

At both low and high temperatures, pressure may be important to electrical properties when differential stresses are generated that change the structure and volume of the pore space. Figure 12 after Brace and Orange (1968), illustrates the effects of confining pressure on the electrical resistivity of water-saturated granite at room temperature. As the confining pressure increases, it reduces the pore volume, thus increasing the resistivity. This effect is different from that discussed in Figure 9, where hydrostatic pressure was changing the electrical resistivity

by altering the electrical properties of the aqueous solution directly. One further effect of pressure is shown in Figure 13 (after Lebedev, 1975), where the labels along the curve are the amount of pressure required to dissolve the indicated weight percent water in a granitic melt. With increasing amounts of dissolved water, the electrical resistivity decreases.

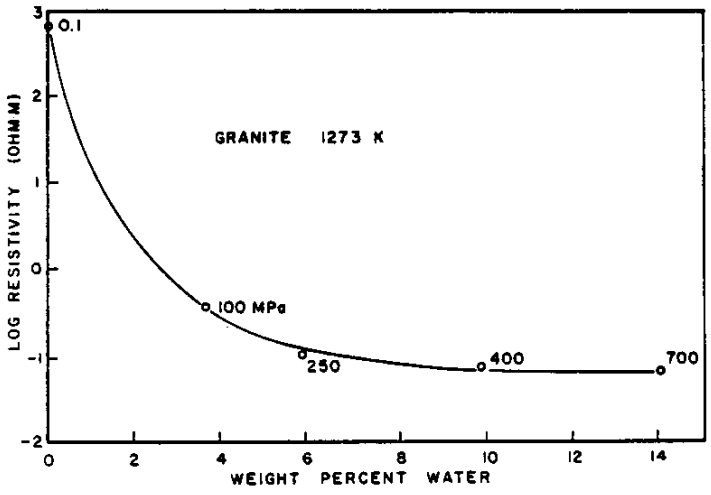

Figure 13 - Resistivity versus dissolved water content (controlled by pressure).

For further reading on the effects of temperature and pressure on electrical conductivity, see Shimizu (1962), Lebedev and Khitarov (1964), Bradley et al.(1964), Lebedev (1965), Quist and Marshall (1968), Marshall (1968), Holzapfel (1969), Watanabe (1970), Timur et al.(1972), Yoon and Lazarus (1972), Parkhomenko and Bondarenko (1972), Bondarenko (1974),

Duba et al.(1974), Volarovich and Parkhomenko (1976), Lastovickova and Parkhomenko (1976), Schock et al.(1977), Bloch et al.(1977), Cleaver (1979), Chelidze et al.(1979), Will et al.(1979), Karato (1981), Parkhomenko et al.(1981), Rai and Manghnani (1981), Hamann (1981), Shankland et al.(1981), Hinze et al.(1981,1982), Frantz and Marshall (1982), Duba (1982), Waff and Bulau (1982), Hsieh et al.(1982), Ishikawa et al.(1982), Parkhomenko (1982), Lacam (1983), Tyburzy and Waff (1983, 1985), and Walsh and Brace (1984).

ELECTRICAL PROPERTIES SHORT COURSE - Gary R. Olhoeft

Charge Separation

Electrical properties are transport properties in that they exist because of the motion of charge through the transport of either electrons, protons, or ions. Most electrical properties are directly related to the charge transport process itself. However, some electrical properties are related to the distribution of charge immediately before or after transport, or to the accumulation of charge at discontinuities during charge transport. The properties related to charge distribution and accumulation are various aspects of polarization phenomena.

The ancient Greeks knew of polarization phenomena, though extensive investigations were not started until the late 1600's and early 1700's when materials were classified by their ability to hold charge. Polarization is the physical displacement or separation of a charge in distance from its normal equilibrium by some applied force. These forces may result from mechanical deformation, electrical fields, chemical reactions, or a variety of other processes.

The principle mechanisms of charge separation due to an applied, external electric field are:

1) electronic polarization: the distortion of an atom's

electron cloud in response to an external electric field in which one side of the atom becomes effectively more positive and the other side more negative than the normal equilibrium,

2) molecular polarization: the distortion of an entire molecule ...
3) ionic polarization: a redistribution of ions within a material ...
4) orientational polarization: realignment or re-orientation of polar molecules without distortion of shape ...
5) interfacial polarization: charge separation and accumulation at local variations in electrical properties during migration of charge in response to an external electric field.

In the order listed, these polarization mechanisms occur from high to low frequency, and they are simply additive to each other in going from high to low frequency. At the highest frequencies of excitation, the electronic polarization is the sole process (up to 10^{24} Hz) as the electrons have the smallest mass and respond very quickly. The polarization of even vaccum is never zero as the small charge separation during the continual creation and annihilation of electron-positron pairs results in the free space dielectric permittivity of $8.8541818782 \times 10^{-12}$ F/m (Dirac, 1967; Heitler, 1954). At lower frequencies, the

heavier mass mechanisms sum: near 10^{14} Hz molecular and ionic polarizations begin to respond as shown in Figure 14, near 10^{12} Hz orientational polarization appears, and roughly below 10^{8} Hz appear the interfacial

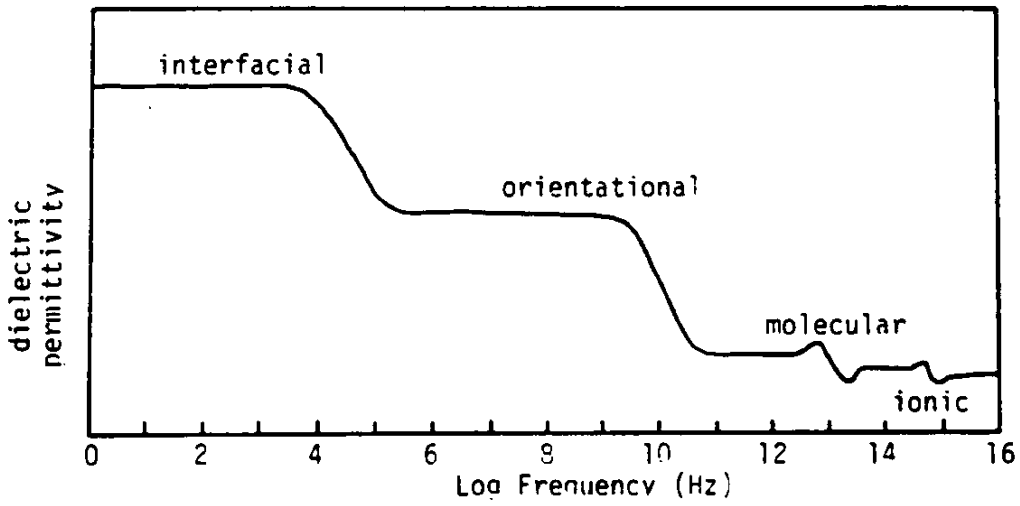

Figure 14 - Polarization versus frequency.

polarizations. Note also that the highest frequency polarizations occur as resonance phenomena while the lower frequency polarizations are relaxation phenomena. Charge separation processes also occur due to coupling between electrical and other forces such as stress (piezoelectric), thermal (pyroelectric), and others as will be discussed in the next section. The best general discussions of polarization phenomena occur in Bottcher (1973) and Bottcher and Bordewijk (1978). Interfacial polarization has been discussed in Butler (1951), Davies and Rideal (1963), Bockris

and Reddy (1970), Hoekstra and Doyle (1971), McCafferty and Zettlemoyer (1971), Gileadi et al.(1975), Antropov (1977), Bockris and Khan (1979), Boguslavsky (1980), Vold and Vold (1983), White (1983), Fuerstenau (1984), and Kitahara and Watanabe (1984). In most geophysical applications, the most important mechanism is interfacial polarization which dominates all other processes except the orientational polarization of the water molecule.

Returning to the simple circuit that was discussed on page 12, recall the expression for the admittance in terms of electrical properties of a material (neglecting the DC conductivity term in [6])

$$K' - iK'' = K_\infty + \frac{K_0 - K_\infty}{1 + i\omega\tau} \qquad [57]$$

which may be rewritten as

$$K' - iK'' = K_\infty \{ 1 + \varsigma \frac{1}{1 + i\omega\tau} \} \qquad [58]$$

where $\varsigma = (K_0 - K_\infty)/K_\infty$ = dielectric chargeability.

For a series of separate mechanisms, this expression and the corresponding electrical circuit may be generalized to

$$K' - iK'' = K_\infty \{ 1 + \varsigma_1 \frac{1}{1 + i\omega\tau_1} + \varsigma_2 \frac{1}{1 + i\omega\tau_2} + \ldots \} \qquad [59]$$

and, as before,

$$K_e = C_1/C_o$$

where C_o = the vacuum capacitance of the empty space occupied by the material,

$$\$_1 = C_2/C_1$$

$$\tau_1 = R_2C_2$$

$$\$_2 = C_3/C_1$$

$$\tau_2 = R_3C_3$$

and so forth.

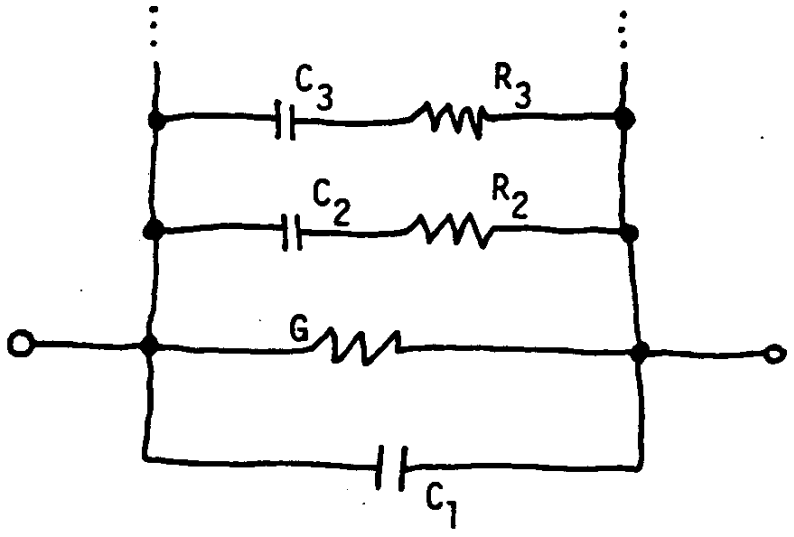

Figure 15 - Distributed circuit model with multiple relaxations.

This extension of a Pellat/Debye single relaxation (first proposed in 1899 by Pellat; see Gevers, 1945,

excellent review) to a continuous distribution of relaxation times by von Schweidler (1907; see Gevers, 1945) resulted in the integral summation

$$K' - iK'' = K_\infty \left(1 + \xi \int_0^\infty K(\tau)\ (1 + i\omega\tau)^{-1}\ d\tau \right) \qquad [60]$$

where $K(\tau)$ is a distribution of time constants, defined such that $\int_0^\infty K(\tau)\ d\tau = 1$, and ξ is equal to a summation of all of the individual ξ_j's above, or $\xi = (K_0 - K_\infty)/K_\infty$

with $K_0 = \lim_{\omega \to 0} K'$

and $K_\infty = \lim_{\omega \to \infty} K'$.

Wagner (1913; in Gevers, 1945) assumed that $K(\tau)$ could be given as the Gauss probability function

$$K(\tau)\ d\tau = \frac{1}{\pi\sqrt{2}}\ e^{-[b\ \ln(\tau/\bar{\tau})]}\ d\ \ln(\tau/\bar{\tau}) \qquad [61]$$

which is thus called the Wagner time constant distribution function with

b = density parameter (greater b causes denser grouping about $\bar{\tau}$)

and $\bar{\tau}$ = mean time constant around which distribution is centered.

In the limiting case of b → ∞, the equations reduce to those of a single relaxation time, and for very small b

$$K' = (K_o + K_\infty)/2$$

and [62]

$$D = \text{loss tangent} = b\,(2\pi)^{1/2}\,\frac{K_o - K_\infty}{K_o + K_\infty} + \frac{\sigma}{\omega\epsilon_o K'}$$

The dielectric literature has many examples of specialized time constant distributions. If equation [58] is rewritten as

$$K' - iK'' = K_\infty\,(1 + \phi Q) \qquad [63]$$

then several of these may be given as

$Q = (1 + i\omega\tau)^{-1}$ is the Pellat/Debye single relaxation of [57]

$Q = \int_0^\infty K(\tau)\,(1 + i\omega\tau)^{-1}\,d\tau$ is the von Schweidler distribution of [60]

$Q = (1 + (i\omega\tau)^{\alpha})^{-1}$ is the Cole-Cole distribution [64]

$$Q = (1 + i\omega\tau)^{-\beta}$$ is the Cole-Davidson distribution [65]

and there are many others. Further discussion of dielectric relaxation may be found in Garton (1946), Cole (1955), Daniels (1967), Schwarzl and Struik (1968), Onsager and Runnels (1969), Addison (1970), Hoekstra and Doyle (1971), Shuey and Johnston (1973), Olhoeft et al.(1973, 1974), Bertelsen and Lindgard (1974), Brun and Dansas (1974), Chu and Hwang (1974), Crossley and Walker (1974), Mason et al.(1974), Bernsaconi (1976), Alvarez and de Paiva (1979), Braunlich (1979), Matsumoto and Watanabe (1979), Vaughn (1979), Rosseinsky et al.(1981), Jonscher (1981, 1983), Hall et al.(1983, 1985), and Wait (1984).

The distribution of Cole and Cole (1941) is the most useful in the earth sciences. It has the form

$$K' - iK'' = K_\infty \left\{ 1 + \xi \frac{1}{1 + (i\omega\tau)^{\alpha}} \right\} \qquad [66]$$

where α is one minus the Cole-Cole distribution parameter. In the limit as α becomes very small, the result is very similar to that found for the Wagner distribution in [62]. As α goes to 1, the result is a single relaxation. A plot of log loss tangent versus log frequency exhibits slopes of $-\alpha$ and α on either side of the maximum loss, which occurs at

$$\omega_m = \frac{(1+\xi)^{1/(2\alpha)}}{\tau} \qquad [67]$$

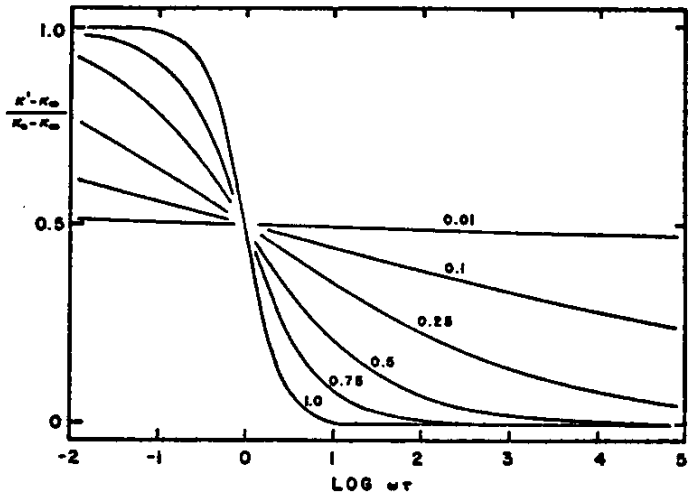

Figure 16

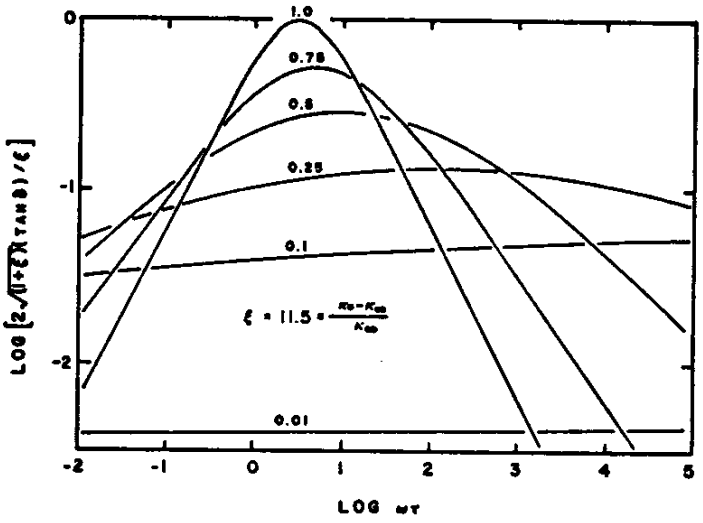

Figure 17

Figures 16 and 17 show the functional form of [66] in terms of the normalized log loss tangent and normalized permittivity as a function of α. Note that the peak in the loss tangent shifts to higher frequencies with decreasing α, even though the time constant is not changing.

Nearly all electrical properties of rocks are sensitive to a wide variety of environmental parameters. The effects of water are most pronounced and will be discussed in detail below. Current density and electric field strength have very little effect on most dielectric properties except in extreme situations (see reviews in Kielich, 1972; Parry-Jones, 1975). Some dielectric properties are pressure dependent, but the effects are usually secondary to the dependence of density changes caused by pressure (see Olhoeft, 1975; 1977). Next to water, the most important environmental influence is exerted by temperature. Normally, K_∞ is independent of temperature, and K_0 may or may not be dependent upon temperature. The time constant, τ, is always strongly dependent upon temperature with a form

$$\tau = \tau_0 \, e^{+E_0/kT} \qquad [68]$$

where E_0 = activation energy (eV)

k = Boltzamnn's constant

T = temperature (K)

and τ_0 = time constant at infinite temperature.

With increasing temperature, the time constant decreases and the relaxation process goes toward higher frequencies as shown in the Figure 18 with $T_2 > T_1$. The loss tangent is

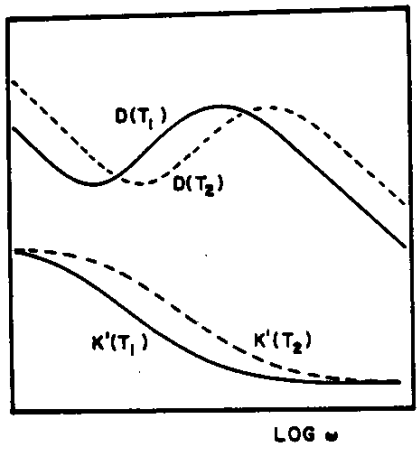

Figure 18

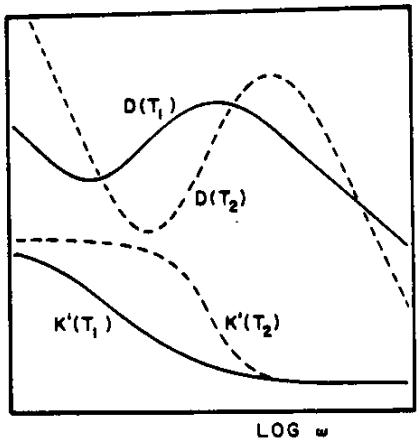

Figure 19

shown as D including both dielectric and conduction loss terms as in equation [9] with conductivity varying with temperature according to equation [55]. Figure 19 illustrates the same situation with regards to temperature, but also including a time constant distribution of the Cole-Cole type that has a temperature dependent distribution

parameter according to (Olhoeft et al., 1973)

$$\alpha = \frac{1 - e^{-\beta T}}{1 + e^{\beta (T_o - T)}} \qquad [69]$$

where β and T_o are empirical constants (Olhoeft, 1976). Most time constant distributions are related to a common mechanism such as a distribution of particle sizes, resulting in the entire distribution shifting uniformly with temperature and retaining its spectral shape. As shown in Figure 19, however, equation [69] describes a change in spectral shape with a change in temperature. This is caused by several distributions with differing activation energies, thus changing time constants at different rates with changing temperature.

One of the most remarkable features of the dielectric properties of rocks is the finding (Olhoeft and Strangway, 1975) that the high frequency relative dielectric permittivity, K_∞, is primarily determined by bulk density. Figures 20 and 21 illustrate this dependence upon bulk density from measurements made at 1 MHz.

Figure 20 plots log relative dielectric permittivity versus dry bulk density with the line labelled 2.39 equal

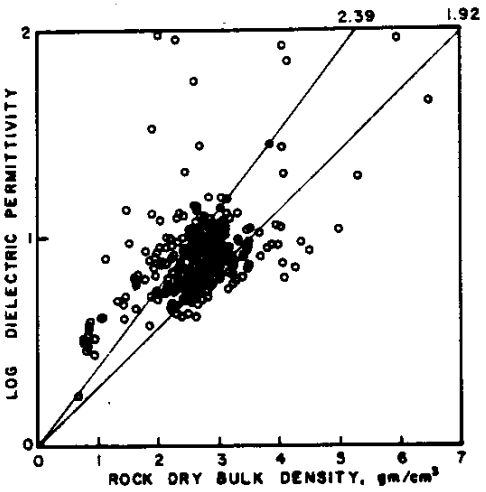

Figure 20- Log relative dielectric permittivity versus dry bulk density.

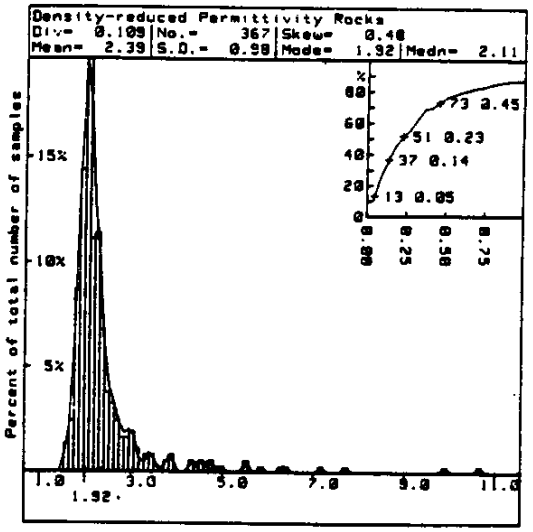

Figure 21 - Histogram of density-reduced permittivity.

to the least squares fit to the logarithmic sum Lichteneiker mixing formula which gives

$$K_m = 2.39^d \qquad [70]$$

where d is the dry bulk density in gm/cm^3. However, as shown in Figure 21, the histogram of the data is highly skewed, biasing a least squares fit. The histogram of the density-reduced permittivity is given from

$$K_{dr} = K_m^{1/d} \qquad [71]$$

where K_{dr} is the density reduced relative dielectric

permittivity from a sample with measured permittivity, K_m, at a density d. The correct formula for the density reduced permittivity is derived from the modal value of the histogram

$$K_e = 1.92^d \qquad [72]$$

as shown by the second line in Figure 20. Olhoeft (1979) has compiled the statistics of the density-reduced permittivity separately for suites of measurements as shown in the table below:

Table 3 - Density-reduced permittivity statistics

	114 lunar samples	261 pure minerals	367 rocks
mean	1.93+-0.17	2.00+-0.67	2.39+-0.98
mode	1.92	1.91	1.92
median	1.93	1.89	2.11
skewness	0.07	0.13	0.48

As the histograms are typically skewed, the modal (or most probable) values should be used in the mixing formula. It is remarkable that all three data suites above result in

$$K_e = 1.92^d \qquad [73]$$

The outstanding exception to this formula is water in all of its forms. The density reduced permittivity of water ranges

from 3.2 (solid ice) to 4.2 (liquid). For rocks, containing water, formula [73] becomes

$$K_e = 1.92^d K_w^v \qquad [74]$$

with a volume fraction of v water of relative dielectric permittivity, K_w, in the rock. However, while this logarithmic mixing formula works well for dry rocks, it fails for wet rocks. The reasons for this along with better wet rock mixing formulas will be discussed later.

In addition to the mixing of two different materials to produce a composite dielectric permittivity as in equation [74], another phenomenon occurs. This results from the additional polarization due to charge accumulation at the boundaries between two dissimilar materials, called interfacial polarization or the Maxwell-Wagner effect. Dukhin (1971) and Hasted (1973) have excellent reviews of this phenomenon. Briefly, two dissimilar materials are uniformly mixed with a volume fraction, v, of particles (subscript 2) in a medium of another material (subscript 1). The resultant mixture exhibits the properties of a lossy dielectric with a strong single relaxation. This takes the form of

$$K' - iK'' = K_e + \frac{K_o - K_e}{1 + i\omega\tau} \qquad [75]$$

which is very similar to the formulas described earlier, except

$$K_\infty = K_1 \frac{2K_1 + K_2 + 2v(K_2 - K_1)}{2K_1 + K_2 - v(K_2 - K_1)} \qquad [76]$$

$$K_0 - K_\infty = \frac{9(K_1\sigma_2 - K_2\sigma_1)^2 v(1-v)}{(2K_1+K_2-v(K_2-K_1))(2\sigma_1+\sigma_2-v(\sigma_2-\sigma_1))^2} \qquad [77]$$

$$\text{and} \quad \tau = \frac{2K_1 + K_2 - v(K_2 - K_1)}{2\sigma_1 + \sigma_2 - v(\sigma_2 - \sigma_1)} \epsilon_0 \qquad [78]$$

with a composite DC conductivity of

$$\sigma_{DC} = \sigma_1 \frac{2\sigma_1 + \sigma_2 + 2v(\sigma_2 - \sigma_1)}{2\sigma_1 + \sigma_2 - v(\sigma_2 - \sigma_1)} . \qquad [79]$$

This Maxwell-Wagner effect is an interfacial polarization resulting because there can be no permanent distribution of free charge within any material of non-zero conductivity (Stratton, 1941). If a force perturbs the charge to create a charge distribution within a uniform material, the removal of the force will result in a divergenceless flow of the charge out of the material. The charge is then trapped in the energy barriers at the edges of the material (e.g., at interfaces). The Maxwell-Wagner effect assumes the thickness of this interfacial region is negligible in comparison to the physical scale of inhomogeneity (e.g., small compared to the average particle

size). For further discussion, see reviews in Sixou et al.(1967), Hasted (1972), van Beek (1967), Dukhin (1971), Pethig (1979), Perram and Anastasiou (1981), and de Loor (1983) in which the effect of particle size and shape are also discussed.

If the thickness of the interfacial region (space-charge layer or double-layer: see Bockris and Reddy, 1970; van Olphen, 1977) approaches or exceeds the particle size, then surface conduction, ion exchange and adsorption, distortion and the independent polarization of the interphase region may become important. In such cases as colloidal clays, the effective dielectric permittivity of the mixture may exceed that of the individual components (relative permittivities on the order of 10^5 are not unusual). When charge transport to and from the interface is also diffusion-limited, the time constant distribution will depend explicitly on the particle size distribution (Pethig, 1979; Schwan et al., 1962; Duhkin and Shilov, 1972; Schwarz, 1972; Chew and Sen, 1982). With simple systems, the theories appear to work very well (Williams and James, 1976; Sen et al.,1981; Sen, 1984), but clays (Arulanandan and Mitchell, 1968; Weiler and Chaussidon, 1968; Forslind and Jacobsen, 1972, 1973, 1975; Calvet, 1975; Hall and Rose, 1978; Lockhart, 1980) and zeolites (Jones and Davies, 1975; Jones, 1975) give conflicting results.

To illustrate the dielectric properties of rocks, consider the electrical properties of monomineralic pyroxene from Olhoeft (1976) as illustrated in Figures 22 and 23.

Figure 22 shows how the conductivity becomes frequency dependent when dielectric displacement currents are strong. Note the convergence of the curves at high temperatures as the conduction effects increase faster with increasing temperature than the dielectric effects, and eventually completely dominate. This data is shown for pyroxene dry in 10^{-7}Torr vacuum, because even the smallest amount of water can completely dominate these dielectric polarization and relaxations related to the structure of the mineral.

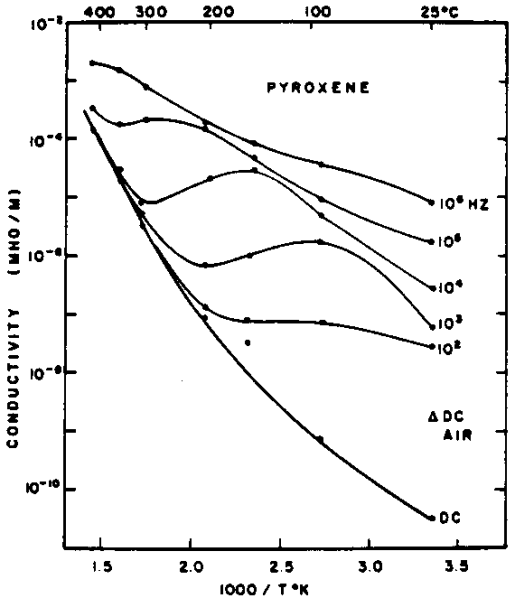

Figure 22

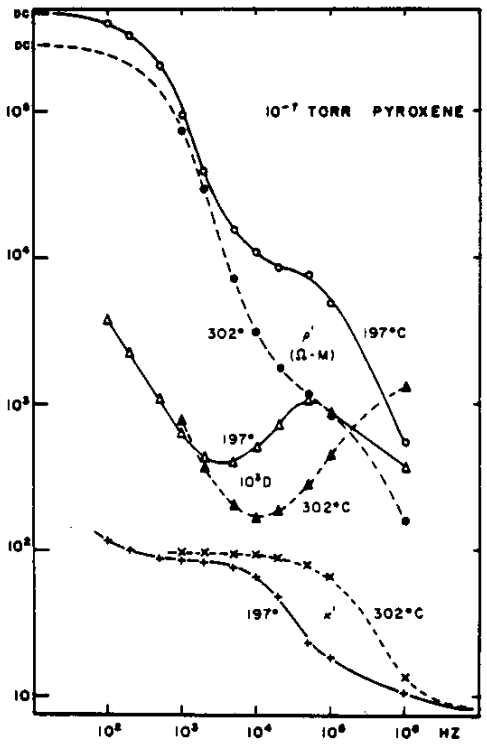

Figure 23 illustrates a portion of the pyroxene data replotted as real resistivity, ρ', relative dielectric permittivity, K', and loss tangent, D, (note scale offset) versus frequency at two temperatures. Note the frequency shift indicative of the change in time constant with

temperature. This sample also exhibits a slight change in the time constant distribution shape with temperature after equation [69] that is shown and discussed further in Olhoeft (1976).

The dielectric properties are dramatically different when water is present. This is shown in Figures 24 and 25 for typical permafrost. Figure 24 shows the behavior of conductivity, resistivity, relative dielectric permittivity, and loss tangent versus log frequency. Above 1 MHz, the electrical properties are strongly temperature dependent but independent of pressure. Below 1 MHz, the electrical properties are both strongly temperature and pressure dependent (Olhoeft, 1975, 1977). Figure 25 schematically illustrates the polarization mechanisms that are causing the observed properties. The region labelled "D" is controlled by the DC ionic conduction through the unfrozen pore water lining the pore walls and clay particles. "M" is a region controlled by Maxwell-Wagner interfacial polarization effects (the dashed line shows the loss tangent after removal of the DC conduction effects). "B" is the region dominated by the relaxation of Bjerrum defects in water ice (Onsager and Runnels, 1969). "U" is a region dominated by clathrate-hydrate relaxations or by clay-organic interactions. "W" is the relaxation of the orientational polarization of the free unfrozen water lining pore walls and surrounding clay particles. Above roughly 10^{11} Hz, the electrical properties are independent of temperature and

pressure.

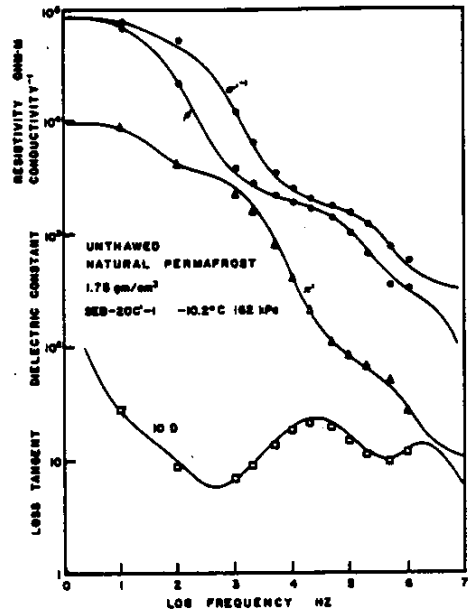

Figure 24

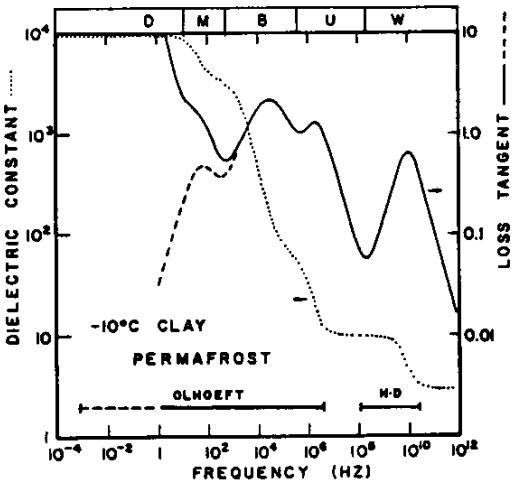

Figure 25

Further studies of dielectric relaxation may be found in Bayley (1933), Berg (1936), Sillars (1936), Akerlof and Oshry (1950), Mayburg (1950), Cumming (1952), Lane and Saxton (1952), von Hippel (1954, 1972), Matsonashvilli (1958), Baldwin (1959), Keller and Licastro (1959), Howell and Licastro (1961), Stacey (1961), Trukhan (1962), Bondarenko (1963), McIntosh (1966), Griffin and Marovelli (1967), McCrum et al.(1967), Scott et al.(1967), Cole and Worz (1969), Hill et al.(1969), Saint-Amant and Strangway (1970), Zheludev (1971), Wiebe (1971), Davies et al.(1972), Geiger and Williams (1972), Bassett and Shackelford (1972), Westphal and Sils (1972), Winkelmolen (1972), Alvarez (1973), Cavell (1973), Chung and Westphal (1973), Hansen et al.(1973), Ho

and Hall (1973), Pearce et al.(1973), Pottel (1973), Young and Frederikse (1973), Benin et al.(1974), Cihlar and Ulaby (1974), Hoekstra and Delaney (1974), Tam (1974), Klein and Swift (1977), Wobschall (1977), Grant et al.(1978), Okrasinski et al.(1978), Poley et al.(1978), Tuck and Stacey (1978), Bergman (1978, 1980), Burfoot and Taylor (1979), Bussey (1979), Nottenburg et al.(1979), Gross et al.(1980), Akhadov (1980), Wang (1980), Brylkin (1981), Miyake et al. (1981), Sen (1981, 1982, 1984), Sen et al. (1981), Yu (1981), Varadan et al.(1982), Bartnikas (1983), Eberle (1983), Bigelow and Eberle (1983), Palaith and Chang (1983), Sherman (1983, 1985), Bunget and Popescu (1984), Hinch et al.(1984), Kenyon (1984), Knight and Nur (1984), Korringa (1984), Mandel and Odijk (1984), Ramdeen et al.(1984), Hall et al.(1985), Hallikainen et al.(1985), Dobson et al. (1985), Shen et al.(1985), Stogryn and Desargent (1985), and De (1985).

Spontaneous Polarization

Charge separation processes also exist due to coupling between electrical and other forces. These include:

1) piezoelectric polarization: asymmetrical displacement of ions in a polar crystal due to external stress,
2) pyroelectric polarization: charge displacement due to asymmetrical alteration of interatomic distances from external heating or cooling of a polar crystal (in order to be pyroelectric, the crystal must first be piezoelectric),
3) ferroelectric: permanent charge polarization in the absence of external forces, but which may be polarity-reversed by an external electric field (must be pyroelectric to be ferroelectric),
4) magnetoelectric polarization: charge separation due to the external application of a magnetic field.

There also exist multiply coupled phenomena like the Hall effect in which an external current and an external magnetic field are required to produce a polarization, or like electrooptical and elastoptical effects. Of these processes, no ferroelectric or magnetoelectric pheonmena have

been found in naturally occuring materials; though synthetic materials with perovskite structures do exhibit ferroelectricity, leading to speculation that such may exist in the upper mantle.

Charge separation phenomena as discussed above normally result from an external force providing the stimulus to displace or separate charge, resulting in an electric field internal to the crystal in opposition to the external force. The following are examples of charge separation phenomena in which an internal process results in a measurable electric field or potential external to the material due to charge separation within the material:

1) contact (Galvani) potential: the differences between the inner potentials of two materials in contact (where the inner potential is that corresponding to the work done to bring a unit negative charge from infinity in vacuum into the bulk of the material),
2) Nerst potential: the differences in inner potential between a liquid and solid in contact,
3) thermoelectric (Seebeck) potential: the potential generated by more rapid diffusion of charge from cold to hot regions than the reverse in the presence of a thermal gradient,
4) streaming (electro-osmotic) potential: the potential along the length of a pore due to flowing

fluids under a pressure gradient forcing charges along the surfaces of the pore walls (the potential generated is opposing the electric current from the charge transport),

5) sedimentation potential (Dorn effect): the potential from the precipitation of charged solid particles from suspension in a fluid,

6) diffusion potential: the potential between two regions with unequal ionic mobilities and an interconnecting chemical gradient,

7) redox (oxidation-reduction) potential: the potential from the charge transfer process during an oxidation-reduction reaction.

In these charge separation potentials, the Nernst, streaming, sedimentation, diffusion and redox potentials are most important in earth materials. Of equal importance, though not readily classified, are charge separation phenomena such as the adsorption-desorption of charge to an interface during ion exchange, chemical complexing, intercalation, and related phenomena. As water freezes to ice, it generates a little studied potential known as the freezing potential (Parameswaran and Mackay, 1983).

For general discussions of these phenomena, see the literature review in Hulse (1978) and detailed discussion in Davies and Rideal (1963), Bates (1972), Antropov (1977), Adamson (1976), Bockris and Reddy (1970), Pourbaix (1973),

Dukhin (1974), Dukhin (1975), Dukhin and Derjaguin(1974), Derjaguin and Dukhin (1974), Dobos (1975), Milazzo and Caroli (1978), Hunter (1981), Antelman (1982), and Bard et al.(1985).

Streaming potential results from a flow of liquid through a tube in which the electrical double layer near the tube or pore wall is sheared by the liquid motion. The shearing of the double layer separates charge, with some being fixed to the pore wall and some moving with the liquid. The charge per second being carried by the fluid is the streaming current. A reverse electrical current flow must occur to balance this mechanically-induced streaming current so that there is no net flow of electricity at steady state. Due to the finite volume conduction of the liquid and the finite surface conduction of the pore wall, there is a voltage generated due to IR drop along the length of the pore. This voltage is the streaming potential, given as (see excellent derivation in Davies and Rideal, 1963)

$$E_{str} = \frac{P\epsilon\zeta}{4\pi\eta_o(\sigma + 2S/a)} \qquad [80]$$

where P = pressure

ϵ = dielectric permittivity of liquid in the pores

η_o = liquid viscosity

ζ = zeta potential (potential at point of shear in

liquid near pore wall)

σ = liquid bulk electrical conductivity

S = surface conductivity

and a = radius of tube or pore.

This formula is only valid if the radius of the pore is much larger than the thickness of the double layer, the flow is laminar, and the length of the pore is greater than the characteristic flow length of the liquid given by $u\zeta/(4\pi^2a^2\sigma)$ where u is the volume flow rate through the pore. The zeta potential is the least known quantity, varying from -36 to -200 mV for water against silica and also varying with the solution type and salinity (ζ generally becomes more positive with increasing salinity) (Ney, 1973; Hunter, 1981). The streaming potential coefficient, $E_{str}/\Delta P$) has been observed to be independent of temperature to 130°C (Johnson and Olhoeft, 1980, unpublished), but it also has a widely varying range including sign reversals from -12 to +500 mV/bar, with most rocks about +10mV/bar. In very fine capillary pore systems, the apparent viscosity is much higher than the actual viscosity of the free liquid due to the effects of double-layer interactions. This results in much lower streaming potentials than would be expected from the properties fo the materials alone.

The sedimentation potential results from a solid particle moving through a liquid, leaving a portion of its double

layer trailing behind like a wake. This distortion of the double layer results in a charge separation and the sedimentation potential

$$E_{sed} = \frac{a^3(D_p - D_l)n_o g f \epsilon \zeta}{3\eta_o \sigma} \qquad [81]$$

where g = gravitational constant

D_p = density of particle

D_l = density of liquid

a = radius of particle

n_o = number of particles

and the other parameters are the same as for streaming potential, except f is a parameter depending upon the ratio of particle radius, a, to double layer thickness, $1/\chi$. For insulating particles that are large compared to the double layer thickness, $f \rightarrow 1$ while for conducting particles, $f \rightarrow 0$. For either conducting or insulating particles that are small compared to the double layer thickness, $f \rightarrow 2/3$ (see Davies and Rideal, 1963, figure 3-11).

The explicit formula for sedimentation potential including volume conductivity of the liquid, σ, volume conductivity of the particle, σ_p, surface conductance, S, and the ratio of particle radius to double layer thickness, χa, is

$$E_{sed} = \frac{2a^3(D_p-D_1)n_o\epsilon\zeta z}{9\eta_o}\left(1+2\frac{\sigma-(\sigma_p+2S/a)}{2\sigma+\sigma_p+2S/a}(f(\chi a)-1)\right) \quad [82]$$

where

$$f(y) = 1 + \frac{y^2}{16} + \frac{5y^3}{48} - \frac{y^4}{96} + \frac{y^5}{96} - \left(\frac{y^4}{8} - \frac{y^6}{96}\right) e^y \int_e^y \frac{e^{-t}}{t}\,dt \quad [83]$$

and the Davies and Rideal (1963) f of [81] = (2/3) f(χa) of [82] in Dukhin and Derjaguin (1974).

Surface conductance for most materials in contact with water is about 10^{-9} mhos (Davies and Rideal, 1963, Table 3-1). Thus, in the streaming potential, the surface conductance becomes important for pore radii smaller than 10^{-6} m with groundwater of 0.01 mho/m. A similar argument follows for sedimentation potential. The result is a significant impact of surface conductance on streaming potential in most rocks, particularly igneous rocks, but a significant impact on sedimentation potential only for colloidal particles (e.g., clays). For further, detailed discussions see Dukhin (1974, 1975). The thickness of the electrical double layer becomes important for pore/particle radii on the order of 10^{-5} m in very dilute solutions or 10^{-7} m in normal ground waters.

Streaming potentials commonly occur wherever ground water is flowing. The most extreme example known is on Adagdak volcano, Adak Island in the Aleutian Chain of Alaska. With extensive rain and snow melt supplying very pure water, 2693 mV was measured between the topographic peak at 645 m and a reference at 15m above sea level. This is explainable solely on the basis of streaming potential and topography by using a streaming potential coefficient of 100 mV/bar (Corwin and Hoover, 1979).

For further discussion of electrokinetic effects, see Bull and Gortner (1932), Toth (1941), Wiley (1951), Bernstein and Scala (1959), DeSilva and Toth (1964), Gay (1967), Lorenz (1969), Bogoslovsky and Ogilvy (1970), Mandel and Edwards (1971), Anderson and Johnson (1976), Zablocki (1976), Corwin et al.(1977, 1979, 1981), Shriever and Bleil (1977), Fitterman (1978, 1979, 1984), Horn (1978), Hulse (1978), Hall (1980), Ishigo and Mizutani (1981), Ucok (1981), Sill (1982, 1983), Warringer and Taylor (1982), Vink (1982), Madden (1983), McConnel (1983), Agarwal (1984), Anderson (1984), Black and Corwin (1984), Cooper and Koester (1984), Corwin (1984), Ishido and Nishizawa (1984), Markiewicz et al.(1984), Ohshima et al.(1984), and Vochten and Goeminne (1984).

The Nerst, redox, and diffusion potentials all have the same form:

$$E = E_o + \frac{RT}{zF} \ln(a_1/a_2) \qquad [84]$$

where RT/F = 0.02569 V at 298.15 K,

and for a redox system

z = number of electrons transferred in a redox reaction

a_1 = activity of oxidizing side of the reaction

a_2 = activity of reducing side

E_o = standard redox potential (tabulated in Dobos, 1975)

The redox potential, E_{red}, is related to the pressure of hydrogen gas, p_{H_2}, and the pH of the solution through

$$E_{red} = -0.029 \log p_{H_2} - 0.058 \text{ pH} \qquad [85]$$

The diffusion potential in a concentration cell with transference of ions is given as

$$E_c = \left(\frac{1}{z} + \frac{\lambda_- - \lambda_+}{\lambda_- + \lambda_+} \right) \frac{RT}{F} \ln(a_1/a_2) \qquad [86]$$

where λ = ionic equivalent conductivity for cations and anions. This potential for a concentrated electrolyte in contact with distilled water (relative to distilled water) is -241 mV for saturated NaCl/water and +84 mV for sulfuric

acid/water. Other examples are tabulated in Dobos (1975).

For further discussion of chemical potentials, see Hulse (1978), Sill (1982, 1983), Corry (1985), Poldini (1938), De Witte (1948), Yungul (1950), Wilckens (1955), Kelly (1957), Sato and Mooney (1960), Meiser (1962), Gast and East (1964), Becker and Telford (1965), Paul (1965), Sato (1966), Smits (1968), Logn and Bolviken (1974), Thomas (1976), Noguchi and Endo (1978), Trasatti (1980), Bhattacharya and Roy (1981), Semenov (1981), Nosal (1982), Burr (1982), Atchuta and Ram Babu (1982), Kilty (1984), Rodriguez (1984), and Steward and Burck (1985).

Water

Pure water is an electrolyte with an electrical conductivity of 5×10^{-6} mho/m and a relative dielectric permittivity of 78 near room temperature at low frequencies. The electrical properties are strongly dependent upon temperature, frequency, impurity chemistry, and physical state, but are relatively independent of pressure in the liquid state below the critical point. In the solid state (ice) and above the critical point or in the gaseous state, the electrical properties of water are strongly pressure dependent. Excellent review discussions of the electrical properties of water include Bockris and Reddy (1970), Hasted (1972), Franks (1972, Quist and Marshall (1968), Wooten (1973), Marshall (1968), Ucok (1979), Akhadov (1980) and Olhoeft (1981).

The electrolytic conductivity of water varies with the concentration of electrolyte according to (Fuoss and Hsia, 1967)

$$\sigma = 0.1\ c\ (B_o - B_1 c^{1/2} + B_2\ c\ \ln c + \ldots) \qquad [87]$$

where

σ = DC conductivity (mho/m)

c = molar concentration of electrolyte

and B_i = coefficients dependent upon the electrolyte (see Table 4).

The conductivity of water depends upon temperature according to the empirical equation (Ucok et al., 1979)

$$\sigma^{-1} = b_o + b_1 T^{-1} + b_2 T + b_3 T^2 + b_4 T^3 \qquad [88]$$

where T is temperature (^oC) and the b_i are coefficients dependent upon the electrolyte. These two equations were combined by Ucok et al. (1979) and fit to experimental data for NaCl, KCl, and $CaCl_2$ brines by three-dimensional regression analysis. The resultant formula predicts the electrical conductivity of salt solutions to within 2% accuracy from 0 to 6 molar (0 to 25 wt%) over the temperature range 25 to 375^oC. Olhoeft (1981) has also analyzed the data of Quist and Marshall (1968) to produce a predictive formula accurate to within 6% for 0.01 m NaCl as a function of temperature from 0 to 800^oC and pressure from 0.5 to 4 kbars. The electrical conductivity of steam is effectively zero, with the conduction in steam-filled rocks being largely due to vapor condensation and surface conduction along pore walls.

Table 4

Electrical Conductivity versus Temperature and Salt Concentration

$$\sigma(T,c) = S_{11} = CBT \quad (mho/m) \qquad [89]$$

from data in Ucok et al. (1979) by three-dimensional linear regression analysis where C and T are matrices with

$C_{11} = c$ (c in molar concentration)
$C_{12} = c^{3/2}$
$C_{13} = c^2 \ln c$

and $T_{11} = 1$
$T_{21} = T^{-1}$
$T_{31} = T$ (T in °C)
$T_{41} = T^2$
$T_{51} = T^3$

and the B_{ij} coefficient matrix for each salt is given as:

NaCl:

3.470	-59.21	0.4551	-9.346×10^{-5}	-1.766×10^{-6}
-6.650	198.1	-0.2058	7.368×10^{-5}	8.768×10^{-7}
2.633	-64.80	0.005799	6.741×10^{-5}	-2.136×10^{-7}

KCl:

5.783	-59.23	0.2051	1.815×10^{-4}	-1.094×10^{-6}
-6.607	149.7	0.1064	-7.037×10^{-4}	1.080×10^{-6}
1.665	-31.21	-0.03418	1.539×10^{-4}	-1.945×10^{-7}

$CaCl_2$:

-34.62	780.3	1.050	-0.002459	9.986×10^{-7}
24.64	-492.3	-0.5922	0.001461	-7.109×10^{-7}
-3.907	64.59	0.06735	-1.216×10^{-4}	-4.731×10^{-9}

The polar water molecule has a very strong orientational (rotational) polarization resulting in a large dielectric permittivity. The polarizaton of an individual water molecule is independent of temperature and pressure (Todheide, 1972), but the dielectric permittivity is polarizability per unit volume and is altered by temperature and pressure as the density of water is changed (just as the dielectric time constant and electrical conductivity vary with changing viscosity). The temperature and frequency dependence of the relative dielectric permittivity is given by Hasted (1972, 1973)

$$K' - iK'' = n^2 + \frac{K_s - K_\infty}{1 + (i\omega\tau_1)^{1-\alpha}} + \frac{K_\infty - n^2}{1 + i\omega\tau_2} \qquad [90]$$

where $n^2 = 1.8$ (independent of temperature)

$$K_s = 295.68 - 1.2283\ T + 2.094\times10^{-3}\ T^2 - 1.41\times10^{-6}\ T^3 \qquad [91]$$

$K_\infty = 4.2$ (relatively independent of temperature)

$\alpha = 0.012$ (independent of temperature)

$$\tau_1 = 5.62\times10^{-15}\ e^{0.188/kT}\ \text{(sec)} \qquad [92]$$

$\tau_2 \sim 4.2\times10^{-14}$ sec

T = temperature (K)

$\omega = 2\pi f$ (f in Hz)

and k = Boltzmann's constant = 8.61735×10^{-5} eV/K.

The relaxation associated with τ_2 is very little understood and its temperature dependence is unknown. The relative dielectric permittivity, K', is effectively K_s for any frequency below several hundred megaHertz. The above formula is valid between freezing and boiling temperatures (273-373 K) and for any frequency below the infrared. At higher temperatures, the principal change occurs in K_s, with Akerlof and Oshry (1950) finding from 373 to 643 K

$$K_s = 5321T^{-1} + 233.76 - 0.9397T + 1.417\times10^{-3}T^2 - 8.292\times10^{-7}T^3 \quad [93]$$

Heger (reported in Todheide, 1972) measured dielectric properties from 373 to 823 K between 0.1 and 5 kbar pressure. Using three-dimensional regression analysis, Olhoeft (1980) found a formula for K_s fitting the data to an accuracy of within 1% for $K_s>20$ and 10% for $K_s<20$.

The dielectric permittivity of ice is given as

$$K' - iK'' = K_\infty + \frac{K_s - K_\infty}{1 + i\omega\tau} \quad [94]$$

$$\text{where } K_s = 3.2 + \frac{20715}{T - 38} \quad \text{(Cole and Worz, 1969)} \quad [95]$$

$$K_\infty = 3.2$$

$$\tau = 4.76 \times 10^{-16}\ e^{0.577/kT} \quad \text{(Camp et al., 1969)} \quad [96]$$

The dielectric permittivity of water is also strongly dependent upon the concentration of impurities (Pottel, 1973; Hasted, 1973). Water molecules have the highest polarizability of any liquid, and any added impurities tend to reduce the volume average polarizability and hence the dielectric permittivity (although colloidal materials tend to increase the apparent polarizability at low frequencies). The relative permittivity of water varies with the concentration of LiCl salt (and similarly for NaCl) according to the formula above for liquid water with

$$K_s = K_s(T) - 13.00\ c + 1.065\ C^2 - 0.03006\ c^3 \quad [97]$$

where $K_s(T)$ is from the formula for pure water above and c is the salt concentration in mole/liter.

$$K_\infty = 4.2 + 0.2145\ c \quad \text{(Hoekstra and Cappillino, 1971)} \quad [98]$$

$$\alpha = 0.0026 + 0.02676\ c - 0.00123\ c^2 + 2.71 \times 10^{-5} c^3 \quad [99]$$

$$\tau = (8.25 - 0.347c) \times 10^{-12} \text{ sec at } T = 298K \quad [100]$$

and the refractive index, n, does not appreciably change with salt concentration. These formulas were derived from linear

regression of data by Gottlob, by Adolph, and others and published in Pottel (1973). Other formulas are discussed in Pottel (1973) and Hasted (1973). The most significant effect of salt is to change K_s and α. For other salt solutions and binary liquids, see Akhadov (1980).

Although mixing laws are explicityly addressed elsewhere, it should be noted here that the mixing of water with any other material produces a composite material with electrical properties unlike the mixture of any two other matierals. Mixtures of most materials tend to produce composite properties somehwere along a geometric mean path between the two end members (see Madden, 1976; Landauer, 1978), and in some cases add properties due to Maxwell-Wagner effects. Mixtures containing water may result in properties very different from any one component through water-mineral interactions such as surface diffusion and corrosion (the basis of induced polarization, Wong, 1979), pore structure interaction (Rangarajan, 1969; Olhoeft, 1977), and colloidal polarization effects (Pethig, 1979; Duhkin, 1971).

In fractional-monolayer quantities, adsorbed water has been studied by a variety of investigators (see review in McIntosh, 1966; Baldwin, 1959; Fripiat et al., 1965; Hoekstra and Doyle, 1971; Clifford, 1975; Kaneko and Inoue, 1979; Fahim et al., 1982; Jenkins and Hartman, 1982; Anastasiou et al., 1983; Tennakone, 1983; White, 1983; Ramdeen et al.,

1984; Clark et al., 1985; Hall et al., 1985). McCafferty and Zettlemoyer (1971) and Zettlemoyer et al.(1975) studied adsorption onto α-Fe_2O_3 powder. Olhoeft (1975) studied sorption on pore walls in basalt. Hall and Rose (1978) studied adsorption by kaolinite clays.

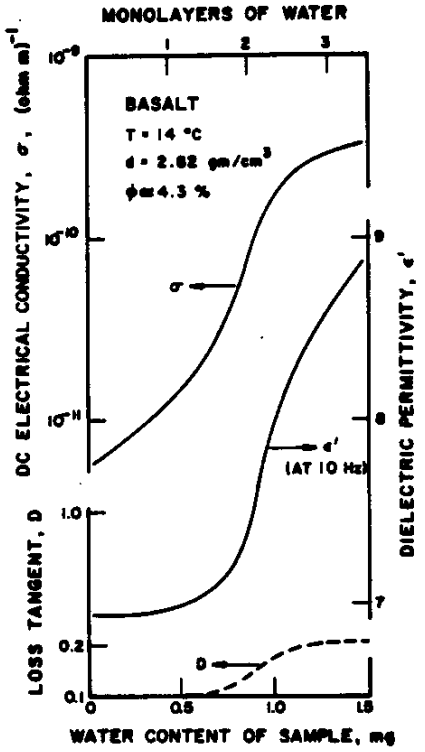

Figure 26 -

Figure 26 (from Olhoeft, 1975) illustrates the typical effect of small amounts of water added to a dry silicate. The DC electrical conductivity does not begin to change until

there is sufficient water adsorbed in the sample to create a connected path from one measurement electrode through the sample to the other (e.g., exceed the percolation threshold; in this case, about 0.002 wt% water or about 20% of a monolayer). At 10 Hz, the dielectric permittivity and loss tangent do not begin to change until more than a full monolayer (about 0.01 wt%) of water has entered the sample, by which time the DC electrical conductivity has increased by an order of magnitude.

The dielectric properties do not change in the first monolayer as the water molecules are strongly bound to the surface and hindered from rotational polarizaton. McCafferty and Zettlemoyer (1971) have estimated the rotation time for water in the first monolayer to be less than 1 second (compared to roughly 10^{-11} sec for free water at room temperature and 10^{-6} sec for ice). With such a reduced rotational polarization, the relative dielectric permittivity is reduced from 78 to about 6 (or roughly the same as the material onto which it is adsorbing). With increasing water content, the rotational freedom of the added water molecules increases with corresponding rises in the time constant and permittivity. By the time roughly seven layers are adsorbed, the additional water behaves as free water. When the sample of Figure 26 has its 4.3% porosity saturated with water, the dielectric properties at high frequencies (above several megaHertz) are barely changed while the lower frequencies show distinctive dispersion or increasing dielectric

permittivity with decreasing frequency. At the same time the DC electrical conductivity has increased by up to 9 orders of magnitude.

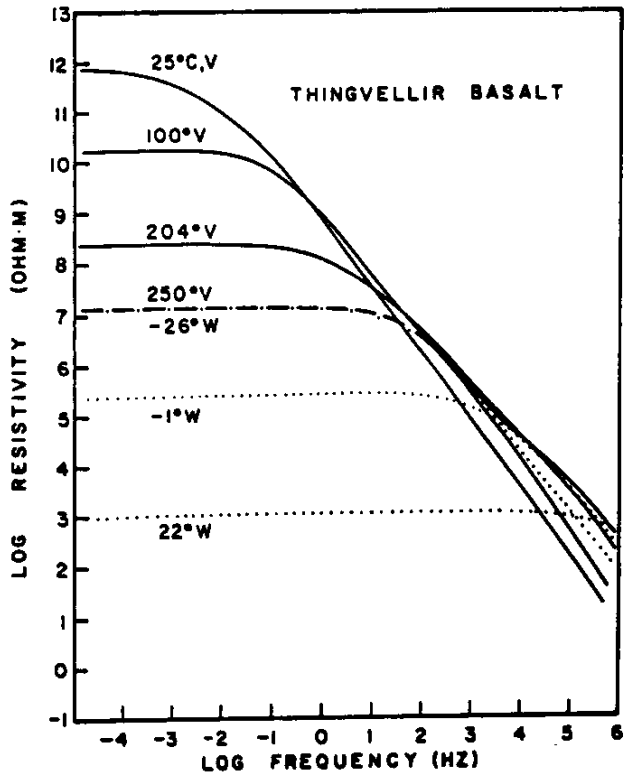

Figure 27 -

Figure 27 compares the temperature dependence of the electrical resistivity of basalt when vacuum dry and when saturated with distilled water. The conduction process dominates in the frequency independent portions of the curves, while the dielectric polarization (displacement currents) dominate in the frequency dependent portions. Note that the 250°C vacuum dry curve is nearly identical to the -26°C water-saturated curve of resistivity versus frequency. It also requires nearly a 250°C temperature

change in the dry sample to equal the change in resistivity of a 50°C temperature change in the wet sample. Also, as the frequency increases, the effects of temperature and water content decrease.

This filling of pores with water to increase conduction and the reduction of water polarizability near solid surfaces are the simplest water-rock interactions and are common in silicates. The next complication arises through chemical reaction between the water and the rock. Very little water-rock chemistry occurs in materials like sandstone while basalts will react with water to grow measurable amounts of zeolite in a month at room temperature (or a few hours above 100°C) and granites rapidly dissolve in water above 200°C. Many sulfides and oxides undergo electrochemical corrosion in contact with water at room temperature, and most high surface-area, high cation-exchange capacity clays and zeolites exhibit strong electrical responses from ion exchange reactions. Some clays and zeolites also act as catalysts for oxidation-reduction rections between water and other materials, and these catalytic effects appear to accelerate with clays in the presence of organic compounds (Eltantawy and Arnold, 1973; Fripiat and Cruz-Cumplido, 1974; Tan, 1975; Poutsma, 1976; Johns, 1979; Trasatti, 1980; Elenkova and Kostadinova, 1981; Kinoshita, 1982; Ovcharenko, 1982; Appleby, 1983; Birkett et al., 1983; Freund and Spiro, 1983). Further, the electrical double layers surrounding

clay particles may be larger than the physical clay particle size, thus leading to cooperative electrical behavior as the double layers overlap. Most of these water-rock interactions will participate in electrical transport or polarization mechanisms and thus be observable through measurements of electrical properties (see review in Olhoeft, 1985). One example discussed earlier was the effect of surface conduction along pore walls in water saturated basalt.

To adequately model this behavior, an additional circuit element must be added to those discussed earlier -- the diffusion-limited Warburg impedance. These diffiusion mechansims usually are observed with a square-root frequency dependence, giving rise to a similar frequency dependence in the Warburg model. However, the Warburg impedance is a special case of a more general interfacial impedance involving both activation and diffusion through the distributed impedance characteristic of porous or particulate elements (see excellent discussion in Rangarajan, 1969; Sluyters-Rehbach and Sluyters, 1970, 1984). The Warburg impedance may be added to the earlier circuit representation of a rock and also distributed to generalize the model and include water-rock interfacial impedances. This will be discussed in the modelling section.

In the Figure 28, experimental data and electrochemical models are used to show the relationship between particle

size and time constant in diffusion-limited systems (discussion under modelling). The models may be shifted about an order of magnitude to right or left depending upon the parameters chosen, but the slope may not be changed. Very similar results have been found in porous systems by Rangarajan (1969). The dotted line is given by

$$\text{time constant} = \frac{a^2}{3.4\times10^{-6}} \qquad [101]$$

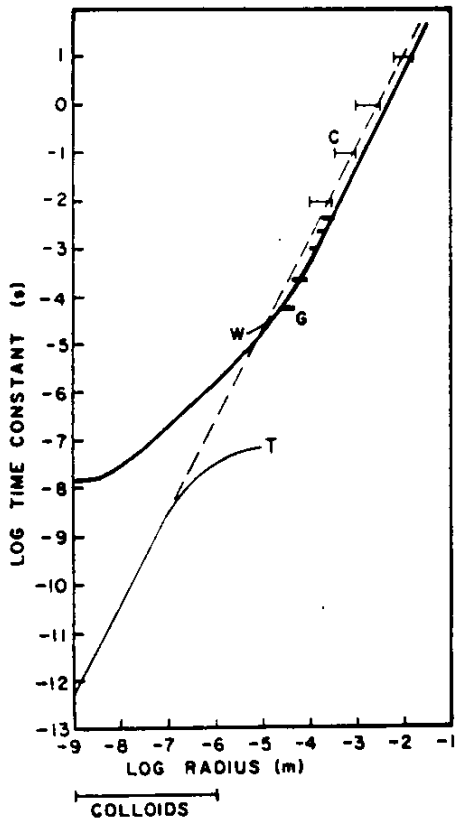

C = Collett (1959) data

G = Grissemann (1971) data after Pelton (1977)

W = Wong (1979) model

T = Trukhin (1962) model

Figure 28

Clay particles commonly exist as small as 2×10^{-8}m (Grim,

1968) with the thickness of the electrical double layer roughly 10^{-9}m. Disseminated sulfide particles range from 10^{-4}m up until they merge with massive and veined sulfides on the order of 10^{-1}m and larger. Paramagnetic oxide particles also exist down into the 10^{-9}m range. As the earth also has large faults and fractures running down to common pore structures in the 10^{-6}m and microcracks in the 10^{-9}m range, it should be apparent that both particle size distributions and pore size distributions will tend to produce very broad distributions of time constants in electrical properties.

Figures 29 and 30 illustrate the complex resistivity spectra of a pyrite-bearing shale from Tiger-Government 2-22 oil well at T37N R78W in Wyoming. Figure 29 is the sample measured "as received" while Figure 30 is the same sample saturated with distilled water. Note that the resistivity changes dramatically, but the phase angle is relatively unchanged. Further, the water saturated sample has a much higher chemical reactivity as evidenced in the increased electrial nonlinearity (higher total harmonic distortion, THD). Further discussion of nonlinearity will come later.

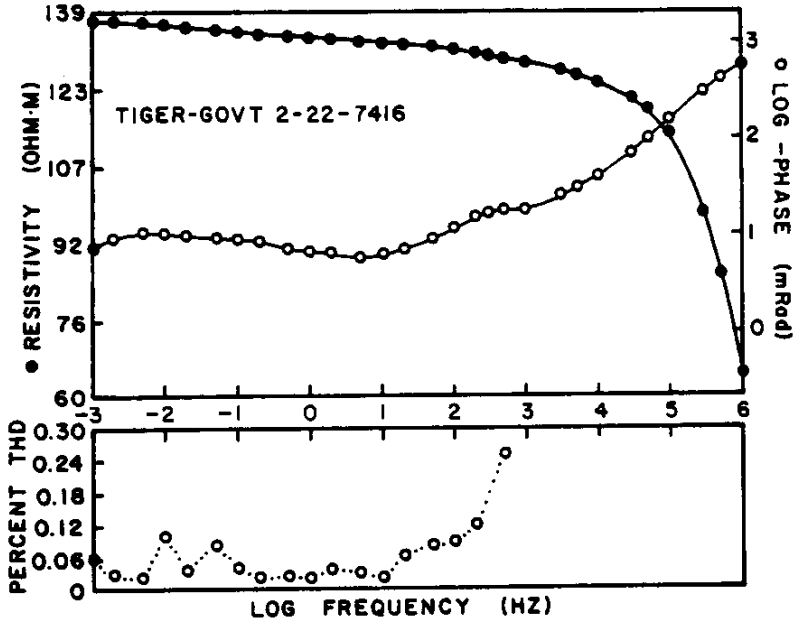

Figure 29 - Measured "as received".

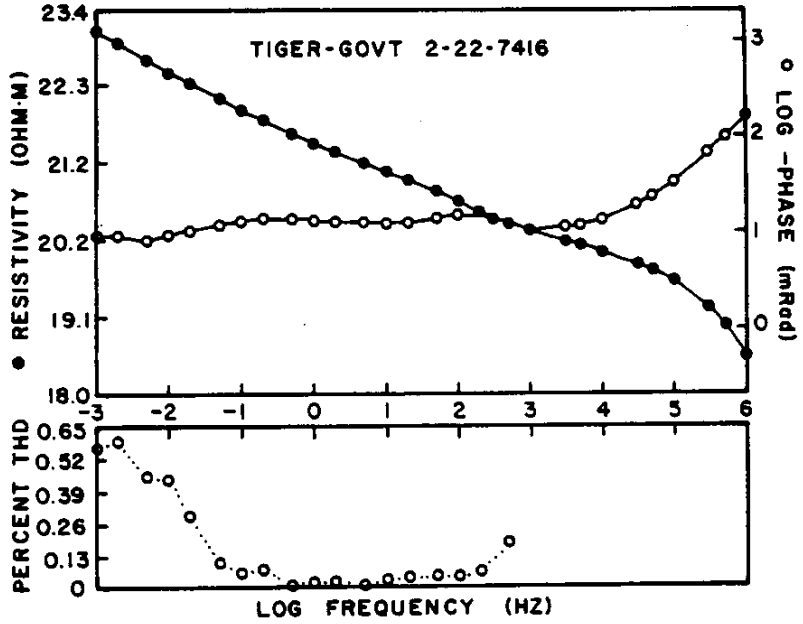

Figure 30 - Measured saturated with distilled water.

For consistancy, all of the following figures are samples measured water saturated in 0.001m KCl solution at a current density of 100 A/m2. Figure 31 illustrates the electrical

properties of the simplest type -- a clean, barren sandstone (e.g., no clay or mineralization). This sandstone 15C263 has 9.2% porosity and is from the Shinarump member of the Chinle Formation near White Canyon, Utah. At low frequencies it

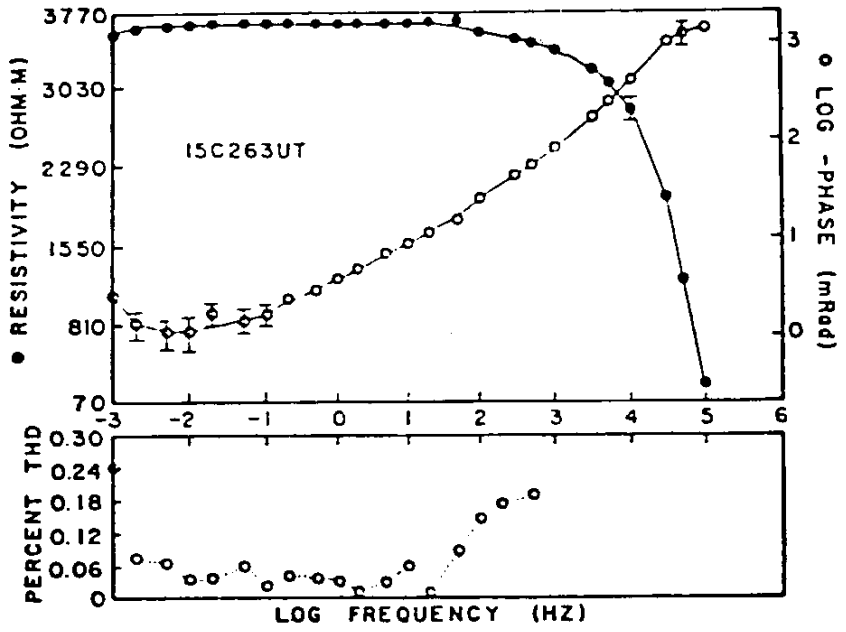

Figure 31 -

shows the characteristic frequency independent resistivity due to domination by the DC conduction (current flowing through the volume conduction of the pore water). At high frequencies, it becomes nearly a pure dielectric (the transition is not entirely sharp due to small Maxwell-Wagner effects from the pore stucture). The phase angle parallels the resistivity with a very small phase angle characteristic of conduction at low frequencies and the $-\pi/2$ radians of a dielectric at high frequencies. Note that the THD is very low, indicative of a linear electrical response with no

evidence of any chemical reactions between the water and the rock.

In contrast, the Figure 32 is the electrical spectra of a sandstone containing both clays and minerals from the Powder River Basin near Pumpkin Buttes, Wyoming with 37.3% porosity. Note the two distinctive relaxations ("bumps" in the phase spectrum) near 0.003 Hz and 3 Hz and the corresponding nonlinear THD. Below 0.001 Hz, the conduction through water-filled pores is dominant. Between 0.001 and 0.1 Hz, the cation exchange reaction of the clays (and surface conduction) is dominant. From 0.1 Hz to 1 kHz, the oxidation-reduction reaction of sulfide and oxide minerals with water is dominant. Above 1 kHz, the sample rapidly turns into a dielectric. A more detailed discussion will come later under modelling.

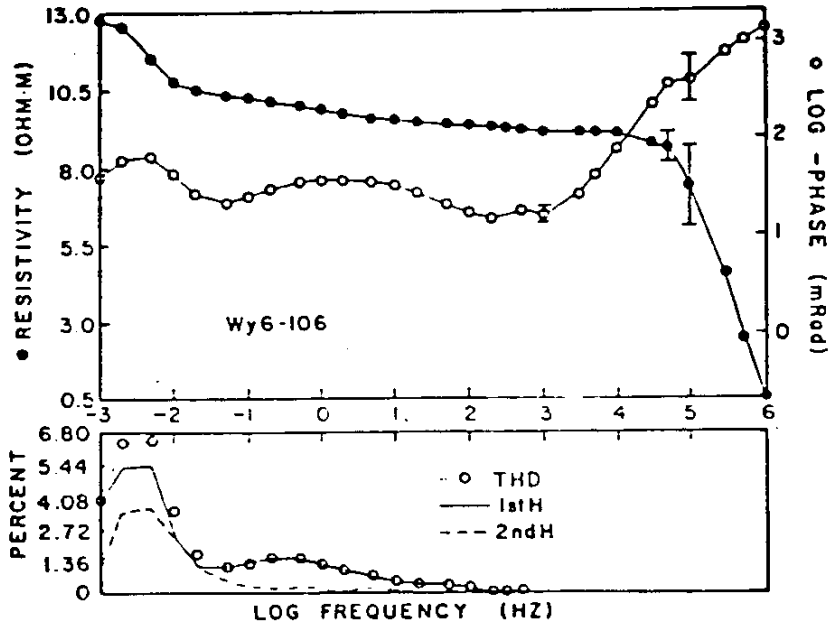

Figure 32 -

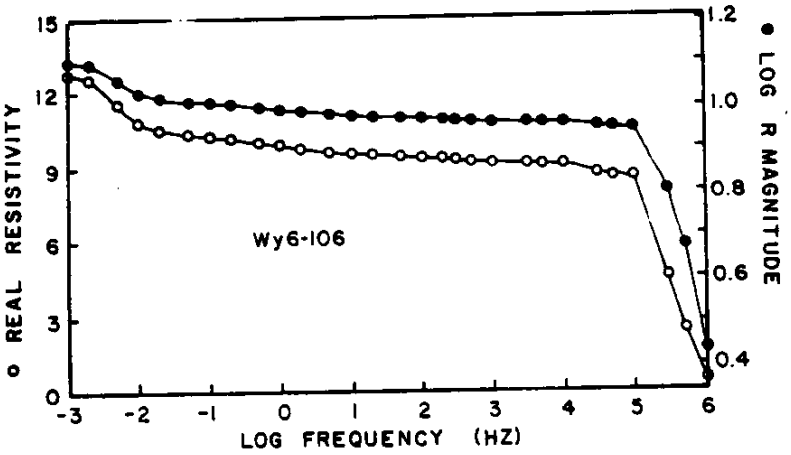

Figure 33 -

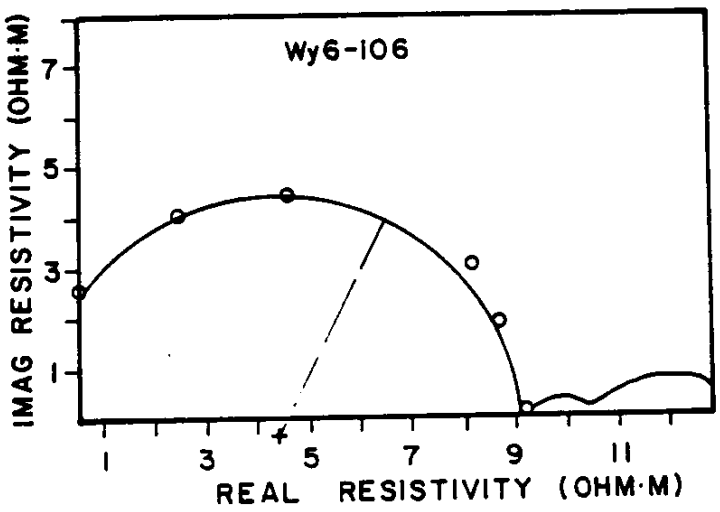

Figure 34 -

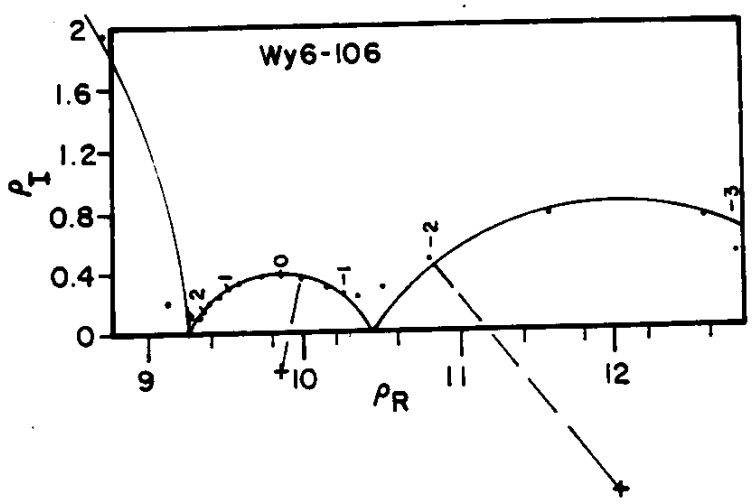

Figure 35-

The next three figures show alternative presentations of the same data. Figure 33 illustrates the difference between plotting the linear real part of the complex resistivity or the log magnitude of the resistivity versus log frequency. Figures 34 and 35 plot two Argand diagrams of imaginary versus real resistivity. Figure 34 plots all of the data as shown above. Figure 35 expands the lower right corner of Figure 34 in order to better see the detail of the sulfide and clay responses (numbers along data curves are log frequency).

Figure 36 illustrates the complex resistivity spectra of a Hawaiian basalt from Kilauea Caldera with 11.3% porosity. This sample is also linear like the sandstone 15C263 above, but notice the more gradual transition from a conductor to a

dielectric with increasing frequency and the higher phase angle in the 10 Hz region due to the greater tendency for basalt to interact with water than exhibited by sandstone.

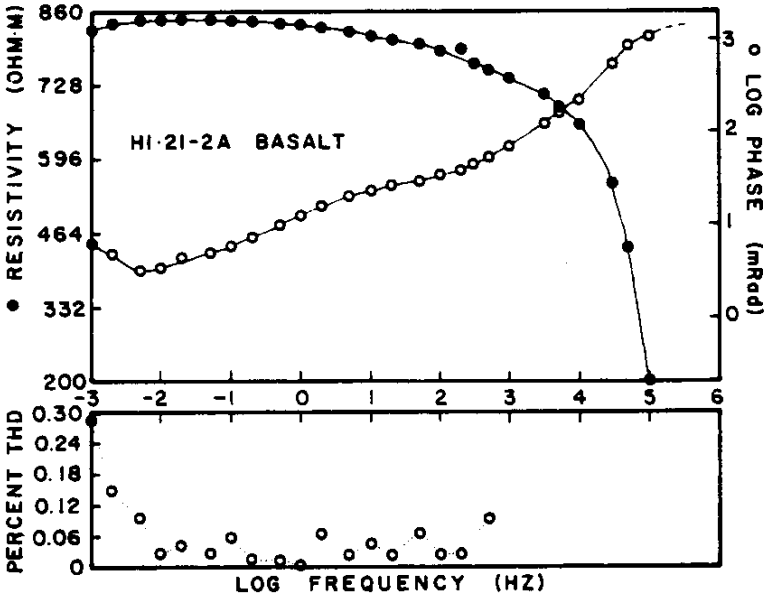

Figure 36

For comparison, the Figure 37 is the specra of a 0.7% porosity granite from Westerly, Rhode Island. The dashed region near 10 Hz is where the impedance-frequency product of the sample exceeds the measurement capability of the instrumentation. Note that the very low porosity and resulting very high resistivity cause the conductor to dielectric transition to occur at much lower frequencies than in previous examples. This granite is a dielectric above 10^2 Hz, while the sandstones earlier are not dielectrics until above 10^4 Hz. The relatively high phase angle at very low frequencies is caused by water-rock interaction, and

values of -15 to -20 milliradians are typical of high resistivity, high quartz materials.

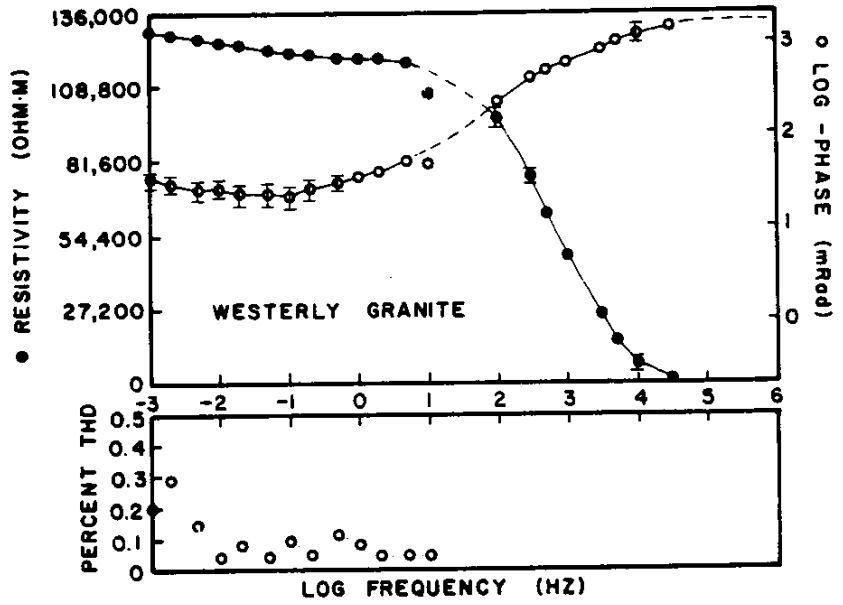

Figure 37

Figure 38 illustrates the electrical specra of another extremely high resistivity material -- a graphite schist from the Dixon Schist near Ticonderoga, Essex County, New York with less than 0.01% porosity. Like the granite above, the schist becomes a dielectric above 10^2 Hz. Unlike the granite, the schist is extremely nonlinear (very high THD) and has an anomalously high phase angle (-172 mRad) at low frequencies. Both are caused by the presence of graphite. Further, note that this sample has a phase response which is independent of frequency from 0.001 to 10 Hz. This could be caused by a uniform, continuous distribution of reactive particles below 1 mm size, but it is generally recognized to

be a characteristic of the electrochemical response of graphite. Thus, while all of the other materials discussed here have become dominantly controlled by pore water conduction at low frequencies, graphite-containing materials are controlled by the electrochemistry of the graphite-water interface.

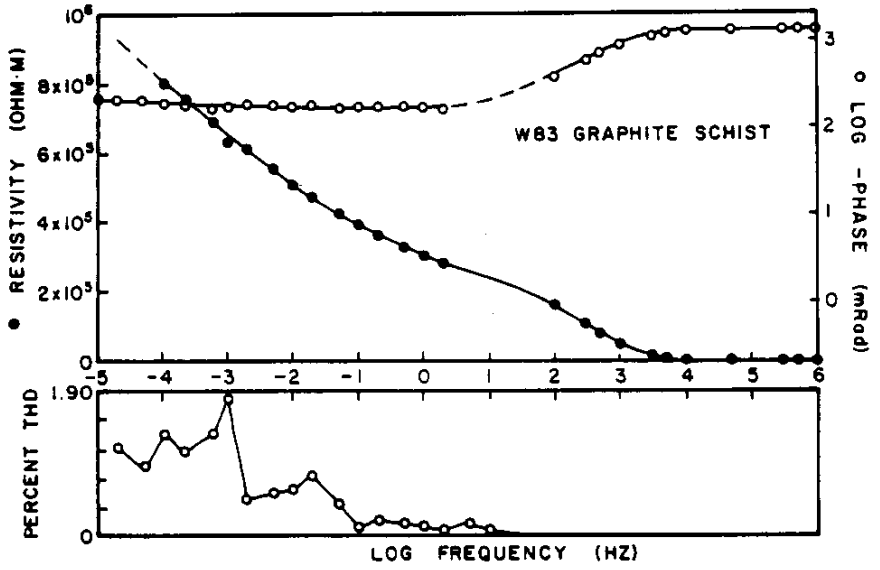

Figure 38 -

All of the preceding examples are of fairly common electrical proerties and materials. The next few are relatively rare at present, but may become more common as more careful field measurements are acquired. Figure 39 illustrates the electrical specra of a sandstone with carbonaceous siltstone and shale from Baggs, Wyoming. It has a porosity of 17% and was measured with its natural water

content intact (preserved by heat sealing in a plastic bag in the field). This unusual response is caused by fine-scale lamination of sandstone, shale, and silt with carbon and clay. The high phase angle and high THD are indicative of electrochemical water-rock interaction with the carbon minerals and shale, but the very strong frequency response around 1 Hz is mainly the result of Maxwell-Wagner effects due to the laminations (e.g., a geometric effect). The presence of clay prevents the material from becoming a true dielectric even at the highest measured frequencies.

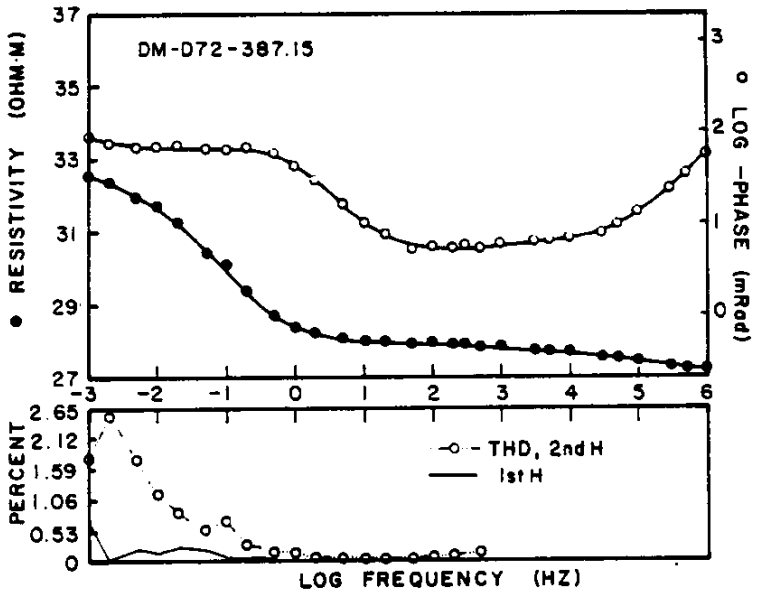

Figure 39 -

Figures 40 and 41 illustrate the electrical propertiees of an Hectorite clay as a complex resistivity spectra and as an Argand diagram. The sample is Clay Minerals Society

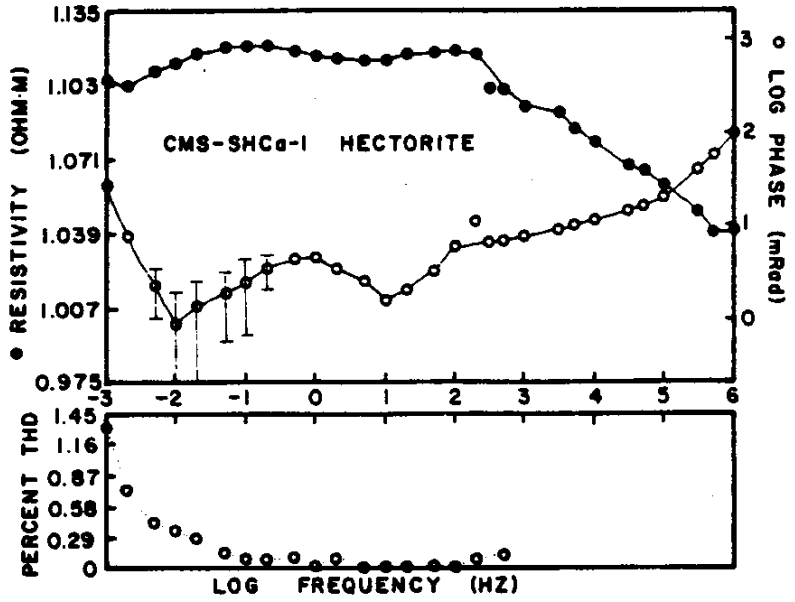

Figure 40

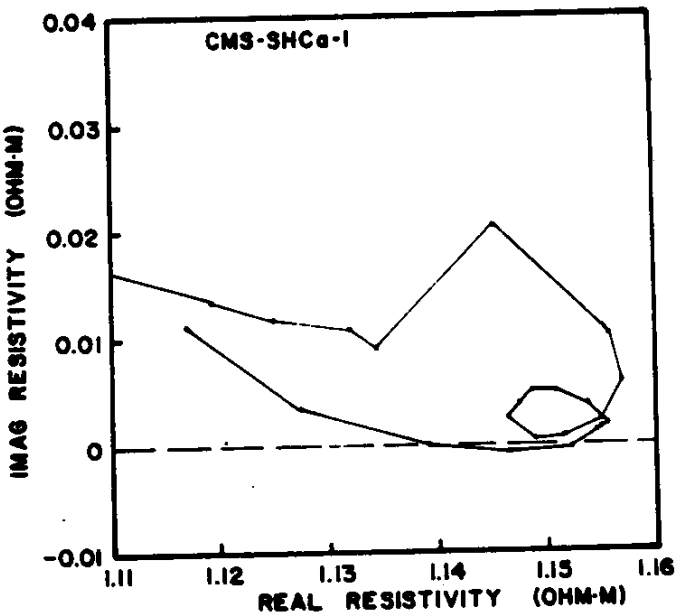

Figure 41 -

standard clay SHCa-1 in a 3:1 mixture of 0.1 m KCl:dry clay

by weight (van Olphen and Fripiat, 1979). Though other materials have been observed to have such unusual electrical properties (Archer and Armstrong, 1980), there is no known explanation for their occurrence.

Figure 42 shows the spectra of an even more unusual type. It is representative of several core materials from oil wells that were provided to the author by oil companies. Unfortunately, the oil companies allowed the samples to be measured only for their electrical properties before returning them. Thus, the mechanisms of many of the observed properties are unknown.

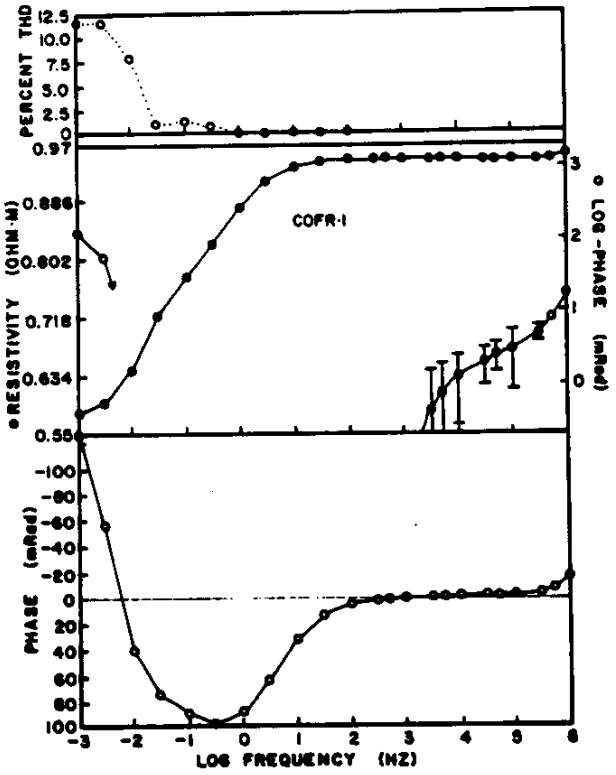

Figure 42 -

However, the very strong negative induced polarization (positive phase angles) of the above materials are also seen

in many clays and in other materials which are very sensitive and reactive to the addition of water (some coals, and "fresh" anhydrous dacite from Mt.St. Helen's eruptive domes). Thus the spectra from the oil core may be related to non-aqueous clay-organic reaction, or to catalytic activity of clays in the presence of organics (Fripiat and Cruz-Cumplido, 1974; Johns, 1979; Ovcharenko, 1982; Elenkova and Kostadinova, 1981; Appleby, 1983; Birkett et al., 1983; Olhoeft, 1985).

Figures 43 and 44 illustrate two typical clay spectra. Figure 43 is an API Standard Clay Mineral number 31 Bentonite from Cameron, Arizona measured as a 1:1 ratio of 0.1 m KCl: dry clay by weight. Figure 44 is API no.7 Kaolinite from Bath, South Carolina measured as a 1:2 ratio of 0.1 m KCl: dry clay by weight. Note that both samples are not dielectrics at the highest frequency measured (1 MHz), and that both samples have reversals in the resistivity curves at low frequencies. These reversals are indicative of nonlinearity as the Hilbert transform is violated (see nonlinear discussion below). Only the bentonite also shows the more conventional total harmonic distortion nonlinearity.

The bentonite example is typical of most smectites, montmorillonites, and other high cation exchange capacity materials. The kaolinite example is typical of low cation exchange capacity materials, and also of modern peptized (or "beneficiated") drilling muds.

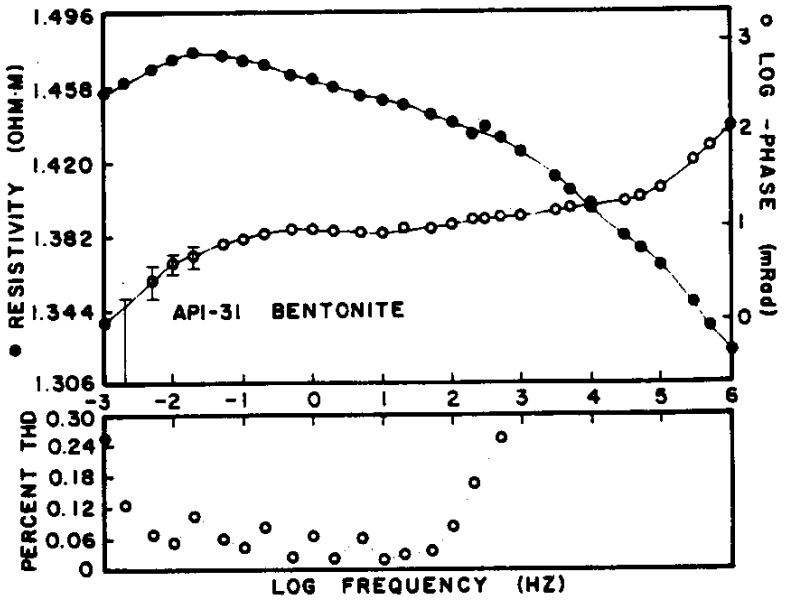

Figure 43

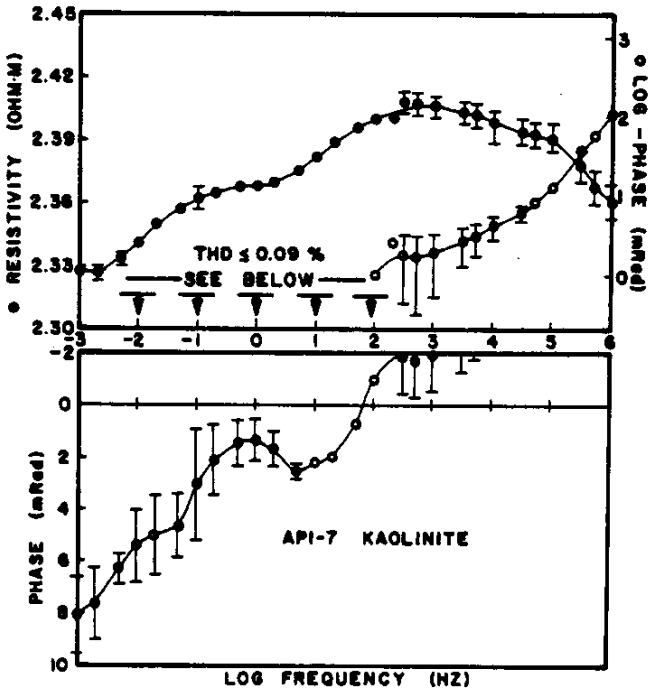

Figure 44

The primary difference between the two clay examples is

the cation exchange capacity (5.1 meq/100g for kaolinite versus 77.0 meq/100g for bentonite; Lewis, 1950). Although there have been reports of a correlation between cation exchange capacity and specific surface area (Patchett, 1975), the electrical properties only appear to "see" the cation exchange capacity. High surface area materials like sepiolite clay (392 m^2/g) but with low exchange capacity (3-15 meq/100g; Grim, 1968) have electrical properties like kaolinite. High cation exchange capacity materials like synthetic cation exchange resins (up to 400 meq/100g) but with low surface areas have electrical properties like the bentonite shown.

Table 5

Surface Area and Cation Exchange Capacity of Various Materials

Material	Surface area m^2/g	Cation Exchange meq/100g	Anion Exchange meq/100g
silica	300-973	10-400	-
zeolites	-	100-620	-
organic matter	10-260	130-350	-
vermicullite	-	100-150	4
montmorillonite	82-767	29-126	23-41
saponite	-	70	21
nontronite	72	60	12-20
halloysite ($4H_2O$)	43	40-50	-
chlorite	42	4-47	-
illite	97-113	10-40	-
palygorskite	-	20-30	-
various soils	-	4-25	-
glauconite	-	11-20	-
attapulgite	140	18	-
sepiolite	392	3-15	-
kaolinite	15-23	3-15	7-20
halloysite ($2H_2O$)	43	5-10	-
pyrophyllite	-	4	-
basalt	0.35	0.5	-
fine sand	1-5	0.8	-

Compiled from the following sources: Almon (1979), Barrer (1978), Grim (1968), Grim and Guven (1978), Lerman (1979), Olhoeft (1975), Unger (1979), van Olphen (1977), and Worthington (1973).

Measurements

There are two natural divisions in the measurement of electrical properties -- the first is a division in frequency at 10^6 Hz, above and below which frequency different sample holders and instrumentation are required. The second is a division in impedance below 10^6 Hz at 10^6 ohms, above and below which impedance different sample holders may be required and different instrumentation is required. Figure 45 outlines in frequency and impedance some of the commerical techniques currently available to measure electrical properties.

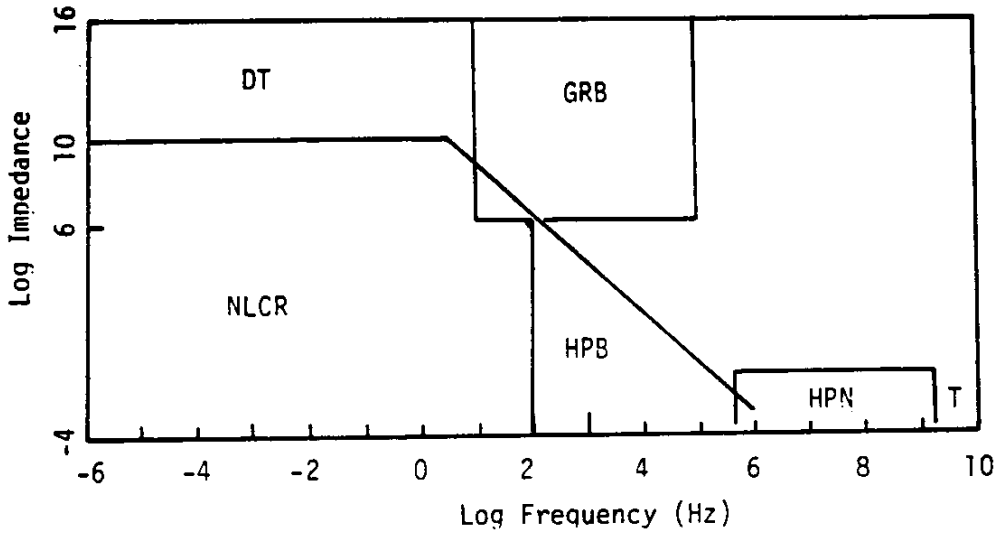

Figure 45 -

DT is a Guildline 9520 digital teraohmeter used in the time-charging mode (or any good electrometer). NLCR is the nonlinear complex resistiviity system described in Olhoeft (1979, 1985). GRB is a General Radio 1620 digital capacitance bridge. HPB is two Hewlett-Packard 4274 and 4275 digital LCR meters. HPN is a Hewlett-Packard 8507 network analyzer system. T is a wide variety of equipment including GR-900 slotted lines, Tektronix time domain reflectometers, and microwave network analyzers from several manufacturers. Other techniques such as resonant cavities, interferometers, and so forth are available, but are usually best suited for very specialized applications. The techniques listed in the figure above are most useful to studying rocks and will be discussed in detail.

Low Frequency Dielectric Measurements

The first technique is the measurement of dielectrics in the DT and GRB regions of the above chart. As dielectric measurements are among the best documented (von Hippel, 1954; Hill et al., 1969) and standardized (see Scheiber, 1960; Charles et al., 1966; and publications of the IEC and the ASTM Standard Tests D150-170 and related), there will only be a quick review here. Figure 46 shows typical dielectric measurement cells for solids (left) and liquids (right).

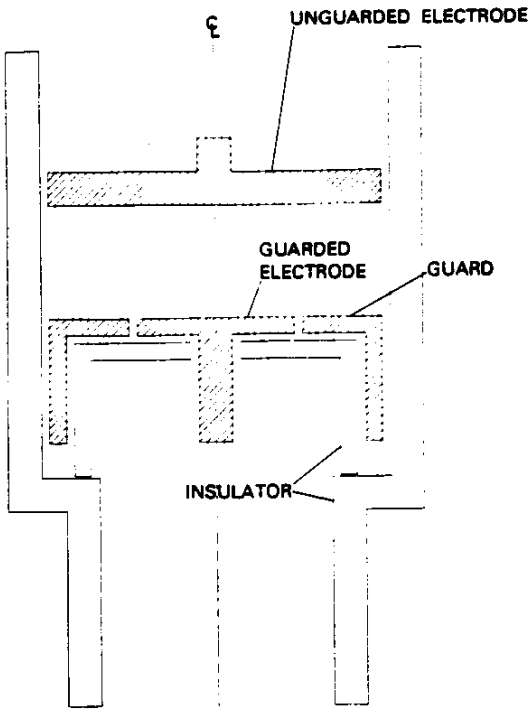

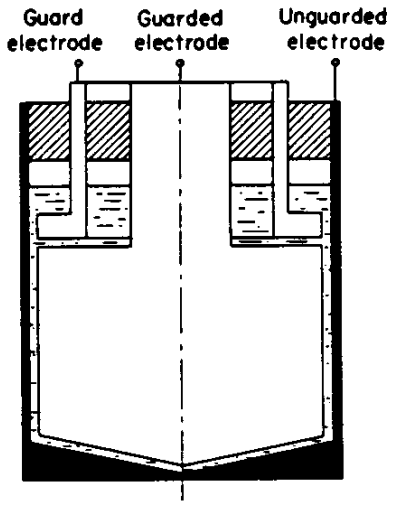

Figure 46 -

Both sample holders employ three terminals or electrodes. The measurement is performed between the guarded electrode and the unguarded electrode. When the bridge is balanced, the guard and guarded electodes are at the same potential. This prevents current from leaking around the sample (through the sample holder or via surface conduction on the sample) and eliminates complications from fringing fields, stray capacitance and cable effects. The best single description of the use of such sample holders is in General Radio application note EID-11. Samples for use in these holders should be thin disks.

Figure 47 illustrates the use of a three-terminal sample holder to measure the dielectric permittivity and loss of a material. The sample holder is first measured without a

sample, acquiring the capacitance, C_F, and loss tangent, D_F, of air with the electrode separation set to the same distance as the sample thickness. The sample thickness should be less than 20% of the sample diameter.

Next, the sample is placed in the sample holder with the same electrode separation as the first measurement, and the capacitance, C_1, and loss tangent, D_1, of the specimen are measured. If the capacitance bridge is well built, the air loss tangent will be zero, $D_F = 0$, otherwise the measured value of D_F will be that of the bridge's internal losses. If D_F is zero, the following formulas yield the relative dielectric permittivity and loss tangent for the sample:

$$K' = \frac{C_1}{C_F} \qquad [102]$$

$$D = D_1$$

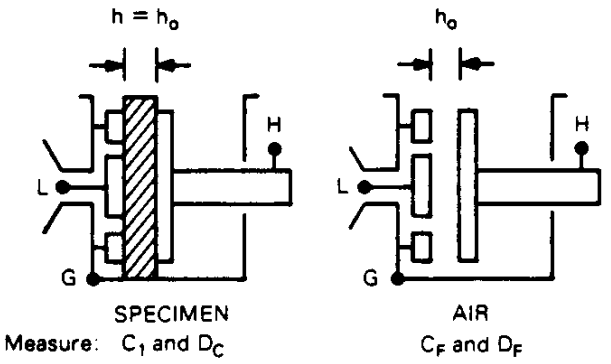

Figure 47

The above method can have a complication if the metal electrodes of the sample holder cause a contact polarization when they touch the sample or if there is a material, such as water, which will adsorb onto the electrodes to create an interfacial polarization. In such situations, C_1 and D_1

will be in error by the amount of the interfacial impedance and polarization in series with the sample. To avoid the problem of contact polarization, the air-gap method is used as outlined in Figure 48. This method requires an accurate knowledge of the separation of the electrodes and of the thickness of the specimen.

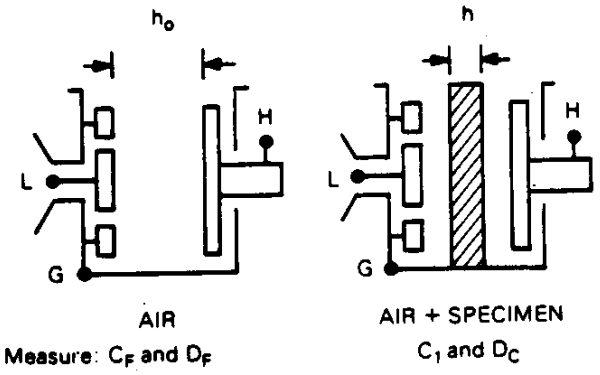

Figure 48 -

$$K' = \left(1 - \frac{(C_1 - C_F)}{C_1} \frac{h_o}{h}\right)^{-1} \qquad [103]$$

$$D = D_C + \left(\frac{h_o}{h} - 1\right) K' (D_C - D_F)$$

In many situations, the sample thickness is not known or cannot be accurately determined (such as with a

rough-surfaced specimen). In such situations, the two-fluid method is used as outlined in Figure 49.

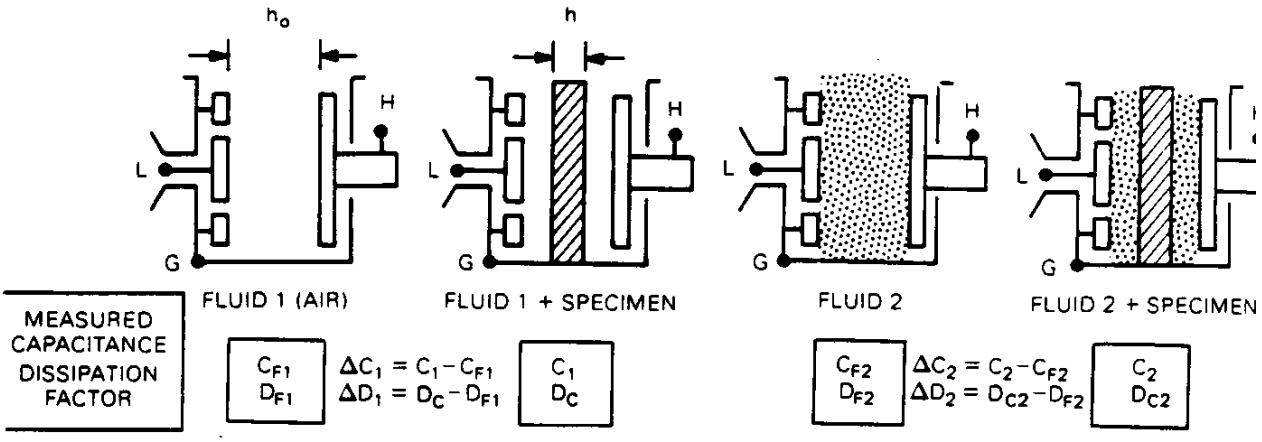

Figure 49 -

This results in the solution for sample relative dielectric permittivity, loss tangent, and thickness:

$$K' = K'_{F1} + \frac{C_2(C_1 - C_{E1})(K'_{E2} - K''_{E1})}{C_2(C_1 - C_{F1}) - C_1(C_2 - C_{F2})}$$

$$D = D_{C2} + \frac{K'(C_{E1}/K'_{E1})}{C_2 - C_{F2}}(D_{C2} - D_{F2}) \qquad [104]$$

$$\frac{h}{h_o} = \frac{C_{E2} - (C_{E1}C_{E2}/C_1) - C_{E1} + (C_{E1}C_{E2}/C_2)}{C_{F2} - C_{F1}}$$

One of the two fluids may be air, and the other should be a stable compound that does not react chemically with the

sample or the sample holder (such as dimethyl siloxane). Since the largest error in measuring dielectric permittivity lies in the measurement of the sample thickness, the two-fluid method is preferred. In such cases, accuracies as high as 0.005% are achievable.

Low Frequency Complex Resistivity Measurements

In dealing with water-saturated samples, the dielectric bridge methods do not work; first, because the impedance is usually lower than most bridges can measure, and second, because water is highly reactive and produces interfacial polarizations at the electrodes and the sample. There are methods to correct for these polarizations, but the simplest technique is to construct a measurement system that does not include the polarizations in the measurement process. This can be done by using a four-terminal sample holder.

Figure 50 outlines some of the problems in measuring the electrical properties of a wet sample. The complex impedance of the sample is determined from the transfer function relating the electric field, E, and the current density, J. These should be related to the voltage drop across the sample due to the volume current flow through the sample, V.

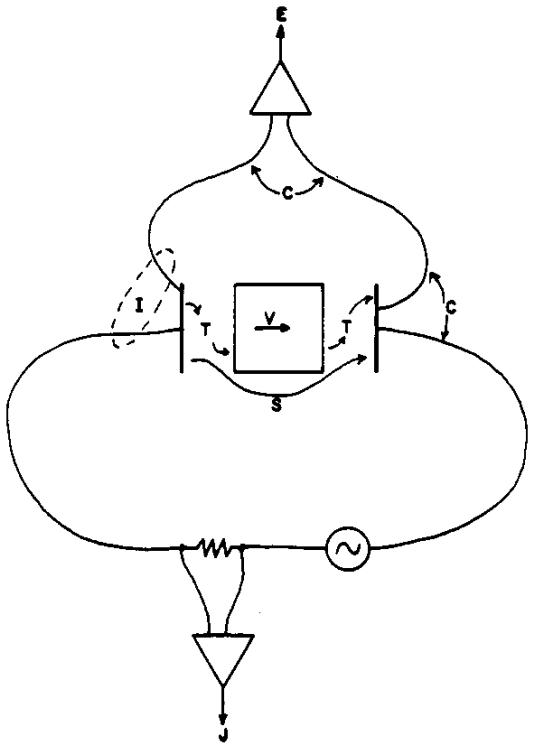

Figure 50

However, there are errors caused by inductive, I, and capacitative, C, coupling between the leads; leakage currents around the sample (either by surface conduction on the sample or through the sample holder), S; and charge transfer impedances, T, caused by the interfacial polarizations at the electrode-water boundary.

The leakage currents, S, can be eliminated by proper sample holder design or by potting the sample. The inductive and capacitative coupling can be eliminated by proper shielding techniques (including the use of driven shields) or may be removed mathematically (see below). The transfer impedances can be removed by separating the electrodes that inject current into the sample (where the interfacial impedance occurs) from the electrodes that acquire the

voltage drop across the sample. If the measurement apparatus has a low noise current (so as to not inject crrent into the voltage-drop measurement circuit) and a high input impedance (so as to not draw current through the voltage-drop electrodes), the transfer interfacial impedance will be bypassed and not cause an erroneous sample impedance to be computed.

A four-terminal sample holder for use with potted samples, water-saturated at room temperature and pressure is shown in Figure 51.

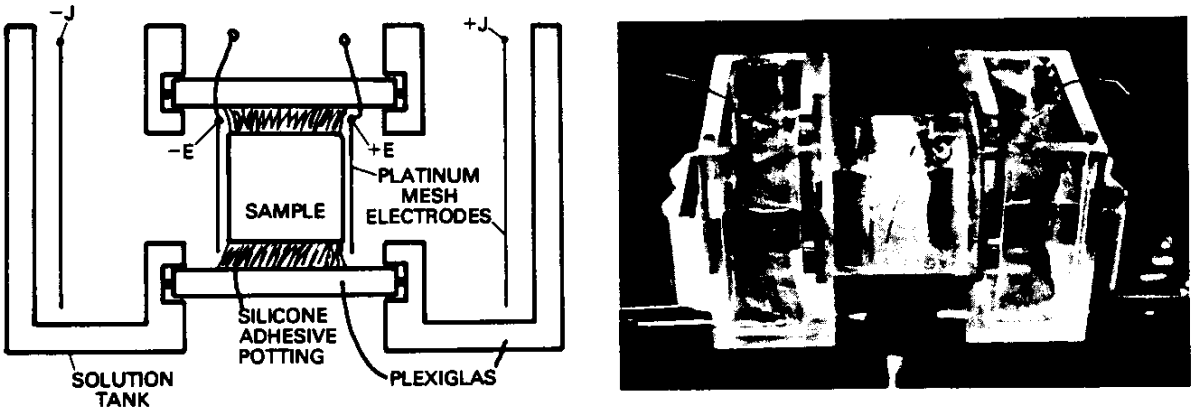

Figure 51

The samples are potted in silicone adhesive which adheres to most rocks and minerals readily and cures in about 48-hours in a high humidity environent. Some epoxies and other compounds do not work well as they do not completely cure, or

the curing process generates an electrical signal, or they do not adhere to rocks and minerals, or they shrink unacceptably. Some plastics and polymers are electrically conductive, thus producing unacceptable leakage currents.

The platinum mesh electrodes are bright platinum as experience has shown that platinized (black) platinum is easily contaminated, is hard to clean, and degrades with time. Bright platinum is easily cleaned in hydroflouric acid, and is readily obtainable in pure quantities (thermocouple grade). The platinum mesh electrodes used to measure the voltage drop across the sample may have platinum wire electrodes substituted if the face of the sample is homogeneous. In either case, the voltage drop electrodes, +E and -E, cannot be allowed to touch the face of the sample or contact polarizations may occur. However, they must be close to the sample to minimize the voltage drop in the solution between the electrode and the sample. Platinum is not the ideal electrode material as it is slightly polarizable in aqueous solution (Sarmousakis and Prager, 1957; Olhoeft, 1985); however, of the available materials, it is the best compromise (silver/silver chloride is better if silver and chloride ion contamination are not problems).

The materials that the sample holder are constructed from must be insulators and they must be chemically inert and not easily charged. Teflon and its relatives are ideal (though expensive). The holder shown in Figure 51 is made from plexiglas, and works acceptably, but nylon is

unacceptable as it accumulates and holds a charge (thus becoming polarized). A disadvantage of the sample holder shown in Figure 51 is that the sample must be potted, which is time consuming, and the sample must be sufficiently well-consolidated to survive the potting process.

Figure 52 illustrates a sample holder that does not require potting and may hold unconsolidated materials. The sample, S, is placed inside a flexible, insulating sleeve such as vinyl or Kalrez (teflon is unacceptable as it does not make a good seal to rocks). Pressure is applied, L, to the ends of the sample holder to seal the sleeve against the walls of the holder. Confining pressure, P_c, squeezes the sleeve to make a seal against the sample and may be used to change the pore volume of the sample. Pore pressures, P_1 and P_2, are used to flow aqueous solutions though the sample for streaming potential or hydraulic conductivity measurements. The stainless steel ends are used as +J and -J current electrodes (they should be platinum plated or they will corrode).

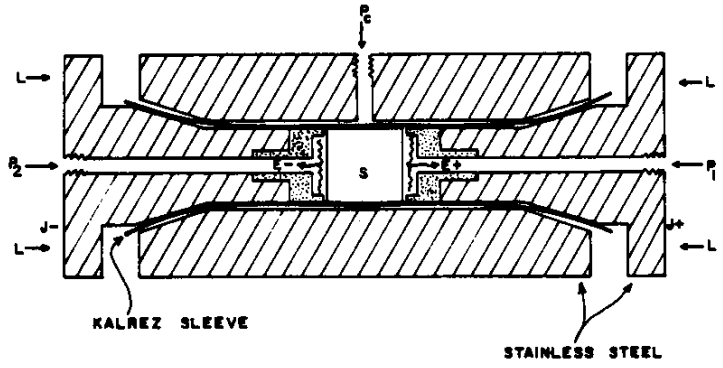

Figure 52 -

Many samples are very unconsolidated and will not even survive the sample holder above. In these situations, the sample is simply poured into a sample holder as in the Figure 53. Surface conduction cannot be eliminated, but then it is probably an important part of electrical conduction in unconsolidated materials and should not be eliminated. When the sample holder is used with materials that contain no metallic or semiconducting oxides or sulfides, the voltage-drop electrodes may touch the sample without adverse effects (as in clean sandstone). When metallic minerals and some clays are present, the voltage-drop electrodes must be isolated from the sample to prevent contact polarization effects. This is illustrated in the drawing by the use of

porous teflon membranes as isolators. In the photograph, it is shown by additional sections of sample holder that are filled with an inert paste made from 0.1 m KCl and fumed silica (Cab-O-Sil or Aer-O-Gel).

Thus, from top to bottom in the photograph, the sample holder is made of an end cap, platinum mesh current electrode, solution reservoir, platinum mesh voltage drop electrode, isolator ring filled with paste, sample ring, isolator ring, platinum mesh voltage drop electrode, solution reservoir, platinum mesh current electrode, and an end cap. All materials are teflon, and the clamp to hold the assembly together is shown in the background. For samples that are to be measured only partially water saturated, the isolator rings and solution reservoirs are filled with fumed silica paste with the appropriate water content. As the paste isolator rings are in the voltage drop circuit, the system must be calibrated to measure and remove the impedance between the voltage drop electrodes and the sample.

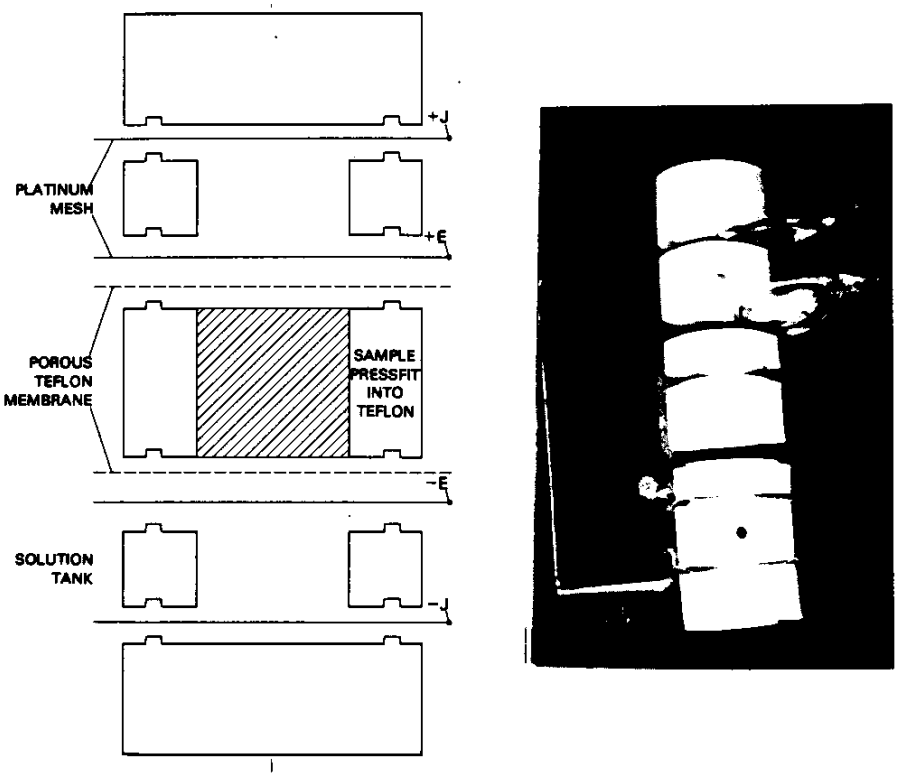

Figure 53

This is simply performed by measuring the sample holder with the two isolator rings shorted together without the sample. The result is then subtracted from later measurements with the sample.

The electronic measurement apparatus to be connected to these sample holders must be linear and capable of measuring the impedance and frequency range of the samples with sufficient accuracy to allow the corrections for residual inductive and capacitative cable coupling (assuming most coupling to have been eliminated by proper shileding). Figure 54 illustrates such a system.

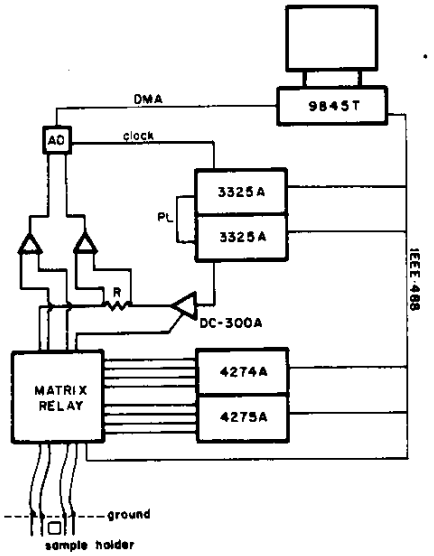

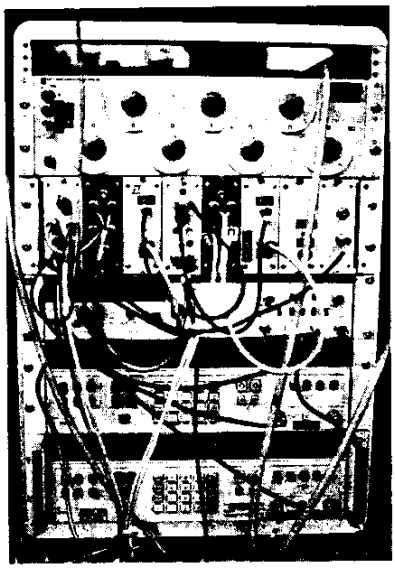

Figure 54 -

The block diagram on the left outlines the system. From 10^2 to 10^5 Hz and overlapping from 10^4 to 10^6 Hz, measurements are performed by Hewlett Packard 4274 and 4275 digital LCR meters under control of the HP9845 computer. The 4275 is capable of measuring to 10^7 Hz if the total cable length from the instrument to the sample holder is under 1 meter. These instruments are first calibrated with an open and a short at their front panels, then again with an open and a short at the sample holder to remove cable effects. The next two pages illustrate the conversions from instrument measured quantities to impedances and corrections for inductive and capacitative coupling.

Table of Measurement Conversions

At any given single frequency, f, only two quantities are measured. With $\omega = 2\pi f$, the conversions are:

The instrument assumes as series circuit:

$$|Z|^2 = R_s^2 + (\omega C_s)^{-2}$$

$$\phi = -\tan^{-1}\left(\frac{1}{\omega C_s R_s}\right) \qquad D = \omega C_s R_s$$

$$Z = R + iX = |Z|\,(\cos\phi + i\sin\phi) \qquad [105]$$

$$R = R_s$$

$$\therefore \quad X = -(\omega C_s)^{-1}$$

The instrument assumes as parallel circuit:

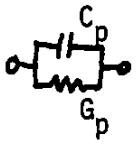

$$|Z|^2 = \{G_p^2 + (\omega C_p)^2\}^{-1}$$

$$\phi = -\tan^{-1}\left(\frac{\omega C_p}{G_p}\right) \qquad D = \frac{G_p}{\omega C_s} \qquad [106]$$

$$Y = G + iB = Z^{-1}$$

$$G = G_s$$

$$B = \omega C_p$$

Conversions:

$$G_p = \frac{R_s}{R_s^2 + (\omega C_s)^{-2}} = R_s^{-1}\,\frac{D^2}{1 + D^2} \qquad [107]$$

$$C_p = \frac{1}{1 + D^2}\,C_s$$

Note: despite the convention addopted on page 11 and equation [15], some instruments use θ instead of ϕ for phase angle.

Example of Cable Correction

At any given single frequency, f, with $\omega = 2\pi f$, the typical circuit including all cable effects is

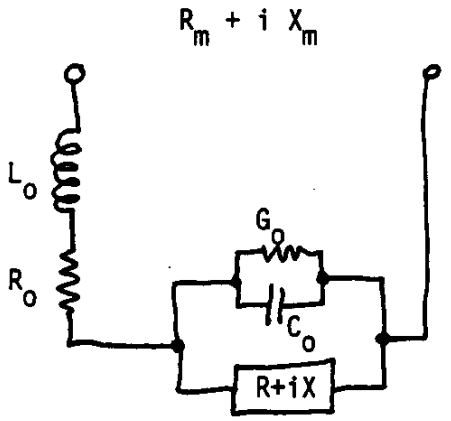

The instrument "sees" R_m+iX_m while the desired parameters are R+iX. R_o is the series resistance of the measurement leads. L_o is inductive coupling. G_o is sample holder leakage. C_o is capacitative coupling.

The solution is $$Z = \frac{Z_m - Z_o}{1 + Y_o(Z_m - Z_o)} \qquad [108]$$

where $Z_o = R_o + i\omega L_o$ and $Y_o = G_o + i\omega C_o$. Z_o is the measured impedance with all of the leads shorted together near the sample holder, and Y_o is the measured admittance with the positive current/potential leads shorted, the negative current/potential leads shorted, but positive-to-negative open. For inductive coupling removal in field situations, see Wynn and Zonge (1975). To remove inductive and capacitative coupling in borehole logging, the hole must be logged three times: once with the cable normally connected to the probe electrodes and thus the formation, a second time with the cable isolated from the probe and shorted at the probe, and a third time isolated and open. The measurements must be performed with high enough accuracy to make the equations above meaningful (see data error analysis next).

The matrix relay switches the center conductor and the shield of the current and voltage drop cables under computer control depending upon which instrument is measuring the sample. Both center conductor and shield must be switched as the digital LCR meters use return-current-loop shielding and the NLCR system uses driven shields.

The remainder of the system shown on the left in Figure 54 is pictured in the right photograph. This is the nonlinear complex resistivity system (NLCR) that measures from 10^{-6} to 10^{3} Hz (it can go to 10^{5} Hz with better pre-amps). This system uses a pair of HP 3325A frequency synthesizers phase-locked together as a precision source and time base. The source drives a Crown DC-300A power amplifier (not required in the laboratory; required for borehole logging) which drives current through a General Radio 1433H precision (0.01%) decade resistor and then through the sample. The voltage drop across the decade resistor, R, and across the sample are fed into two low-noise-current, high-input-impedance, isolation preamplifiers with driven shields. The driven shields preserve the high-input-impedance to the ends of the cables and eliminate some of the capacitative coupling. From the preamplifiers, the signals are simultaneously digitized by two sample-and-holds and a pair of 12-bit A/D converters. The digitized signals are then multiplexed and DMA'd into the HP9845 memory (see Olhoeft, 1979, 1985).

The computer memory thus holds a series of numbers representing voltages and currents taken simultaneously at discrete, known time intervals. After applying the sample geometry to convert these to electric fields and current densities, there is:

$$E_1, E_2, E_3, \ldots E_n$$

$$J_1, J_2, J_3, \ldots J_n$$

$$\text{at} \quad t_1, t_2, t_3, \ldots t_n$$

all measured at a single frequency, f, with $\omega = 2\pi f$. These may then be analyzed by Fourier analysis and deconvolution to arrive at the complex transfer function (and hence complex resistivity), but that does not give a measure of how good the data is: noise spikes, drifting sample, etc. To perform the transformation and obtain the quality of data, matrices are set up and the inverse taken as follows.

$$E(t) = E_s + E_o \sin(\omega t + \phi_e)$$

$$J(t) = J_s + J_o \sin(\omega t + \phi_j) \qquad [109]$$

where E_s = constant DC offset = spontaneous polarization

J_s = constant DC offset (generally zero, but retained for symmetry)

E_o = amplitude of the electric field response

J_o = amplitude of the current density stimulus

and ϕ_e and ϕ_j are phases relative to an arbitrary zero time. Since the measurement system has the source frequency, ω , phase-locked to the digitizing clock (and hence the time-base, t), the times $t_1 \ldots t_n$ are known in terms of ωt. Thus, the pair of equations [109] may be setup in matrix form as 2n equations with 6 unknowns.

This results in the matrix of the form

$$\underline{X} = \underline{I}\underline{\Theta} \qquad [110]$$

where underlined capital letters are matrices, $\underline{X}$ is n x 2, $\underline{I}$ is n x 3, and $\underline{\Theta}$ is 3 x 2 with

$$X_{m1} = E(t_m) \qquad X_{m2} = J(t_m)$$

$$\begin{aligned} T_{m1} &= 1 \\ T_{m2} &= \sin(\omega t_m) \\ T_{m3} &= \cos(\omega t_m) \end{aligned} \qquad [111]$$

$$\begin{aligned} A_{11} &= E_s & A_{12} &= J_s \\ A_{21} &= E_o \cos\phi_e & A_{22} &= J_o \cos\phi_j \\ A_{31} &= E_o \sin\phi_e & A_{32} &= J_o \sin\phi_j \end{aligned}$$

Then by simple inverse theory (Searle, 1971), the solution to the system of equations is

$$\underline{A} = (I^T I)^{-1} I^T \underline{X}. \qquad [112]$$

Algebraic manipulation of $\underline{A}$ yields

$$\begin{aligned} \phi_e &= \arctan(A_{31}/A_{21}) \\ \phi_j &= \arctan(A_{32}/A_{22}) \end{aligned} \qquad [113]$$

$$\begin{aligned} E_o &= A_{21}/\cos\phi_e \\ J_o &= A_{22}/\cos\phi_j \end{aligned}$$

These are converted to the complex resistivity parameters through

$$\begin{aligned} |\rho| &= E_o/J_o = \text{resistivity magnitude} \\ \phi &= \phi_e - \phi_j, \end{aligned} \qquad [114]$$

and these may be converted to other parameters through the equations in the section on Nomenclature.

This NLCR system has the advantage over the digital LCR meters of being able to record and store the full E(t) and J(t) waveforms for later analysis (in the case of nonlinear samples), produce error statistics on each measurement (see

discussion in section on Data Error Analysis), and generate the complex transfer function with higher accuracy (Olhoeft, 1979, 1985).

Figures 55 and 56 illustrate the typical measurement accuracy and range characteristics of the NLCR system. Figure 55 shows (from top to bottom) the error in measuring impedance (typically less than 0.2%), the error in phase (within 0.2 milliradians), and the nonlinearity of the system as total harmonic distortion (THD: typically less than 0.04%). The increased deviation approaching

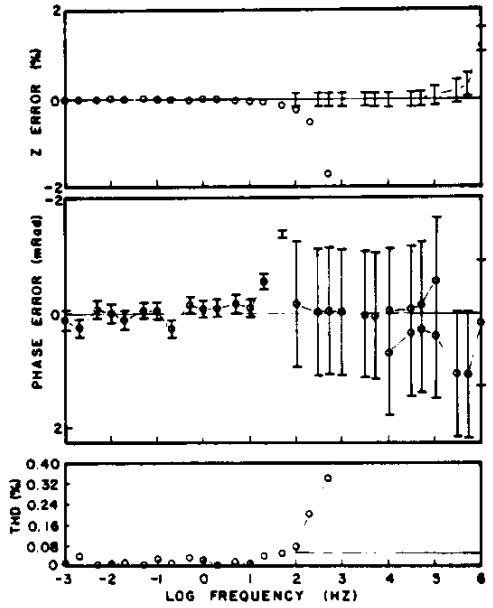

Figure 55

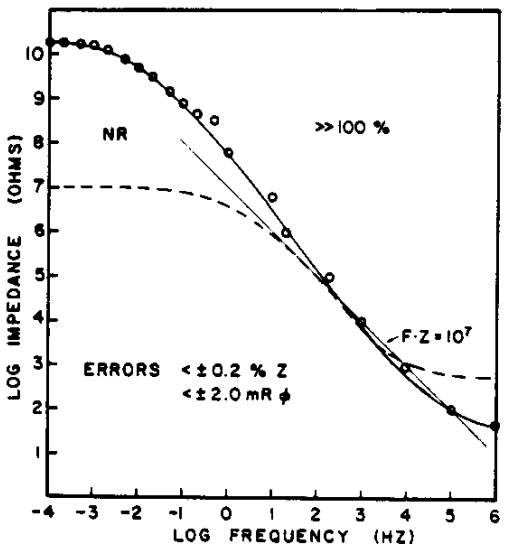

Figure 56

10^2 to 10^3 Hz is caused by the limiting frequency response of the isolation preamplifiers. The higher frequency data is from the 4274 and 4275 LCR meters (which cannot measure THD).

Figgure 56 illustrates the range of frequency and

impedance that can be measured with this system. The circles are the actual, measured input impedance of the system, below which the stated accuracy is correct. The region labelled NR is where the GR 1433H decade resistor fails and must be replaced by individual, precision high-impedance, wire-wound glass resistors.

The measurements shown in Figures 29 through 44 were acquired with this system. Error bars are plotted for all data points, though some may not be visible as they are smaller than the plotting symbol.

This system is also used for classical electrochemistry experiments using corrosion cells (to study single mineral-water interfaces) and others as described in Bard and Faulkner (1980) and Olhoeft (1979, 1982, 1985). For details, see Klein (1980), Cavell (1973), Evans and Matesich (1973), MacDonald (1977), Kuta and Yeager (1972), Weppner and Huggins (1978), and Mansfeld and Bertocci (1981). After acquiring data in the form of [114] it must be corrected through [108] with the open and short measurements at the sample holder to remove coupling.

High Frequency Dielectric Measurements

The region labelled HPN in Figure 45 requires an entirely different type of sample holder and measurement technology than that already discussed. There are a variety

of methods that have been developed to perform measurements above 10^6 Hz, but the most versatile employs a microwave network analyzer measuring samples inside coaxial waveguides. Figure 57 illustrates a 14 mm, General Radio 900 coaxial airline. The photograph shows examples of these airlines (two at the bottom), one with adaptors installed to convert to type-N connectors, and three examples of rectangular microwave waveguides. To use these, samples must be precisely machined to tighly fit between the

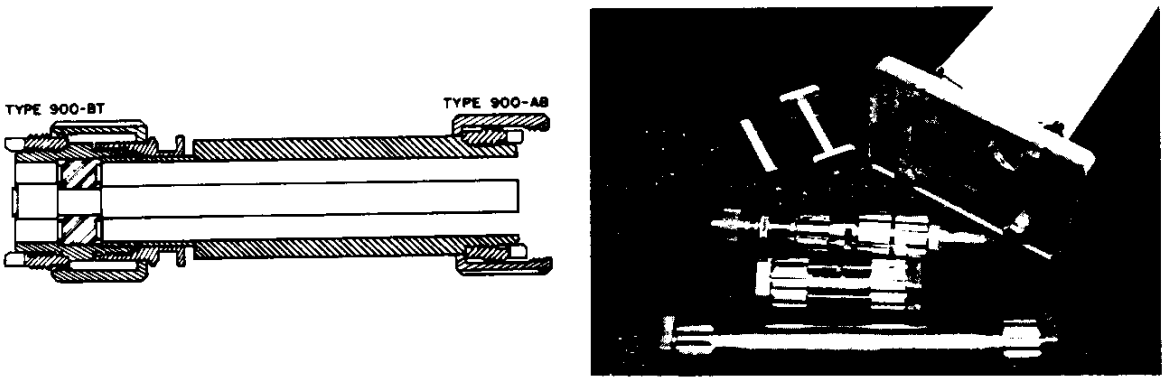

Figure 57

outer conductor and inner rod of the coaxial line or completely fill the rectangular waveguide (there also exist perturbation techniques for small samples that only partially fill the waveguide, see von Hippel, 1954; Adam, 1969, 1978; Hewlett Packard, 1985). Incomplete filling of the waveguides

requires complicated and uncertain corrections. Further corrections are required for any adaptors, feedthroughs, and cables required to connect the sample holder to the network analyzer. These will be discussed in detail below

The desired physical properties from the propagation of electromagnetic energy are the relative dielectric permittivity and relative magnetic permeability, given as

$$K' - iK'' = (c_2/c_1)^{1/2} \qquad [115]$$

$$\mu_r' - i\mu_r'' = (c_1 c_2)^{1/2} \qquad [116]$$

where

$$c_1 = \frac{(1+\Gamma)^2}{(1-\Gamma)^2} \qquad [117]$$

$$c_2 = -\left(\frac{c}{\omega d} \ln\frac{1}{z}\right)^2 \qquad [118]$$

with c = speed of light in vacuum = 2.998×10^8 m/s

d = sample length in meters

$\omega = 2\pi f$

$$z = \frac{V_1 - \Gamma}{1 - V_1\Gamma} \qquad [119]$$

$$\Gamma = \chi \pm (\chi^2 - 1)^{1/2} \qquad [120]$$

$$\chi = \frac{1 - V_1 V_2}{V_1 - V_2} \qquad [121]$$

$$V_1 = S_{21} + S_{11} \qquad [122]$$

$$V_2 = S_{21} - S_{11} \qquad [123]$$

The parameters, S_{11} and S_{21}, along with S_{22} and S_{12}, are the measured quantities. They are complex quantities

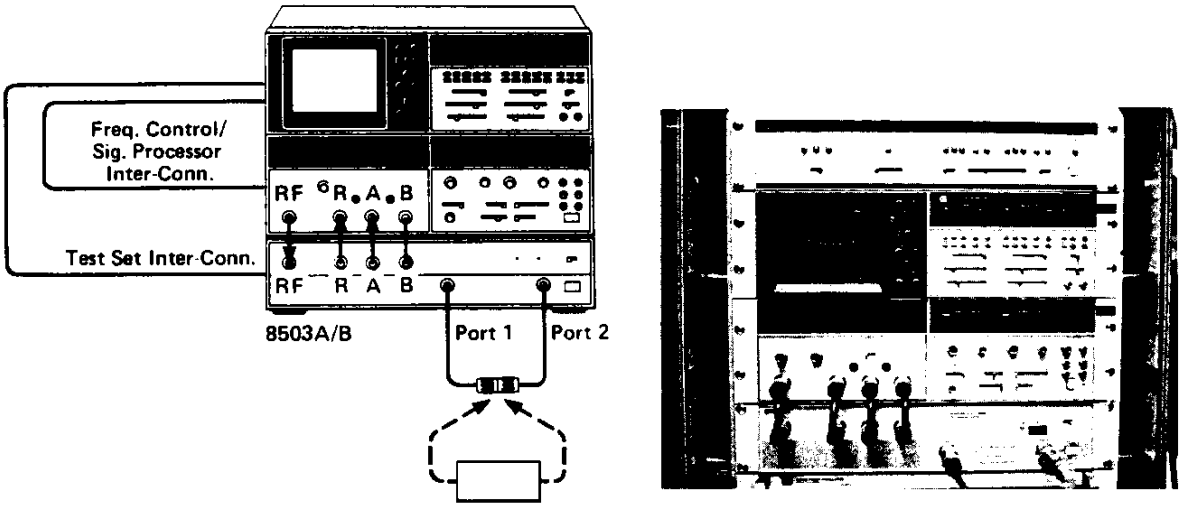

Figure 58

with magnitude and phase measured at each frequency using a network analyzer such as the Hewlett-Packard 8507 system shown in Figure 58.

The S-parameters (sometimes called scattering parameters) are defined for a two-port system as (Kurokawa, 1965; Adam, 1969)

$$b_1 = S_{11}a_1 + S_{12}a_2$$

$$b_2 = S_{21}a_1 + S_{22}a_2 \qquad [124]$$

where a_1 and a_2 are the normalized voltage waves incident on ports 1 and 2 respectively, and b_1 and b_2 are the normalized voltage waves reflected from ports 1 and 2 respectively. This is represented in Figure 59.

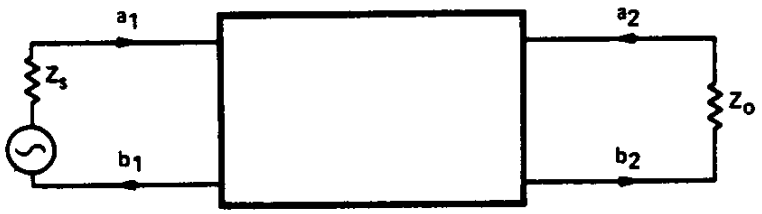

Figure 59-

To determine the quantities in equation [119] in order to solve equations [123] back to [115] and [116] for permittivity and permeability, corrections must be made for errors in the measurement system as outlined in Figure 60.

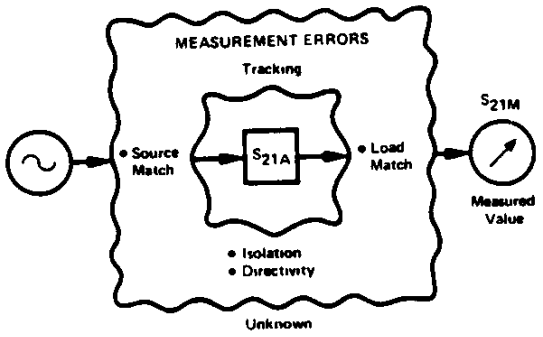

Figure 60 -

and corrections must be made for the cables and adaptors between the sample holder and the instrument. These corrections are made by proper calibration of the network analyzer and the development of corrective equations for the measurement errors in Figure 60. Then, at the ends of the cables and adaptors where the sample holder would normally be placed, both port 1 and port 2 are measured over the desired frequency range with an open, short, and 50-ohm load (assuming 50-ohm network analyzer) and the resultant 6 S-matrices recorded at each measurement frequency. Then an empty sample holder is put into place, connecting port 1 to port 2, and the S-matrix is recorded at each frequency. This results in 7 complex S-matrices or 56 numbers to be stored at each measurement frequency.

The sample holder containing the sample is then placed between the two ports, and the S-matrix of the sample is recorded at each frequency. Following lengthy, but straight-forward algebraic manipulation of these 64 numbers at each frequency, the S-matrix is determined for the sample and plugged back through equations [123] to [115]. The details of this are explained in Kruppa and Sodomsky (1971) and Adam (1968), and have been implemented on pocket calculators (Hillbun, 1980). Hewlett-Packard also has an extensive series of application notes (numbers 221A, 117-1A, and others) and programs (85030B Applications Pac) explaining how to do this with their instruments (Hewlett Packard, 1985).

One useful application of the full S-matrix is the study of the interaction of electromagnetic energy with the scale of inhomogeneity in the material. In equations [122] and [123], only S_{21} and S_{11} are used. These use energy incident on port 1 to measure the transmission through the sample to port 2 and the reflection from the sample surface facing port 1. Similar information is obtained in the other direction at port 2. If the sample is homogeneous at the wavelength of measurement, using S_{21} and S_{11} will provide the same solutions as using S_{12} and S_{22}. However, if the wavelength of electromagnetic energy propagating in the material is less than 3 times the scale of inhomogeneity in the material, then S_{21} and S_{11} will produce a different

solution than S_{12} and S_{22}. Thus, by varying the frequency and measuring from low frequency (long wavelength) to high frequency, the difference between these two pairs may be used to quantitatively determine the amount of volume scattering of electromagnetic energy in the material as opposed to energy lost by conversion to thermal energy.

The network analyzer shown in Figure 58 operates over a frequency range of 5×10^5 to 1.3×10^9 Hz. With coaxial waveguides and additional equipment, network analyzers may be used to about 26 GHz. Above 26 GHz, the microwave frequency range is broken down into bands. For each band (roughly a factor of 1.4 in frequency span), a different rectangular waveguide must be used as a sample holder, and various pieces of ancillary hardware must be changed to connect the sample holder to the network analyzer (or precision microwave source and receiver). Current commercial equipment is available to extend the frequency range in this manner up to 300 GHz (3×10^{11}Hz), beyond which optical techniques are more appropriate.

Examples of the use of network analyzers to measure the high frequency dielectric properties of rocks are found in DuBow (1976), Poley et al.(1978), Freeman et al.(1979), Nottenburg et al.(1979), Rau and Wharton (1982), Huang and Shen (1983), Shen (1983), Kenyon (1984), De (1985), and Shen et al.(1985).

Above about 3×10^8 Hz, network analyzers are the easiest,

but not necessarily the most accurate measurement techniques. For very low loss materials, some network analyzers cannot determine the imaginary part of the permittivity at all. In such situations, resonant cavity or slotted line techniques are to be preferred. Both suffer from the fault that they cannot measure over a continuous range of frequencies, nor measure at any arbitrary frequency, but must measure at half-integer multiples of the wavelength of the electromagnetic energy in the material. Thus, if the dielectric permittivity is unknown, the measurement frequency is also unknown. However, both are very accurately determined during the measurement process. As most rocks contain enough water to have reasonably high loss, neither of these two techniques are widely used. For more details on these types of measurements and others, see the discussions in von Hippel (1954) and Bussey (1967, 1979).

A more widely used alternate technique for high frequency measurements is the use of the time-domain-reflectometer (TDR). Commercially available TDR equipment covers the frequency range 10^5 to 10^{10} Hz and higher, with detailed reviews and discussion available in Fellner-Feldegg (1972), van Gemert (1973), Suggett (1972), Clark et al. (1974), and Cole (1977). The measurements are performed in coaxial and/or rectangular waveguides much the same as discussed above for the microwave network analyzers. However, unlike network analyzers which work in the frequency domain directly, TDR measures in the time domain and transforms the

result into the frequency domain. After the transformation, the same S-matrix computations and corrections may be performed as discussed earlier for the network analysis.

The principal added problems in TDR are the requirement to accurately digitize and transform a fast waveform. A highly accurate time-base is essential, with time-base jitter causing serious errors as the frequency is raised. There are also the usual problems related to digitizing, aliasing and a significant number of digitization levels, but also the requirement to acquire enough data over a long enough time window to make the transformation to the frequency domain meaningful. Laplace and Fourier transforms require infinite time windows to work properly, but such measurements are not possible.

One distinct advantage of TDR is the ability to fine-tune the measurement apparatus to place reflections from cable, adaptors, and so forth at places in the time record where they do not interfere with the sample data. Thus, some of the S-matrix corrections may be eliminated, and in many cases, the directly measured time data may be transformed and used to compute the dielectric permittivity directly. Further, as events are placed in time, it is possible to directly see perturbations in the time record that are caused by electromagnetic scattering due to inhomogeneities within the sample. For examples, see Nicholson and Ross (1970), Lytle and Myers (1977), Stuchly and Stuchly (1980), Topp et al.(1980,1982), Patterson and Smith (1981, 1983), Dalton et

al.(1984), and Delaney and Arcone (1984).

Figure 61 illustrates a microwave anaechoic vacuum chamber that was used to measure the volume and surface scattering characteristics of rock and soils for application to lunar problems (Olhoeft et al., 1979). This is just one example of many that require full scale or fractional scale modelling of electrical and electromagnetic processes in the laboratory in order to understand how electrical properties are observed with geophysical equipment in the field.

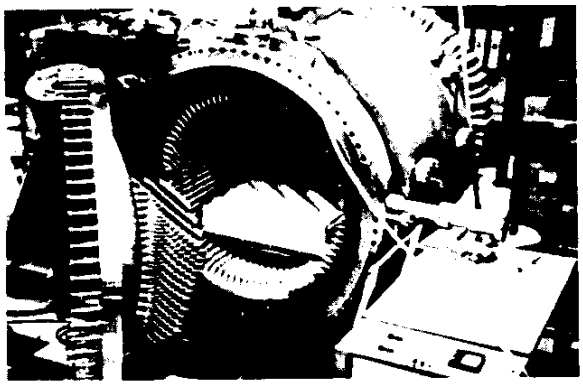

Figure 61

Data Error Analysis

Bevington (1969) and Meyer (1975) give excellent introductions to the error analysis of physical data. From Bevington (1969) come these basic definitions:

N = number of observations

$\mu = \lim_{N\to\infty} N^{-1} \Sigma x_i$ = parent mean

x_i = ith observation

$\bar{x} = N^{-1} \Sigma x_i$ = sample mean ~ μ

$\sigma^2 = \lim_{N\to\infty} N^{-1} \Sigma (x_i - \mu)^2$ = variance

σ = parent standard deviation

where the standard deviation is a measure of the uncertainty in the measured data. The sample standard deviation, s, is

$$\sigma^2 \sim s^2 = (N-1)^{-1} \Sigma (x_i - \bar{x})^2 \qquad [125]$$

where N-1 is the number of degrees of freedom left after determining $\bar{x}$ from N observations.

It is rare that an instrument actually measures the desired quantity, x. Usually an intermediate physical quantity is measured which must be suitably converted into

the desired quantity. For example, by measuring voltage, V, and current, I, Ohm's Law is used to obtain resistance, R.

$$R = V/I$$

Errors propagate from the original measurement to the final parameter through the conversion formula. For any parameter x as a function of u and v

$$x = f(u,v,...)$$

if the most probable value of x is

$$\bar{x} = f(\bar{u},\bar{v},...)$$

then errors in u and v propagate through to x and yield

$$s_x^2 = s_u^2\left(\frac{\partial x}{\partial u}\right)^2 + s_v^2\left(\frac{\partial x}{\partial v}\right)^2 + 2s_{uv}^2\left(\frac{\partial x}{\partial u}\right)\left(\frac{\partial x}{\partial v}\right) + \ldots \qquad [126]$$

where $s_u^2 = N^{-1}\,\Sigma(u_i - \bar{u})^2$ and similarly for s_v^2 [127]

and $s_{uv}^2 = N^{-1}\,\Sigma((u_i - \bar{u})(v_i - \bar{v}))$ = covariance uv [128]

Thus, in the example for resistance with

$$R = V/I$$

$$s_R = R^2\left(\frac{s_V^2}{V^2} + \frac{s_I^2}{I^2} - 2\,\frac{s_{IV}^2}{IV}\right) \qquad [129]$$

Note that for proper values of the covariance, the errors could cancel giving a zero standard deviation in R. This requires high correlation in the errors of I and V. If the I and V errors are totally uncorrelated, then $s^2_{IV} = 0$. Similar examples hold for the propagation of errors in capacitance bridge measurements of dielectric permittivity and loss tangent through

$$K' = C/C_o$$

$$D = G/\omega C$$

and a three-terminal sample holder is assumed so there are no corrections for fringing fields, surface conductance, and cable coupling.

In the examples just noted, the individual variances are computed by large numbers of measurements to determine the statistics of the measurement system or by using the manufacturer's stated accuracy statistics for the instrument. In the following example, linear regression analysis of the NLCR system described earlier will show how the variance may be computed directly from the measured data.

Equations [110] through [114] described how to proceed from a series of voltages and currents measured at specified times (not necessarily uniformly spaced) through use of the sample holder geometry to convert them into electric field and current density values at discrete times

$$E_1, E_2, E_3, \ldots E_n$$

$$J_1, J_2, J_3, \ldots J_n$$

$$t_1, t_2, t_3, \ldots t_n$$

all at a specific frequency, f, and solve the linear system of equations to arrive at the matrix form

$$\underline{X} = \underline{I}\underline{\theta} \qquad [110]$$

with the solution

$$\underline{\theta} = (\underline{I}^T\underline{I})^{-1}\underline{I}^T\underline{X} \qquad [112]$$

eventually resulting in the complex resistivity with

$|\rho| = E_o/J_o$ = resistivity magnitude

$\phi = \phi_e - \phi_j$ = phase angle between E and J

The propagation of errors from E's and J's at various t's is followed by first finding the errors in the E's and J's. Assume the errors in time, t, and frequency, f, are negligible by using 0.1 ppm accurate time bases in comparison with 12-bit A/D digitization of E and J (244. ppm).

$$\underline{S} = (\underline{X} - \underline{I}\underline{\theta})^T(\underline{X} - \underline{I}\underline{\theta}) \qquad [130]$$

where the matrix, $\underline{S}$, contains both the variance and covariance information for the E's and J's. Dividing $\underline{S}$ by

the number of degrees of freedom, n - 6 (as there are n measurements and 6 elements in $\underline{A}$) yields

$$\underline{L} = (\underline{I}^T\underline{I})^{-1}B_{11}B_{22}/2 \quad \text{where} \quad \underline{B} = (n-6)^{-1}\underline{S} \qquad [131]$$

with the phase error

$$s_\phi = \frac{(A_{31}/A_{21})^2\left(\frac{L_{31}}{A_{31}^2} + \frac{L_{21}}{A_{21}^2}\right)}{1 + \frac{A_{31}^2}{A_{21}^2}} + \frac{\frac{L_{32}}{A_{32}^2} + \frac{L_{22}}{A_{22}^2}}{1 + \frac{A_{32}^2}{A_{22}^2}} \qquad [132]$$

and the resistivity magnitude error

$$s_\rho^2 = \frac{J_o}{E_o}\frac{A_{21}^2 + A_{31}^2}{A_{22}^2 + A_{32}^2}\left(\frac{L_{21}A_{21} + L_{31}A_{31}}{(A_{21}^2 + A_{31})^{3/2}} + \frac{L_{22}A_{22} + L_{32}A_{32}}{(A_{22}^2 + A_{32}^2)^{3/2}}\right) \qquad [133]$$

As it was experimentally determined that the covariances, B_{12} and B_{21}, are invariably several orders of magnitude smaller than B_{11} and B_{22}, and also determined that $B_{11} \sim B_{22}$, the above derivation was performed assuming that $B_{12} = B_{21} = 0$ and $B_{11} = B_{22} = (B_{11}+B_{22})/2$.

The error bars that result from this analysis are what are plotted on complex resistivity spectral plots. A further error must be added to these however to arrive at a better understanding of the total errors in the system. In converting from measured voltages and currents to electric

field and current density or from measured resistance to material resistivity, one of the largest errors is in the sample dimensions. These appear as

E = V/thickness (thickness or length of sample)

and J = I/sample-area (cross-sectional area of sample through which current flows)

or

ρ = R area/thickness.

The error in the measurement of the ratio area:thickness is given as

$$s^2_{a/t} = (a/t)^2(s^2_a/a^2 + s^2_t/t^2) \qquad [134]$$

with covariance assumed to be zero. If the error in measurement of resistance, R, is s^2_R, then

$$s^2_\rho = \rho^2(s^2_R/R^2 + s^2_{a/t}/(a/t)^2) \qquad [135]$$

In the Petrophysics Laboratory, typical values of these parameters are

R = 100

a/t = 0.5, a = 0.02, t = 0.04

ρ = 50

$s^2_R = 9\times10^{-8}R^2 = 9\times10^{-4}$ (0.03% error)

$s^2_a = 1\times10^{-4}a^2 = 4\times10^{-8}$ (1%)

$s^2_t = 1\times10^{-4}t^2 = 1.6\times10^{-7}$ (1%)

thus

$$s^2_{a/t} = 0.0001 \qquad (1\%)$$

$$s^2_{\rho} = 1.000225 \qquad (2\%)$$

Thus a 0.03% error in measuring R and a 1% error in measuring sample thickness and area translate into a 2.0% error in resistivity. Similarly, a 0.03% error in R and 0.1% error in a and t result in a 0.2% error in resistivity. These latter errors are typical of measurements on well-consolidated samples which machine easily. For dielectric permittivity presented relative to free space, loss tangent, and phase angle the geometry errors tend to cancel out, leaving oly the measurement error. Accuracies as high as 0.005% in relative dielectric permittivity are readily attained. Accuracies as high as 0.2 milliradians in phase are typical (see Olhoeft, 1980, 1985).

In microwave measurements, network analysis offers direct measurement of phase angle with accuracies as high as 0.7 milliradians available on commercial instruments. Error estimates of dielectric permittivity require similar derivative error analysis depending upon exactly how the measurements and mathematics were performed. Typical dielectric permittivity measurement accuracies are 0.2%.

ELECTRICAL PROPERTIES SHORT COURSE - Gary R. Olhoeft

Linear Models

In contrast to nonlinear properties (discussed in the next section), there are a wide variety of models that may be applied to linear system electrical properties. Linear models also exist which include a wide variety of environmental parameters, most of which have not yet been applied to nonlinear electrical properties. The purpose of a model is to reduce a large number of measurements to a manageable number of parameters, aid in the interpretation of the physical-chemical mechanisms behind the observed properties, and help in predicting similar properties under related conditions.

For example, magnetotelluric depth soundings provide information about the lower crust and upper mantle. Yet, current drilling technology cannot reach those depths, so there are no pristine specimens of materials from those depths. To aid in the interpretation of the magnetotelluric data, extensive laboratory measurements are performed on likely materials under appropriate conditions of temperature, pressure, water content, and so forth. The lab data are synthesized into a petrophysical model (including a variety of physical properties as functions of various environmental parameters). The resultant model is then used to generate fits to the magnetotelluric data through the forward problem

or is used to constrain parameters in the inverstion of the field data. The most likely candidate suite of model parameters fitting both the petrophysical and field data is used as a basis for interpretation (Hermance et al., 1972; Stanley et al., 1977; Beblo et al., 1983; Flovenz et al., 1985; Schmeling, 1985).

Mathematical models may always be constructed to fit experimental data. However, purely mathematical models are rarely useful. To have meaning in a geological context, the models must be developed with proper considerations of physical and chemical laws of nature. The models must then be used in the context that they were developed to address and not abused.

Several simple models were introduced earlier for dielectric systems. It is convenient to be able to use models that are available in either complex dielectric permittivity or complex conductivity or complex resistivity. For multiple mechanisms, several terms of an equation like [59] may be added together, such as

$$K' - iK'' = K_{n+1} \left\{ 1 + \sum_{q=1}^{n} \frac{\$_q}{1 + (i\omega\tau_q)^{\alpha_q}} \right\} \qquad [136]$$

where

$$\$_q = \frac{K_q - K_{q+1}}{K_{q+1}} .$$

Olhoeft (1977) has used such a model to characterize

permafrost as illustrated in Figure 62. The triangles are the data points. The dashed line is a DC conductivity term with

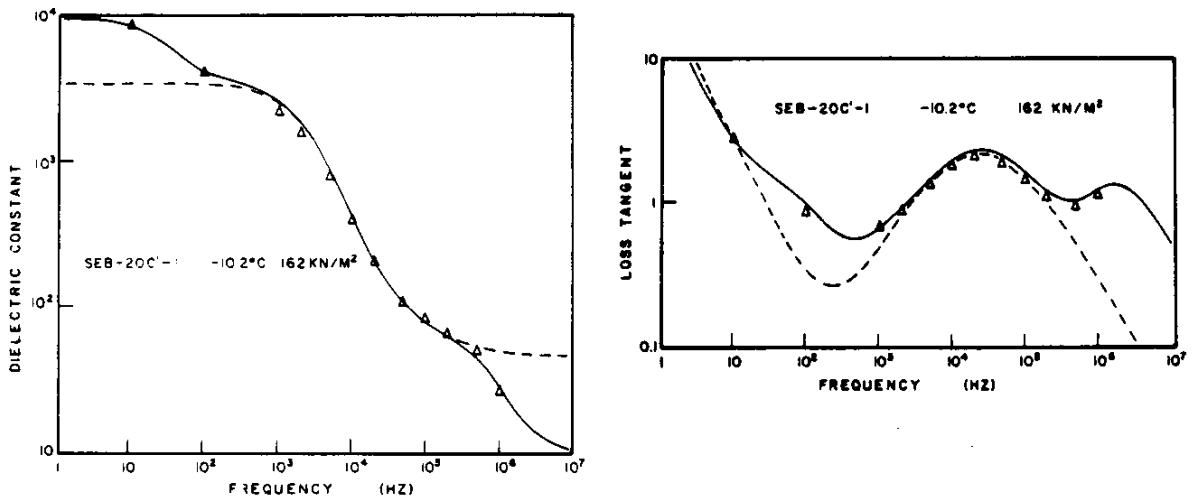

Figure 62 -

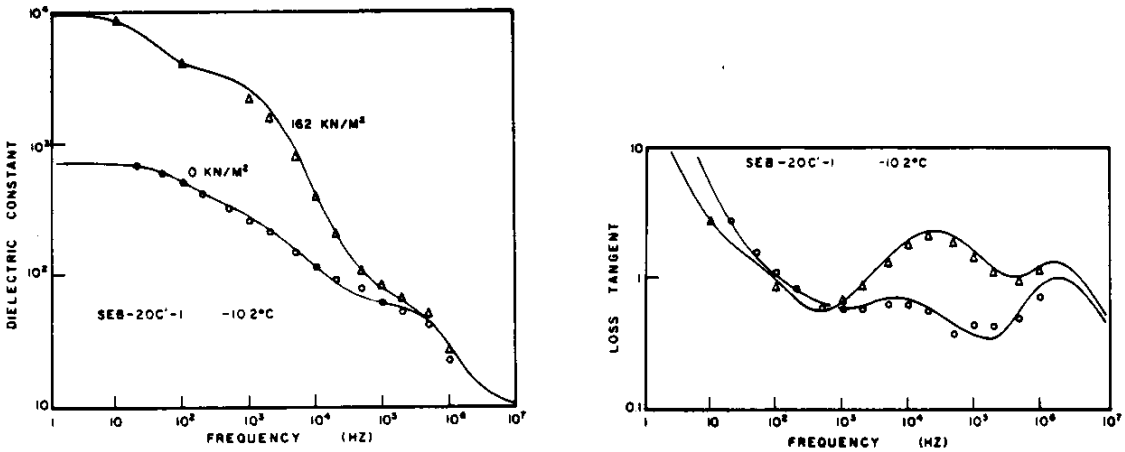

Figure 63 - .

a single Cole-Cole relaxation distribution using n = 1 in [136] and the loss tangent from [9]. The solid line adds two more distributions to increase n to 3. By fitting this model while uniaxial confining load is applied to the sample (Figure 63), a series of model parameters were found which describe the frequency and pressure dependence of the electrical properties. For this permafrost material, it was determined that ε_1, ε_2, and ρ_{DC} varied strongly with pressure as

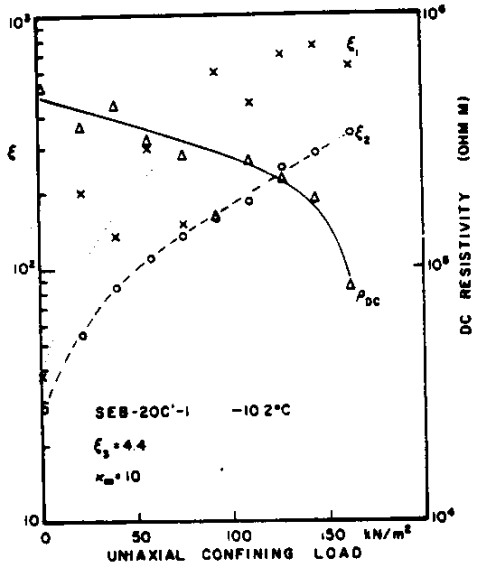

Figure 64 -

shown in Figure 64. α_2 varied slightly with pressure from 0.75 at 0 kN/m^2 to 0.86 at 162 kN/m^2. The remaining

parameters were independent of pressure and found to be

$$\alpha_1 = 0.90 \qquad \tau_1 = 0.553\times10^{-2} \text{ seconds}$$

$$\tau_2 = 0.791\times10^{-4}$$

$$\phi_3 = 4.4 \qquad \alpha_3 = 1.00 \qquad \tau_3 = 0.188\times10^{-6}$$

and $K_\infty = 10$. For further details see Olhoeft (1975, 1977). Similar models have also been developed for temperture and frequency dependence (Olhoeft et al., 1973, 1974).

In the modelling of the electrical properties of mineral deposits, Collett (1959), Grissemann (1971), van Voorhis (1973), Zonge and Wynn (1975), Gateau et al. (1976), Pelton (1977), Wong (1979), Halverson et al. (1979), and others have demonstrated that the frequency dependence of linear induced polarization is related to mineralization through water-mineral interfacial electrochemistry. If high current densities are used, the system goes nonlinear and the following discussion does not apply (see next section). The evidence is conclusive that the time constant distribution is dominantly controlled by grain size distribution in diffusion-limited systems. The amplitude of the relaxation is mainly determined by the amount of reactive redox mineral present and available for water contact.

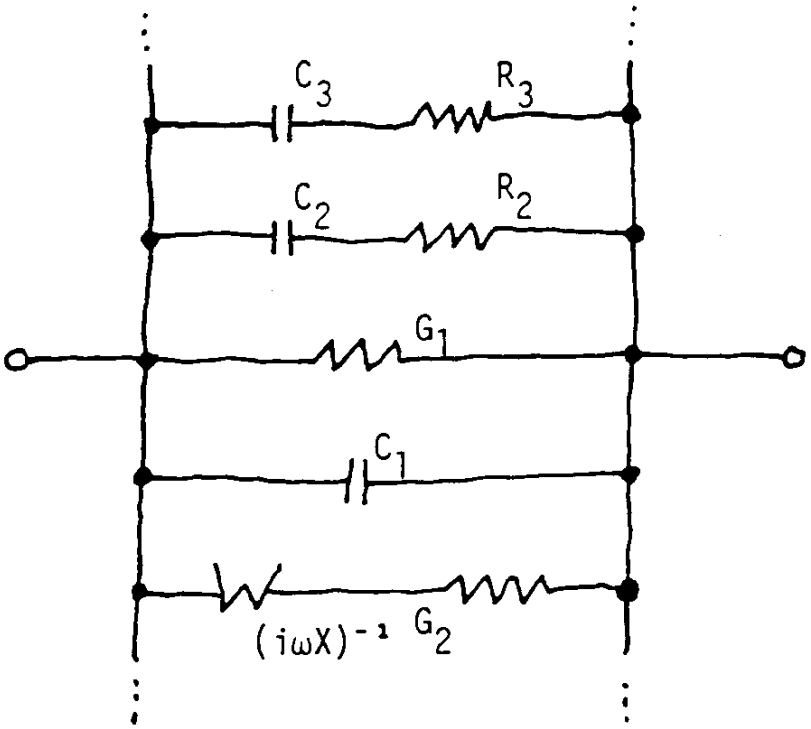

Figure 65

In such systems, the distributed circuit of Figure 15 is modified to look like Figure 65 with the equivalent total material conductivity given as

$$\sigma_T + i\sigma_T = \sigma_{DC} \left(1 + m \int_0^\infty \frac{i\omega\lambda\, F(\lambda)}{1 + (i\omega\lambda)(1-m)}\, d\lambda \right) + i\omega\epsilon_0 K_\infty \left(1 + \xi \int_0^\infty \frac{K(\tau)}{1 + i\omega\tau}\, d\tau \right) \qquad [137]$$

where σ_{DC} = DC conductivity

m = volume chargeability = (the same quantity as

defined by Seigel, 1959, and Pelton, 1977, for induced polarization)

$F(\lambda)$ = Faradaic time constant distribution with

$$\int_0^\infty F(\lambda)\, d\lambda = 1.$$

λ = Faradaic time constant

ϵ_o = vacuum permittivity = $8.85418782 \times 10^{-12}$ F/m

K_∞ = high frequency limiting relative dielectric permittivity

η = dielectric chargeability

$K(\tau)$ = dielectric time constant distribution with

$$\int_0^\infty K(\tau)\, d\tau = 1$$

and τ = dielectric time constant. The loss tangent and phase angle are given as

$$D = \cot\phi = \frac{\sigma_I'}{\sigma_T} \qquad [138]$$

The circuit element  is called a Warburg impedance, and it usually behaves as $(i\omega X)^{-n}$ where $n = 0.5$ for pure diffusion. Pure diffusion is rarely observed, and the situation of $n = 0.5$ is a special case of a more general diffusion model as discussed by Rangarajan (1969).

Note that when the chargeability, m, is zero, equation

[137] reduces to the dielectric equations based on [57], and when both m and ξ are zero, the total conductivity in [137] reduces to

$$\sigma_T' + i\sigma_T'' = \sigma_{DC} + i\omega K_\infty \epsilon_0 \qquad [139]$$

σ_{DC} may become very small ($\sim 10^{-17}$ mho/m) but never equal to zero, and K_∞ may never be less than 1.

If equation [137] is rewritten as

$$\sigma_T' + i\sigma_T'' = \sigma_{DC}\{1 + m\, G(n,m,\omega\lambda)\} + i\omega K_\infty \epsilon_0 \{1 + \xi\, K(\alpha,\omega\tau)\} \qquad [140]$$

then any distribution function such as the Cole-Cole distribution may be introduced through (see page 56ff)

$$G(n,m,\omega\lambda) = \frac{(i\omega\lambda)^n}{1 + (i\omega\lambda)^n(1-m)} \qquad [141]$$

$$K(\alpha,\omega\tau) = \{\, 1 + (i\omega\tau)^\alpha \,\}^{-1} \qquad [142]$$

Note the similarities and differences between the two distributions. If the conductivity distribution is written alone in the form of a resistivity (Pelton, 1977) ignoring the dielectric portion, it appears as

$$\rho' - i\rho'' = \rho_{DC}\{\, 1 - m\,(\, 1 - [\, 1 + (i\omega\lambda)^n \,]^{-1}\}. \qquad [143]$$

Equation [143] is identical in form with the models of Wait

(1959) and Halverson et al. (1979).

If equation [143] is rewritten as

$$\rho' - i\rho'' = \rho_{DC}\{1 - m\,(\,1 - Q\,)\} \qquad [144]$$

then other time constant distributions may be inserted (just as was done on page 59 for dielectrics) with the forms

$$Q = (\,1 + (i\omega\lambda)^{c}\,)^{-1} \qquad [145]$$

is the Cole-Cole distribution

with c = 1 is the Debye/Drude distribution

c = 0.5 is the Warburg distribution

c = 0.25 is the Madden-Cantwell distribution.

$$Q = (\,1 + i^{b}(\omega\lambda)^{c}\,)^{-1} \qquad [146]$$

is the modified Cole-Cole distribution

$$Q = \frac{(b + i\omega\lambda)^{c} + b}{(b + i\omega\lambda)^{c} + (b + i\omega\lambda)^{2c}} \qquad [147]$$

is the Glarum distribution

$$Q = \frac{\tanh(i\omega\lambda)^{c/2}}{(i\omega\lambda)^{c/2}} \qquad [148]$$

is the Zonge distribution

and others, such as the Fuoss-Kirkwood distribution, which is equivalent to the Cole-Cole but with the Fuoss-Kirkwood distribution parameter, β , given as

$$\beta = \frac{c}{2^{1/2}\cos(c\pi/4)} \qquad [149]$$

where c is the Cole-Cole distribution parameter in [145]. Another distribution with a different form than the above is the Drake, given as

$$\rho' - i\rho'' = \rho_{DC} (1 + i\omega\lambda)^{-a}. \qquad [150]$$

The key difference between the dielectric interfacial polarizations, such as the Maxwell-Wagner type discussed on page 68, and the water-rock interfacial polarization is the strong dependence of the latter relaxation time constant upon particle size and diffusion coefficient, roughly proportional to

$$\text{time constant} \sim \frac{a^2}{D_e} \qquad [151]$$

where a is the particle radius and D_e is the effective diffusion coefficient for charged particles (up to a factor of 2000 slower than the actual diffusion coefficient).

Pelton et al (1978) used formula [143] to fit the laboratory data of Grissemann (1971) to determine the dependence of the following parameters on mineralogy, finding:

σ_{DC} depends upon pore water conductivity and pore

structure connectivity relatively independent of mineralogy and grain size,

m has a slight dependence upon grain size and a strong dependence upon the volume fraction mineralization,

n most frequently falls between 0.4 and 0.6, with 0.5 the expected value for a diffusion-dominated process,

and λ is strongly dependent upon BOTH grain size and volume fraction of mineralization.

Figure 66 summarizes Grissemann's data as fitted to [143] by Pelton.

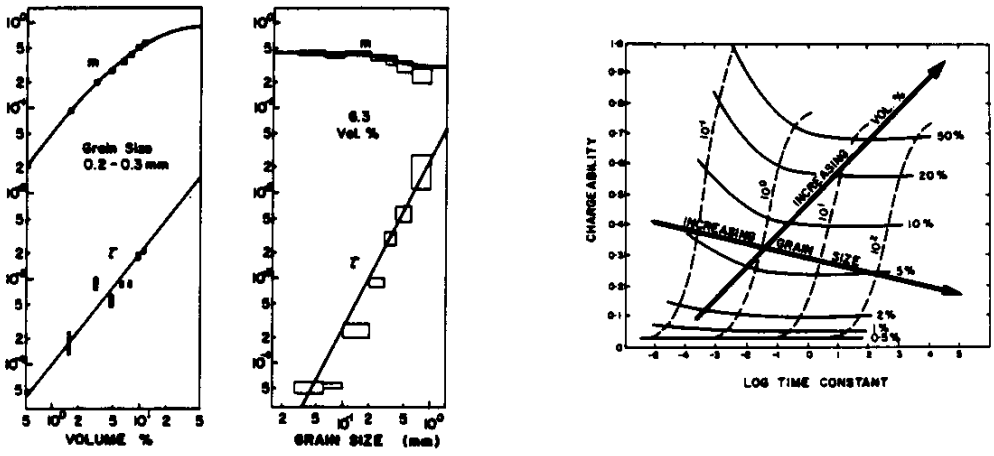

Figure 66 -

The theoretical electrochemical models of Wong (1979) and Wong and Strangway (1981) accurately predict the dependence of chargeability, m, on volume fraction and of time constant,

λ , upon grain size, but fail to duplicate the observed dependence of time constant upon volume fraction. The models also predict n ~ 0.5. The slight variations in n away from 0.5, the slight dependence of m upon grain size, and the dependence of λ upon volume fraction may all result from pore structure effects which were not explicitly considered in Wong's model (see Rangarajan, 1969). Wong and Strangway (1981) improved the original model based upon spherical particles to include particles of spheroidal shape, and this particle shape improved some of the model fits to real data, but still missed the dependence of λ upon volume fraction mineralization.

In equation [151], it was noted that the time constant was inversely proportional to the effective diffusion coefficient, D_e. The temperature dependence of the diffusion coefficient is (see discussion in Fyfe et al., 1978, p.113ff)

$$D_e = D_o \, e^{-E_o/kT} \qquad [152]$$

where D_o = diffusion coefficient at infinite temperature,

E_o = activation energy (typically 0.5-1.0 eV),

k = Boltzmann's constant,

and T = absolute temperature. This yields a temperature dependence of the time constant that is (compare to [68])

$$\lambda \sim e^{+E_o/kT} \qquad [153]$$

Thus, the time constant distribution may be shifted by one order of magnitude by changing the grain size distribution by a factor of 3.2, or by changing the temperature by 20°C (assuming E_o = 1.0 eV), or by changing the volume fraction of minerals by a factor of 3.5 (Pelton et al, 1978), or by changing the concentration of reactants by a factor of 3 (Wong, 1979). A change of mineral volume fraction by a factor of 10 produces a factor of 20 change in chargeability. Thus, by working in chargeability-time-constant space as proposed by Pelton et al. (1978) in Figure 66, it should be possible to determine the grain size and volume fraction from the complex resistivity spectra. This has been further demonstrated by the models of Wong (1979) and Wong and Strangway (1981), in which it is demonstrated that the shape of the mineralized particles may also be determined.

In some situations, the type of mineralogy may also be determined in chargeability-time-constant space. Pelton et al. (1978) show several examples; the sulfide-graphite separation is the most clear cut (as seen in Figure 67). For most minerals, the regions overlap somewhat.

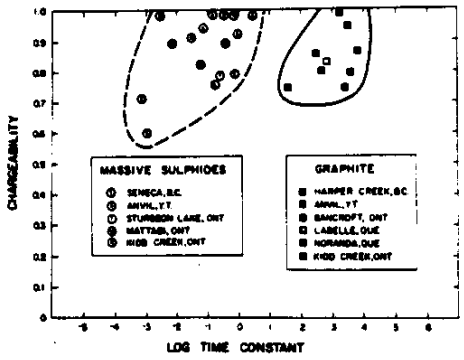

Figure 67 -

The DC conductivity will also vary with volume fraction mineralization, the concentration of reactants, and the temperature (as well as the porosity and pore connectivity or tortuosity). Since diffusion is involving the same ions in the polarization process that determines the relaxation time constant, and also in the conduction process, the activation energy and the temperature dependence of the DC conductivity will be similar to that of the Faradaic time constant and given by

$$\sigma_{DC} = \sigma_o \, e^{-E_o/kT} \qquad [55]$$

as discussed on page 43. Note the change in sign of the activation energy in [55] and [153] due to conductivity being

directly proportional to the diffusion coefficient while the time constant is inversely proportional to the diffusion coefficient (Erdey-Gruz, 1974). The activation energy will change slightly with the size, charge, and polarizability of the diffusing ion, with the fastest moving ion (generally a cation) dominating the electrical properties.

The model just outlined (based upon Wong, 1979) depends upon the following assumptions:

1) linear behavior following Ohm's law, equation [11],
2) the conductivity of the mineral particles is very much higher than that of the surrounding medium,
3) the space-charge layers inside the semiconducting mineral particles and at the water-mineral interface (electrochemical double layer) are negligibly small in comparison to the particle size, and these layers do not significantly polarize nor participate in surface conduction
4) the concentrations of ions involved in the induced polarization process at the water-mineral interface are small perturbations on a larger background concentration,
5) cations are the only active charge carriers, anions are inactive,
6) all diffusion coefficients, mobilities, charge valences, and concentrations for individual ionic species are equal,

7) no adsorption or ion exchange occurs at the mineral-water interface,

8) the volume fraction of mineral particles is small so there is no mutual interaction or cooperative phenomena between particles,

9) no corrosion or metallic dissolution processes are occurring, and

10) the particles may be statistically treated as if they were all spheroids.

If the first assumption is violated, the system goes nonlinear with many oxidation-reduction reactions (redox) occurring. In that situation, the system is usually not diffusion limited (assumption 4) and the kinetics of the reactions may determine the time constant distribution instead of the grain size and diffusion coefficients. If the conductivity of the mineral particles is not very high (assumption 2), then space charge layers may polarize inside the particles and assumption 3 concerning the size of the double layer relative to the particle size may also be violated. This is common in colloidal particles such as clays, zeolites, and paramagnetic oxides (colloidal pyrite is common in coal). Coincidently, the grain size may still control the time constant distribution (see Trukhan's model below). There will also be a very large change in the chargeability, m, accompanying this behavior.

Experimentally (Olhoeft, 1979; Klein, 1980), cations

dominate over anions so assumption 5 appears to be valid. Usually cations have diffusion coefficients that are a factor of 10 to 40 times faster than anions, but this does not appear to alter the model results, so assumption 6 is probably valid. The cation exchange capacity of clays and zeolites may create a significant polarization (Olhoeft, 1979), so assumption 7 is invalid in such systems. Massive and veined sulfides exist, so assumption 8 will be invalid in those cases. Corrosion processes are rampant in most mineral systems (that is how many deposits are formed), so assumption 9 may be invalid. Assumption 10 is realistic only for random particles of arbitrary shape and orientation. It will be violated in dentritic hematite, minerals filling cracks with preferred stress orientations, and related situations.

Despite the potential problems, the model works very well in assisting in the interpretation of surface-acquired IP surveys of disseminated sulfide ore deposits. It has very limited applicability to the interpretation of massive sulfide surveys, borehole logging, and related situations where one or more assumptions are invalid. It may also fail in disseminated sulfide systems where pore structures are more important than mineral-grain distribution (a la Rangarajan, 1969) or where mineral-water interaction is not diffusion limited (very high current densitities or very low reactant concentrations). The largest problem to this model is presented by clay and zeolite systems which violate several assumptions.

At any abrupt material boundary, there exists an electrical potential which decreases with distance away from the boundary due to the accumulation of charge in the energy barriers at the boundary. The local electric potential in such a situation is given by

$$e^{y/2} = \frac{e^{z/2} + 1 + (e^{z/2} - 1)\, e^{-\kappa x}}{e^{z/2} + 1 - (e^{z/2} - 1)\, e^{-\kappa x}} \qquad [154]$$

where $y = Ze\phi/kT$

$z = Ze\phi_o/kT$

with k = Boltzmann's constant

T = absolute temperature

e = electron charge

Z = valence of ion

ϕ = local electric potential as a function of x,

ϕ_o = surface potential at interface

κ = the reciprocal of the thickness of the electrochemical double layer, given as

$$\frac{1}{\kappa} = \left(\frac{\epsilon kT}{8\pi n e^2 Z^2}\right)^{1/2} \qquad [155]$$

with $\epsilon = K'\epsilon_o$ = dielectric permittivity of the medium

n = concentration of ions = solution molarity times Avogadro's number.

For small surface potentials, ϕ_o, the solution to [154] is

$$\phi = \phi_o\, e^{-\kappa x} \qquad [156]$$

The surface potential is obtained from the solution to

$$\sinh\left(\frac{z}{2}\right) = \sigma\left(\frac{\pi}{2n\epsilon kT}\right)^{1/2} \qquad [157]$$

where σ is the surface charge density (not the electrical conductivity), and for typical values of 0.001m NaCl aqueous solution against a flat surface with a constant charge density of 11.7 $\mu C/cm^2$, the thickness of the double layer is about 10^{-8}m with a surface potential of 0.025 V (see detailed discussion in van Olphen, 1977). The thickness of the double layer varies inversely with the square-root concentration of the aqueous solution, and for normal groundwaters is about the same size as many clay particles. Other colloidal materials such as organic compounds and paramagnetic oxides may be an order of magnitude smaller than the thickness of the double layer.

When the thickness of the double layer approaches the particle size, the electrical properties are strongly dominated by the interaction of the double layers. Verwey and Overbeek (1948) discuss these interactions in detail, and two situations are observed. It is possible to have either a surface of constant charge or a surface of constant potential. In the surface of constant charge (as in montmorillonite and other materials with constant cation exchange capacity), the surface potential increases with increasing interaction between particles. For a surface of

constant potential (as in amorphous clays and many oxides where cation exchange capacity increases with increasing solution concentration), the surface charge decreases with increasing interaction.

Systems containing clays are very complicated due to multiple reaction and interaction paths. Generally, the presence of colloidal clay particles causes catalytic oxidation of many compunds (particularly iron and manganese), effectively raising the Eh (oxidation potential) of the system. However, organic compounds generally are responsible for a drop in Eh towards reducing chemistries. Organic materials also interact with the clays directly or through catalytic reactions on the clay surfaces: oxidation-reduction reactions, polymerization-depolymerization reactions, and transformation, synthesis, and decomposition reactions (for detailed discussions, see van Olphen, 1977; Yariv and Cross, 1979; Theng, 1979). Most of the reactions are electrochemical in nature resulting in alterations of the electrical properties of the system (Eltanawy and Arnold, 1973; Fripiat and Cruz-Cumplido, 1974; Johns, 1979; Trasatti, 1980; Elenkova and Kostadinova, 1981; Ovcharenko, 1982; Appleby, 1983; Birkett et al., 1983).

Figure 68 illustrates some of the proposed interactions between clay particles and elecrical fields.

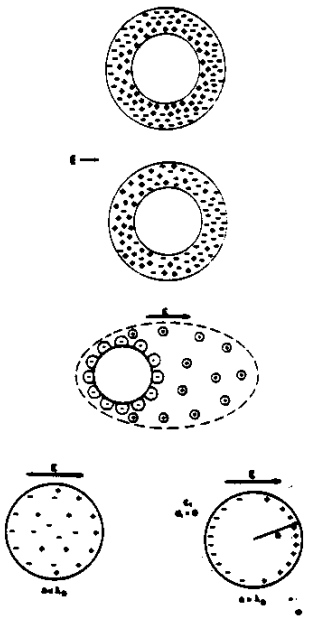

Figure 68

The topmost diagram is a clay particle surrounded by an electrochemical double layer in the absence of any external electrical fields. The next diagram is the same particle with an externally applied field as shown: note the redistribution of charges within the double layer and the resultant polarizaton of the whole particle. The next diagram shows how such redistribution of charge also results in the distortion of the shape of the double layer around the particle. The next pair of figures illustrates the polarization of the space charge layer inside the non-conducting clay particle depending upon the thickness of the internal space charge layer compared to the physical particle size (on the right, the particle is much bigger than the internal space charge layer thickness).

Further, most clay particles are plate-like and not spherical as shown, thus adding a shape factor to the polarization, and the high surface conductivity of clay particles increases the mobility of ions in the double layer. All of these effects cause an increase in the polarizability of the clay-water system. Figure 69 shows (on the left) a series of particles with double layers thin compared to the physical particle size wherein each particle is independent of the rest (particularly if they are dispersed throughout another medium). On the right, in a system such as clays with double layers thick compared to the particle size, the double layers overlap and particle polarizations interact with each other.

Figure 69 -

The result of these polarization enhancements is that

clay particles made from insulating silicate compounds with relative dielectric permmitivities about 6, combined with water (K' around 80), can result in a mixture with a dielectric permittivity thousands of times greater than either component alone.

Several theories have been proposed to explain this (see reviews in Dukhin, 1971; Pethig, 1979; Chew and Sen, 1982); one of the best is that by Trukhan (1962). This is similar to the Maxwell-Wagner theory discussed on pages 68 and following, except the thickness and polarization of the space charge layer are explicitly taken into account. Trukhan obtains the permittivity of the mixture as

$$K_m = K_1 \left(1 + 3v \frac{K_2 - K_1 + \beta}{2K_1 + K_2 - 2\beta} \right) \qquad [158]$$

where

$$\beta = \frac{\kappa^2 \{3 + (\gamma a)^2\} \tanh(\gamma a) - 3\gamma a}{\gamma^2 \{2 + (\gamma a)^2\} \tanh(\gamma a) - 2\gamma a} \qquad [159]$$

and

$$\gamma^2 = \kappa^2 + i\omega D_n^{-1} \qquad [160]$$

where κ is from [155] and D_n is the charge carrier diffusion coefficient. The time constant associated with this interfacial polarization is given by (and plotted in Figure 28)

$$\tau = \frac{\{(2K_1 + K_2)\epsilon_0\}\{(\kappa a)^2 \tanh(\kappa a/2) + 6[2\tanh(\kappa a/2) - \kappa a]\}}{(2\sigma_1 + \sigma_2)\{(\kappa a)^2 \tanh(\kappa a/2) - 4[(K_1/K_2) - 1][2\tanh(\kappa a/2) - \kappa a]\}} \qquad [161]$$

Subscripts 1 and 2 refer to the medium and particle respectively as on page 68. Further discussion will appear in the section on nonlinear electrical properties.

In contrast to the models of linear electrical properties just discussed which rely upon long series of assumptions, consider the total electrical conductivity equation [137] in matrix form as (Olhoeft, 1979, 1985)

$$\underline{S} = \sigma_{DC}(\underline{C}+\underline{Y}\underline{E}) + \epsilon_\infty \underline{D}\underline{W}\underline{K}$$
$$\underline{T} = \sigma_{DC}\underline{W}\underline{E} + \epsilon_\infty \underline{D}(\underline{C}+\underline{X}\underline{K}) \qquad [162]$$

where $\underline{S}$ is the matrix containing the real part of the total conductivity, σ'_T, and $\underline{I}$ contains the imaginary part, σ''_T, such that

$$S_i = \sigma'_T(\omega_i)$$
$$T_i = \sigma''_T(\omega_i)$$
$$X_{ij} = \frac{1}{1 + (\omega_i \tau_j)^2}$$
$$W_{ij} = \omega_i \tau_j X_{ij}$$
$$Y_{ij} = \omega_i \tau_j W_{ij}$$
$$D_{ii} = \omega_i \qquad D_{ij} = 0, \; i<>j$$
$$C_i = 1$$
$$F_j = \frac{m}{1-m} F(\psi_j) \qquad \psi_j = \lambda_j(1-m)$$

and $K_j = \epsilon K(\tau_j)$.

By letting the highest frequency measured data point

determine ϵ_∞ and the lowest measured frequency determine σ_{DC}, solve for $\underline{K}$

$$\underline{K} = \epsilon_\infty^{-1} \left(\underline{W}^{-1}\underline{D}\underline{X} - \underline{Y}^{-1}\underline{D}\underline{W}\right)^{-1}\left(\underline{W}^{-1}\left(\underline{I} - \epsilon_\infty\underline{D}\underline{C}\right) - \underline{Y}^{-1}\left(\underline{S} - \sigma_{DC}\underline{C}\right)\right)$$

then [163]

$$\underline{E} = \sigma_{DC}^{-1}\underline{W}^{-1}\left(\underline{I} - \epsilon_\infty\underline{D}\underline{C} - \epsilon_\infty\underline{D}\underline{X}\underline{K}\right) = \sigma_{DC}^{-1}\underline{Y}^{-1}\left(\underline{S} - \sigma_{DC}\underline{C} - \epsilon_\infty\underline{D}\underline{W}\underline{K}\right)$$

with

$$\phi = \Sigma\ \underline{K} \qquad [164]$$

and

$$m = \frac{\Sigma\ \underline{E}}{1 + \Sigma\ \underline{E}} \qquad [165]$$

This model assumes the material obeys the Hilbert linearity (e.g., the real and imaginary parts of the transfer function are related to each other by the Hilbert transform; see next section) and that only relaxation processes are involved (e.g. no resonances). In most materials, a prior assumption that $\underline{K}$ is zero and solving for $\underline{E}$ is indistinguishable from assuming $\underline{E}$ is zero and solving for $\underline{K}$. In other words, the distincton between Faradaic conduction and dielectric relaxation terms cannot be ascertained from linear electrical data alone (as first discussed by Fuller and Ward, 1970). In these cases, the solutions are

$$\underline{K} = 0, \text{ then } \underline{E} = \left(\underline{Y} - \sigma_{DC}\epsilon_\infty^{-1}\underline{D}^{-1}\underline{W}\right)^{-1}\left(\sigma_{DC}^{-1}\underline{S} - \epsilon_\infty^{-1}\underline{D}^{-1}\underline{I}\right) \qquad [166]$$

$$\underline{E} = 0, \text{ then } \underline{K} = (\epsilon_\infty \sigma_{DC}^{-1} \underline{D} \underline{W} - \underline{X})^{-1} (\sigma_{DC}^{-1} \underline{S} - \epsilon_\infty^{-1} \underline{D}^{-1} \underline{I}) \qquad [167]$$

Some materials have a better fit to their electrical properties spectra with only $\underline{K}$ or $\underline{E}$ and others are better fit with both $\underline{K}$ and $\underline{E}$. In these latter cases, the separation of the Faradaic and dielectric process is distinct with no assumed form for the time constant distribution functions. Further, the solutions in matrix form quickly fit the data including linear regression analysis to give goodness of fit parameters. The output of this model yields the parameters σ_{DC}, m, and $F(\lambda)$ for conductivity relaxations, and ϵ_∞, ϕ, and $K(\tau)$ for dielectric relaxations. Deviation between the data and the model fit, indicates the data (or the measurement instrument) violates the Hilbert transform and thus indicates a measure of the material nonlinearity.

To illustrate the use of these models, the data presented in Figures 31 and following will be fit starting with sample Wy6-106. In Figure 70, on the left, the solid line is the data, and the light dashed line is a simple model assuming only a DC conductivity and a high frequency dielectric permittivity:

$$\sigma_T' + i\sigma_T'' = \sigma_{DC} + i\omega K_\infty \epsilon_o$$

with σ_{DC} = 1/12.1 mho/m and K_∞ = 6430. This simplest model

only fits the complex resistivity spectrum at the very lowest and highest frequencies, and it only fits the phase at the very highest frequencies.

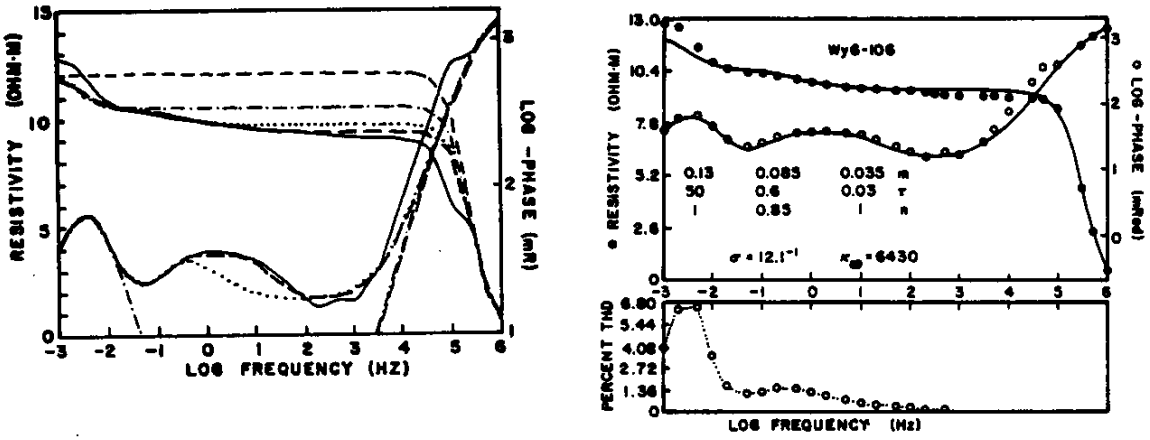

Figure 70 -

The next model includes one Faradaic relaxation process (dot-dash line)

$$\sigma_T' + i\sigma_T'' = \sigma_{DC}\{ 1 + m_1 G(n_1, m_1, \omega\lambda_1)\} + i\omega K_\infty \epsilon_o$$

where $G(n_1, m_1, \omega\lambda_1)$ is the Cole-Cole distribution function from [141] with $n_1 = 1$, $m_1 = 0.13$, and $\lambda_1 = 50$. This improves the fit to the restivity and phase at low frequencies.

Proceeding as above, the model is extended (dotted line) to include a second Cole-Cole distribution with

$n_2 = 0.85$, $m_2 = 0.085$, and $\lambda_2 = 0.6$. Continuing along the same lines, a third relaxation is added (heavy dashed line) with $n_3 = 1$, $m_3 = 0.035$, and $\lambda_3 = 0.03$. The model is beginning to fit the data pretty well (as seen in the right half of Figure 70).

However, there are 56 data points (resistivity and phase at 28 frequencies) and the model now has 11 parameters. To be a really acceptable fit to the data, the model still requires a dielectric relaxation near 100 kHz, which would bring the model parameters to at least 14. Instead, consider the model outlined in equations [162] to [167]. Assuming either K or E is zero, the model results in

$$\sigma_{DC} = 1/12.8$$

$$K_\infty = 6430$$

$$m = 0.99634 \text{ (with } K = 0)$$

and an array F with 28 parameters describing the time constant distribution. Only 8 of the elements of the array E will be significantly greater than zero. Thus, the model could be reduced to 11 parameters with no a priori assumptions made about the shape of the time constant distribution.

Figure 71 illustrates the model fit with both K and E set to zero. In these next figures, across the top are given the σ_{DC}, sample name, and K_∞. In the top left of

each subset figure for resistivity, phase, relative dielectric permittivity, and loss tangent are shown the mean error in fitting the data. The lower left is the K and E time constant distributions in frequency space (to match the upper figures), and the lower right is the total harmonic distortion measure of sample electrical nonlinearity (see next section).

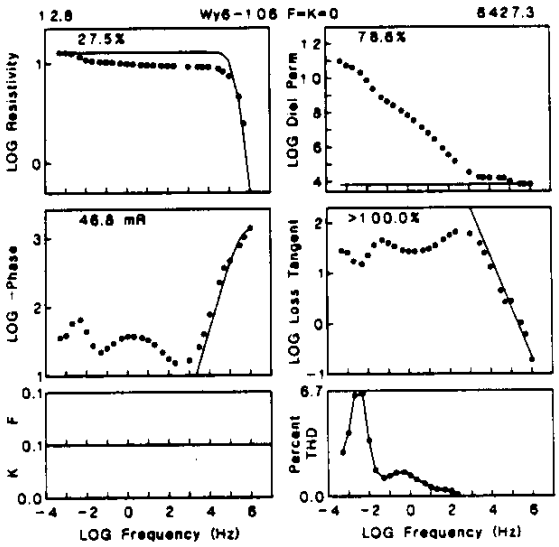

Figure 71 -

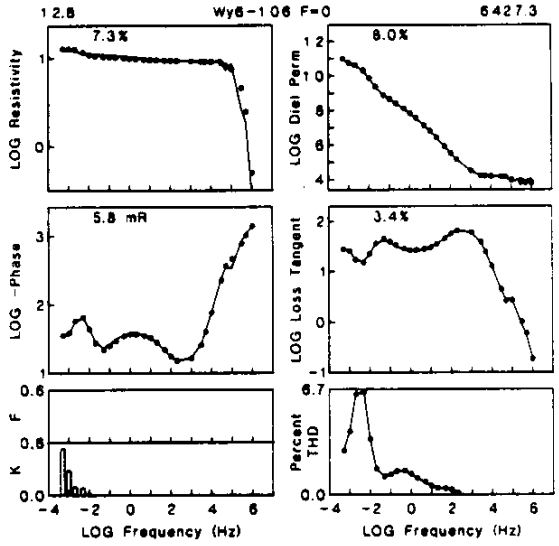

Figure 72 -

Figure 72 illustrates the model fit assuming E = 0 (the figures are identical and indistinguishable from K = 0). The next figure illustrates the fit for equation [163] with both K and E nonzero. Note that by using both K and E, the fit to the resistivity is better than either alone, but that the fits to the permittivity, loss tangent, and phase

are worse. Also note that the fits in any case for sample Wy6-106 are worse than for sample Tiger-Govt 2-22 (Figure 74). This discrepancy in the fit

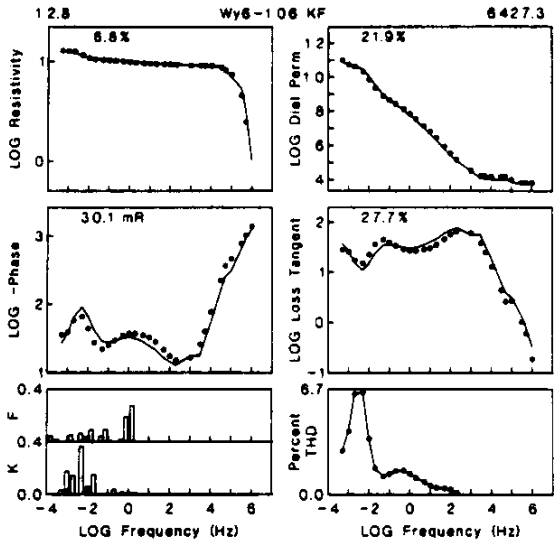

Figure 73 -

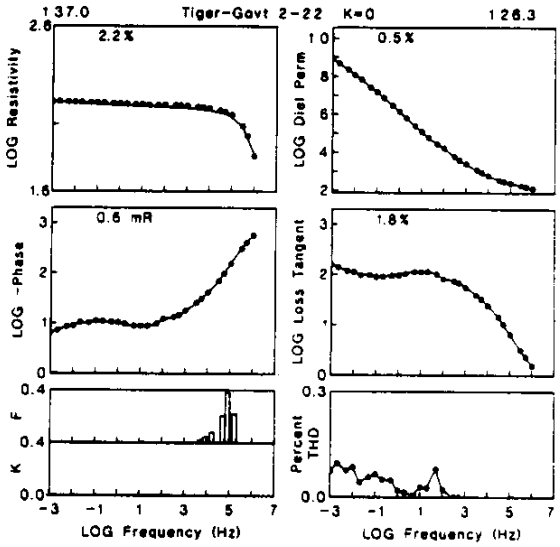

Figure 74 -

for Wy6-106 is caused by the electrical nonlinearity in the sample and is a measure of the nonlinearity through violation of the Hilbert transform in addition to the measure of nonlinearity in the THD. The residuals in the fit for Tiger-Govt 2-22 are approximately the errors associated with the measurement process.

One advantage this model has over the Cole-Cole distribution model is that [162] to [167] are performing linear regression while a fit to [136] requires nonlinear regression such as with the Marquardt algorithm. This use of linear regression simplifies programming and reduces

computation time while also giving goodness of fit parameters.

Figures 75 and 76 illustrate further examples of attempts to fit models against samples exhibiting nonlinear electrical properties with both high THD and violation of the Hilbert transform. Note the large and nearly constant offset in the resistivity of DM-D72 (coal and shale) versus the humic matter. Note also that in none of these examples has the THD been predictable or fit by the linear models. To fit THD requires the use of nonlinear models as discussed in the next section.

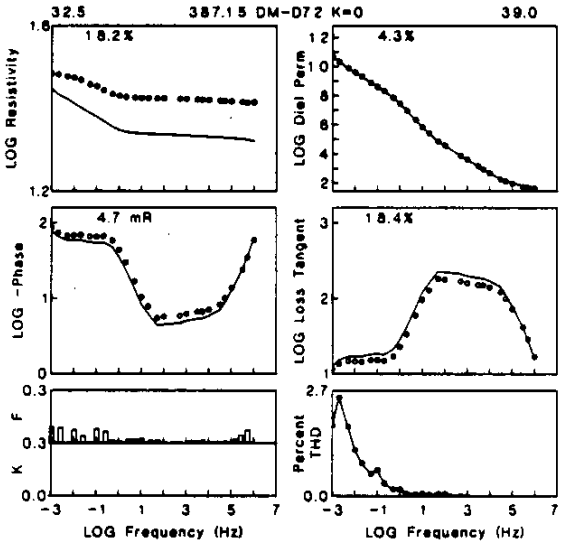

Figure 75 -

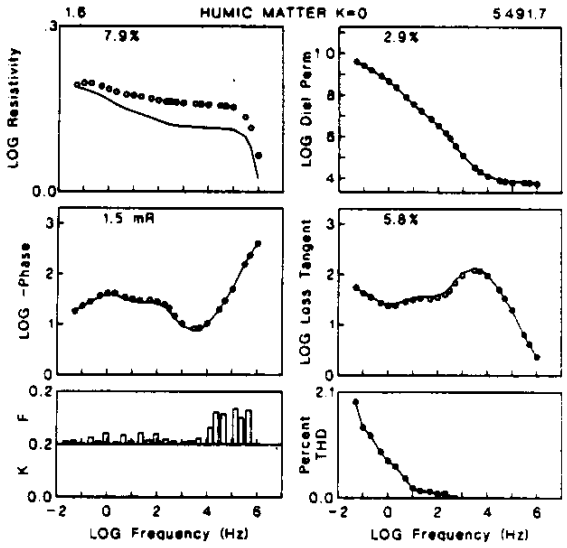

Figure 76 -

Figures 77 and 78 illustrate the fit of the model to two typical clays. Note the kinks in the dielectric permittivity curves as well as the violation of the Hilbert transform.

Note also that the THD declines with increasing frequency and near 10 kHz would indicate amplitude linearity in the sample, except for the very high Hilbert violation that still remains.

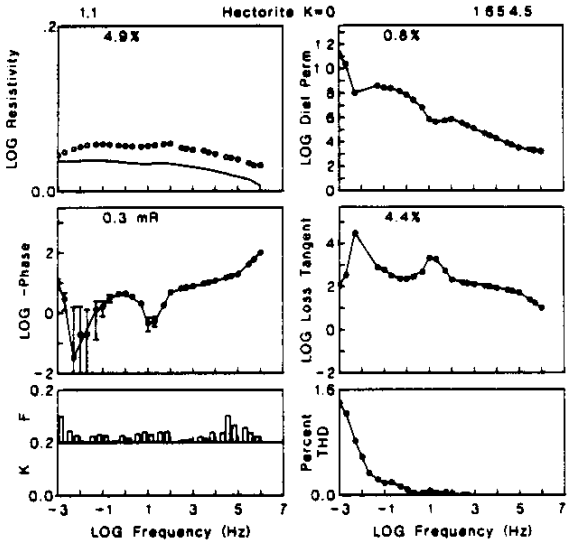

Figure 77 -

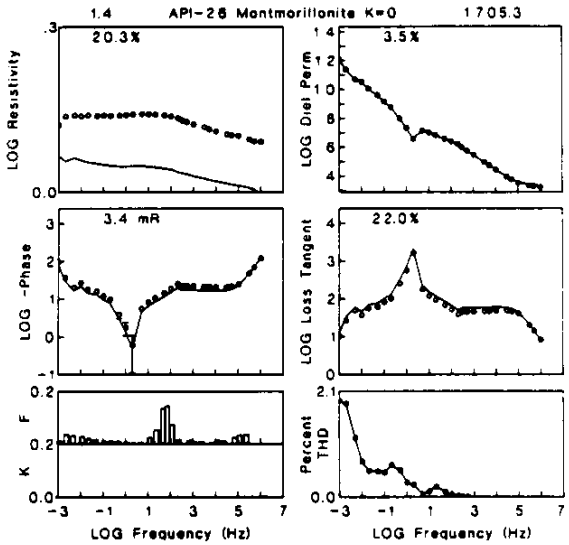

Figure 78 -

ELECTRICAL PROPERTIES SHORT COURSE - Gary R. Olhoeft

Linearity

The following development is abstracted from Olhoeft (1979). In the frequency domain, the electrical properties describing a system response relate the input (or stimulus or excitation) to the output (or response) of the system by a multiplicative factor, the transfer function of the system. If the input to the system is an electrical field and the output is current density, then the transfer function is the complex electrical conductivity. If the input is current density and the output is electrical field, then the transfer function is the complex electrical resistivity.

The equation relating the input and output of a system is called the system equation. If all the derivatives of the input and output in the system equation are raised to the first power only and there are no products of derivatives, then the system is said to be linear. Mathematical properties of linear systems include additivity and homogeneity (together called superposition) which are discussed in detail by Cooper and McGillem (1967). These mathematical properties of linearity result in two measurable properties of linear systems:

(1) the transfer function of a linear system is independent of the amplitude of the input to the system,

and (2) the output of a linear system contains no new

harmonic content that did not appear in the input to the system. In the latter case, if the input to the linear system is a pure sine wave, then the output contains no harmonics.

In addition to linearity, systems are described as being causal or acausal and by being integrably transformable or not. Causal systems have outputs which are independent of future values of input. All physically realizable systems are causal (they cannot predict the future). A system which is linear may be integrably transformable. The integral transforms of the input, output, or system transfer function do not exist unless the integrals are convergent (Sneddon, 1972). Most physically realizable waveforms are convergent in this sense, and it is always possible to choose the input to the system such that the input and the output are both convergent.

The integral transform of a linear causal function has a time function that is completely specified by EITHER the real or imaginary part of the transform (see derivation in Landau and Lifshitz, 1960). Thus, the real and imaginary parts and the amplitude and phase spectra of the transfer function are related to each other. The relation between the real and imaginary parts is called the Kramers-Kronig relation, which is a type of Hilbert transform. If the real and imaginary parts of the transfer function do not obey the Hilbert transform and the input was chosen to give a convergent input and output, then the system is either acausal or nonlinear.

As all physically realizable systems must be causal, such a system must be nonlinear.

As a consequence, there are two additional measures of nonlinearity:
(3) the transfer function of a system in the frequency domain is the Laplace transform of the impulse response of the system in the time domain (see Cooper and McGillem, 1967), and (4) the real and imaginary parts of the complex transfer function are a Hilbert transform pair.

Thus, there are four methods of measuring nonlinearity in an electrical system:

1) Measure the transfer function at two or more different values of input signal amplitude. A measure of non-linearity is the derivative of the transfer function with respect to amplitude of input.

2) Measure the harmonic content of the input and of the output of the system. The root-mean-square difference between the harmonics in input and output is the total harmonic distortion (THD) and is a measure of nonlinearity.

3) Measure the transfer function using a sine wave and a triangular wave input. The difference between the two resultant transfer functions is a measure of nonlinearity. (This approximates the measurement of impulse response and test of the transform to transfer function. In a linear system, the transfer function should be independent of the form of input.)

4) Measure the frequency dependence of the complex

transfer function. Use the Hilbert transform to compare the real and imaginary parts to each other. Differences are a measure of nonlinearity.

There appears to be a degree of independence between the first three measures of linearity and the last. The physical significance is not yet known, but there exist materials which violate all four linearity criteria, materials which only violate the first three, and materials which only violate the last.

Examples of nonlinear electrical properties are numerous in corrosion, solid state physics and electrochemistry (Parmentier, 1970; Hladik, 1972; Pourbaix, 1973; Kuta and Yeager, 1972; Parry-Jones, 1975; Devreese and VanDoren, 1976; MacDonald, 1977; Shetzen, 1980). The best electrochemical description of nonlinear impedance is found in Sluyters-Rehbach and Sluyters (1970, 1984). In minerals, the oxidation-reduction reaction violates Ohm's Law in transferring charge across a water-mineral interface (Klein and Shuey, 1978; Olhoeft, 1979; Olhoeft and Scott, 1980; Klein, 1980). Nonlinear behavior also appears in cation exchange processes (Olhoeft, 1979, 1985; Rubinstein and Shtilman, 1979). The earlist description of nonlinear impedance effects in rocks occurs in Collett (1959) followed by Shaub (1965). The Soviets have been exploiting nonlinear electrochemistry to measure the chemistry of ore deposits via borehole measurements (Ryss, 1973; Shaub and Ivanov, 1971). Extensive laboratory work (Alvarez, 1973; Katsube et al,

1973; St. Amant, 1974; Hall, 1975; Fink, 1976, Klein and Shuey, 1979; Olhoeft, 1979; Anderson, 1981;) is now being applied to modification of existing logging tools (Mitchell and Russell, 1980; Olhoeft and Scott, 1980; Daniels et al., 1983; Olhoeft, 1984) and development of new tools (Klein, 1980). The most recent review is Olhoeft (1985).

Klein (1980) has demonstrated a logging technique based upon nonlinear electrochemistry which can directly log a copper assay accurate to within 1 percentage point at the 5% copper level. Olhoeft and Scott (1980) have modified the surface electronics of a conventional platinum Wenner-array logging probe to directly distinguish between oxidation-reduction and ion-exchange lithologies (e.g., locate sulfides and oxides versus clays), and the tool has more recently been used to monitor clay-organic reactions at toxic waste sites and in petroleum wells (Olhoeft, 1984, 1985).

For direct laboratory electrochemical studies of sulfide ores, see the above references and Warren (1978), Biegler et al. (1975), Beigler (1976), Rand (1977), Biegler and Swift (1976, 1979), Biegler (1977), Biegler et al. (1977), Koch (1975), Richardson and Maust (1977), Vaughn and Craig (1978), Fink (1979), Hamilton and Woods (1981), and Klein et al.(1984). Most sulfides have been well studied, but most oxides have been little studied (Allen and Hampson 1979; Evans, 1980; Morrison, 1980; Dignam, 1981; Trasatti, 1981; Randin, 1981; Olhoeft, 1982; Dare-Edwards et al., 1983;

Furstenau, 1984).

In clays, there are more electrokinetic and dielectric studies (Marshall, 1959; Lorenz, 1969; Weiler and Chaussidon, 1968; Arulanandan and Mitchell, 1968; Waxman and Smits, 1968; Smits, 1968; Almon, 1979; Patchett, 1975) than nonlinear studies (Rubenstein and Shtilman, 1979; Lockhart, 1980; Olhoeft and Scott, 1980). Fewer nonlinear investigations have been performed on zeolites. Insulators are rarely discussed in the electrochemical literature (Boguslavsky, 1980). Nearly as little investigated are the organic electrochemical processes (Zuman, 1969; Allen, 1958; Rudd and Conway, 1983).

The water-metal interface oxidation-reduction systems have been extensively studied. Following the derivation of Sluyters-Rehbach and Rehbach (1970, 1984)(see also De Bruin and Franklin, 1981), the most simple equivalent circuit for an electrode impedance is the Randle's circuit shown in Figure 79,

where C_{dl} = double layer capacitance

R_o = ohmic resistance drop in solution

R_t = transfer resistance

and -W- = Warburg impedance.

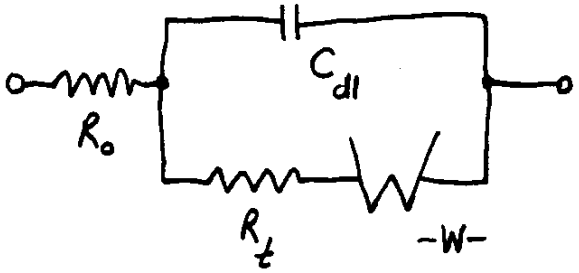

Figure 79 -

Together, the transfer resistance and Warburg impedance comprise the Faradaic impedance. This Faradaic impedance does not obey Ohm's Law, but follows the Butler-Volmer absolute rate equation

$$I = C_1 e^{\alpha f(V)} + C_2 e^{\beta f(V)} \qquad [168]$$

where I = faradaic current

V = applied voltage

f(V) is a linear function of V involving the number of electrons involved in the charge transfer process and the potential across the interface required to initiate the reaction (e.g., the formal standard potential of reaction)

C_1 and C_2 are constants involving the reaction rates and

concentrations of reactants at the electrode surface

α = anodic transfer coefficient

β = cathodic transfer coefficient

and $\alpha + \beta = 1$.

The impedance of this Randle's circuit is

$$Z_R = R_o + \frac{Z_f}{1 + i\omega C_{dl} Z_f} \qquad [169]$$

where

$$Z_f = \Gamma \left\{ \frac{1}{k^a_{sh}} + \frac{1}{(2\omega)^{1/2}} (1 + i) \left(\frac{1}{(D_O)^{1/2}} e^{-\alpha\phi} + \frac{1}{(D_R)^{1/2}} e^{\beta\phi} \right) \right\} \qquad [170]$$

with D_O = oxidation diffusion coefficient

D_R = reduction diffusion coefficient

k^a_{sh} = apparent standard heterogenous rate constant

and

$$\phi = \frac{nF}{RT} (E - E_o) \qquad [171]$$

where n = number of electrons involved in charge transfer

F = Faraday's constant

R = gas constant

T = absolute temperature

E = applied DC potential

E_o = formal standard potential of reaction

$$\Gamma = \frac{RT}{n^2F^2} \frac{1}{\alpha \bar{C}_R e^{\alpha\phi} + \beta \bar{C}_O e^{-\beta\phi}} \qquad [172]$$

where $\bar{C}_R$ = concentrations of reduction components at electrode surface due to DC potential

$\bar{C}_O$ = concentrations of oxidation components at electrode surface due to DC potential.

In order to arrive at this impedance, it was assumed that a small AC potential was superimposed upon a large DC potential. The DC potential put the energy into the system required to initiate the reactions while the small AC potential provided a small perturbation to allow measurement of the reaction process. Note that this Randle's circuit represents a single electrode process at a single water-mineral interface. In a typical porous rock with a complicated mineralogy, there would be a distribution of these Randles' circuits attached to the DC conduction path through the pores and the dielectric properties of the rock as discussed earlier. Further, the pore structure will modify the behavior of the interfacial electrochemistry (Grens and Tobias, 1964; De Levie, 1967; Rangarajan, 1969,

1971; Chizmadzhev and Chirkob, 1983; Hampson and McNeil, 1983).

The reactions can become much more complicated, including coupled reactions, multistep charge transfer, relaxation in the double layer, absorption, and ion exchange. Sluyters-Rehbach and Sluyters (1970, 1984) discuss several of these and reference more detailed discussions in the literature. Measurements exploiting this AC superimposed on DC technique are discussed in detail in the electrochemical literature and in Klein (1980).

While this technique is best suited for studying oxidation-reduction reactions, it is not optimal for studying ion exchange processes. In the redox system, as long as there is a DC current flow across a water-minearl interface, there will be oxidation or reduction reactions occurring (until the mineral or the water is totally used up). Over long periods of time, the mineral chemistry will change and new reactions will occur in place of the old reactions. In an ion exchange process, however, it is possible to totally saturate the surface of the mineral with ions. Once all the ions have been exchanged, the reaction stops. If sufficient current remains applied, redox reactions may begin altering the surface of the exchange mineral or pull cations out of the structure of the mineral, altering the mineralogy.

In order to study both redox and ionex systems, Olhoeft (1979) applied large AC currents to samples. The AC currents generate potentials across water-rock interfaces and excite

chemical reactions. Only cation echange reactions were found to be significantly nonlinear with anion exchange being relatively linear. In comparing the redox systems to the cation exchange systems,

1) at very low current densities ($<10^{-6}$ A/cm^2), nearly all redox systems become linear (as predicted by the Butler-Volmer equation) while many cation exchange montmorillonites remain nonlinear down to 10^{-9} A/cm^2,

2) at very high current densities, redox systems tend to create sufficient potential to cause water to breakdown into hydrogen and oxygen gases while nearly all cation exchange systems saturate and become linear,

3) redox systems are generally symmetrical in their current-voltage Lissajous patterns while cation exchange systems are very asymmetrical,

4) in the nonlinear regime, as the current density is slightly changed, redox systems tend to change both the amplitude and spectral shape of their transfer function while cation exchange systems change amplitude but retain spectral shape,

5) in most minerals the redox system is roughly balanced with $\alpha \sim \beta$ (meaning roughly reversible reactions of equal magnitude) giving rise to high THD with much 2f (1st harmonic) but little 3f (2nd harmonic) while many cation exchange systems have little 2f and much 3f,

6) many redox systems with high THD nonlinearity violate the Hilbert transform while others obey it, most cation

exchange systems have low THD and violate the Hilbert transform (sometimes producing positive phase angles, e.g., negative IP responses).

Theory, laboratory experiments, and field experience all accurately reflect the state of the art in redox systems based upon the broad background of electrochemistry experience (Klein, 1980). However, much more work in all three areas is required before an adequate understanding of nonlinear cation exchange phenomena can be fully exploited. In redox systems, there are tables of standard electrode potentials (Pourbaix, 1974; Milazzi and Caroli, 1978; Antelman, 1982) describing at what stimulus level nonlinearities will occur, but there are no tabulations nor large amounts of data available for the kinetics of such systems (Sarangapani and Yeager, 1984). Neither electrode potential tabulations nor kinetics information are available for most ion exchange systems, and similar situations exist in organic electrochemistry (Zuman, 1969; Birkett et al., 1983; Baizer and Lund, 1983; Rudd and Conway, 1983; Hawley, 1984; Weast and Astle, 1985) and mixed systems such as clay-organic electrochemistry (Solomon, 1968; Theng, 1974, 1982; Olhoeft, 1984, 1985).

The most common observation of nonlinearity in mineral electrical propeties is that the complex resistivity changes value with the amplitude of the current density as shown in Figures 80 and 81 (Olhoeft, 1979).

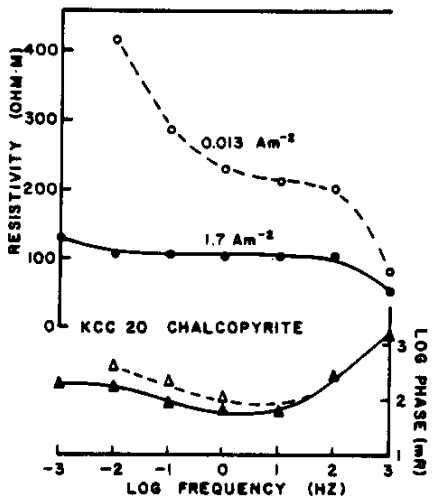

Figure 80 -

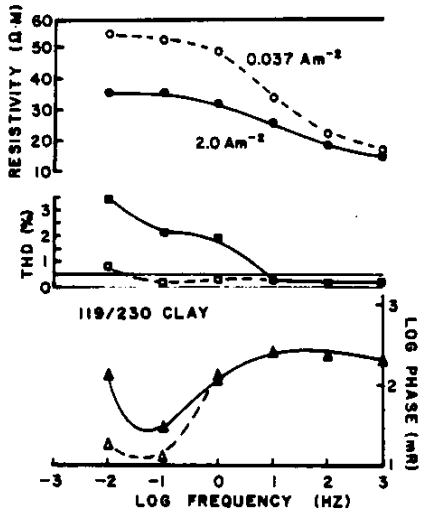

Figure 81 -

Note how the chalcopyrite in the redox system changes both amplitude and shape of the resistivity spectra with changing current density whereas the clay changes amplitude but retains spectral shape.

In Figures 82 and 83, electric field is plotted versus current density in the classic electrochemical cyclic voltammogram type of plot. Note that the chromite redox system is symmetrical whereas the cation exchange resin is highly assymetrical (the numbers on the plot are log frequency). Note also that both systems exhibit linear ellipses as the frequency increases to 100 Hz.

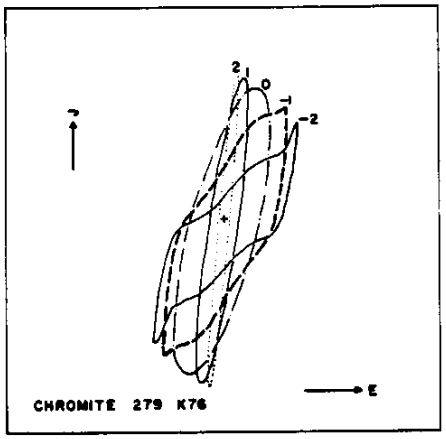

Figure 82 -

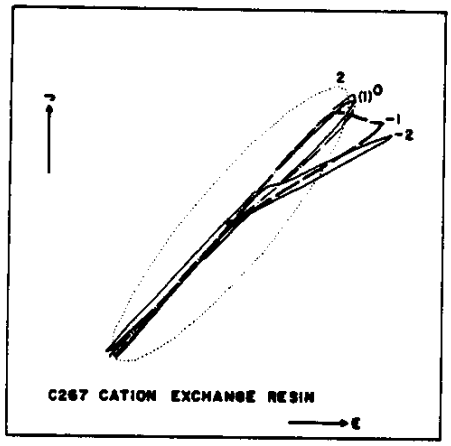

Figure 83 -

In Figure 84, some of the electrochemical processes are outlined. The overall water-mineral system may behave like a battery (e.g., as a source of electrical energy) driving an external load, or it may behave like a load being driven by an external source. In either case, at the water-mineral interface, the mineral will either behave as an anode (taking electrons from solution) or a cathode (putting electrons into solution) depending upon the direction of current flow. At the interface, current flow from the solution to the mineral anode will generate oxidation reactions, dissolve the mineral surface, evolve oxygen gas, and the generate acids.

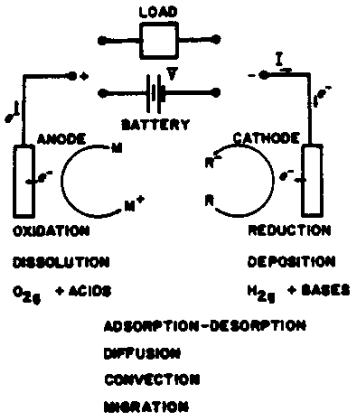

Figure 84 -

For the opposite direction of current flow, the mineral cathode surface will generate reduction reactions, deposit cations onto the mineral surface (plating), evolve hydrogen gas, and generate basic compounds. Which or all of these processes occur is determined by a variety of factors, but they all occur with a similar sequence of events. This sequence begins in the bulk solution with chemical species that must be transferred from the bulk solution to the immediate vicinity of the electrical double layer at the interface. This mass transfer may occur by chemical diffusion, thermal convection, or electrochemical migration. On nearing the interfacial region, various intermediate reactions may occur, such as attachment or detachment of protons or hydroxyls. Adsorption-desorption (ion exchange)

and catalytic phenomena may then occur at the interface, and finally, an electron transfer will occur across or along the interface. The reverse sequence occurs to remove the reactant products from the interfacial region.

The external factors controlling these events include temperture, pressure, and time (including rate-of-exchange). Electrical variables are the potential across the interface, current density, and quantity of electrical charge. Solution variables include the bulk concentrations of the electroactive species, concentrations of other species (including pH and Eh), and type of solvent. Electrode (mineral surface) variables include the material of the surface, surface area, surface roughness and condition, geometry (such as edge versus face in clays), and surface concentrations of chemical species.

Most of the details of these processes are understood fairly well for metallic surfaces (see Bockris and Reddy, 1970; Bard and Faulkner, 1980), corrosion processes (Mansfeld and Bertocci, 1981), and are beginning to be understood for semiconductors and metallic oxides (Trasatti, 1980; Morrison, 1980), but are very little understood for nonconducting materials such as clays (Bockris and Khan, 1979; van Olphen, 1977; Yariv and Cross, 1979; Theng, 1979; Bruggenwort and Kamphorst, 1979; Boguslavsky, 1980, Hunter, 1980).

Composite Media and Mixing Formulas

Mixing formulas are methods of predicting the composite properties of a mixture of several materials from the known properties of the component materials given the ratio in which they are to be mixed. In many cases, mixtures have composite properties that are simply the mean of the properties of the components (Nielson, 1978). In other cases, the mixture exhibits new properties that were not present in any individual component. Mixing formulas are reviewed for dielectrics by Polder and van Santen (1946), Taylor (1965), van Beek (1967), De Loor (1968), Geiger and Williams (1972), Bottcher (1973), Tinga et al.(1973), Cihlar and Ulaby (1974), Hipp (1974), Wobschall (1977), Bergman (1978, 1980), Gubernatis (1978), Milton (1980, 1984), Wang (1980), Sheng (1982), Shutko and Reutov (1982), Bennetto et al.(1983), Dobson et al.(1985), and Hallikainen et al. (1985); for conductors by Cremers et al.(1966), Zuca and Ionescu-Vasu (1967), Kay (1973), Landauer (1978), Madden (1976), Shankland and Waff (1974), Rhoades et al.(1976), Hermance (1979), Islam et al.(1979), Anderson (1981), Milton and McPhedran (1982), and Bussian (1983); and for mixed dielectrics and conductors by Dukhin (1971), Dukhin and Shilov (1972), Hasted (1973), Bergman (1978, 1980), Pethig (1979), and Cummings et al.(1984). There are few discussions

of mixing in the electrochemistry literature (Kay, 1973; Anderson, 1981; Beaunier et al., 1981; Allison, 1982). Also of relevance are reviews of fluid flow through porous media (IAHR, 1972; Scheidegger, 1974; Collins, 1976).

Landauer (1978) and Dukhin (1971) review the history of mixing formulas. The earliest mathematical derivation of a mixing formula is credited to Mossotti in 1846, and has been subsequently re-derived many times by Clausius, Lorenz, Lorentz, and Maxwell. This formula is usually called the Clausius-Mossotti approximation:

$$\frac{K_m - K_1}{K_m + 2K_1} = v \frac{K_2 - K_1}{K_2 + 2K_1} \qquad [173]$$

where K_m is the dielectric permittivity of a composite medium made from a volume fraction, v, of material with K_2 in a material of K_1. Note that solving this formula for K_m yields the same formula as given in [76] for K_∞ in the Maxwell-Wagner model. This formula assumes non-interacting particles dispersed through a second material in a way that effectively acts as though there were a single particle of appropriate volume fraction in the material. Hence, these and related theories are all called effective medium approximations. They only work for very small volume fractions, typically $v < 0.2$.

Bruggeman extended the theory to account for discrete

volume particles in a finite medium, giving a formula accurate to much larger volume fractions: (see reviews in Dukhin, 1971; Sen et al., 1981)

$$\frac{K_m - K_2}{K_1 - K_2} \left(\frac{K_1}{K_m}\right)^{1/3} = 1 - v \qquad [174]$$

The next development resulted from multipole expansion using statistical theory to add mutual interaction between particles by Bunter and Heinrich (1965) as discussed in Dukhin (1971), Bottcher (1973), and Wong and Strangway (1981).

The Bruggeman formula [174] has recently been rederived using self-consistent coherent potential and self-similar (scale invariant) approximations by Sen et al (1981) showing that limiting cases are similar to the familiar Archie's law (see below). Further, their derivation replacing the exponent 1/3 with a variable allows for a link to fractal representations of rock porosity models (Deutscher et al., 1983). Sen (1981) later extended the model to include high aspect ratio particles within rocks. Due to the computational complications of using the Bruggeman formula, Wong and Strangway (1981) introduced the discrete equivalent of it in the form of a recursive formula, easily programmed on a computer:

$$\sigma_e = \sigma_o \prod_{n=0}^{N-1} \frac{1 - (n - 2f)\,\Delta v}{1 - (n + f)\,\Delta v} \qquad [175]$$

where σ_e = complex conductivity of the mixture

$$N = v/\Delta v$$

$$f = \frac{\sigma_p - \sigma_n}{\sigma_p + 2\sigma_n}$$

$$\frac{\sigma_{n+1}}{\sigma_n} = \frac{1 + 2f \dfrac{\Delta v}{1 - n\Delta v}}{1 - f \dfrac{\Delta v}{1 - n\Delta v}}$$

and σ_p is the complex conductivity of the particles in a medium with complex conductivity σ_o. All of these formulas may be used for either dielectric permittivity or electrical conductivity.

The explicit consideration of both conductivity and permittivity was first considered when Wagner added conductivity to Maxwell's formula to result in [74] to [79]. Similarly, Hanai extended the Bruggeman formula [174]. However, all of these formulations and those of Sen (1981) and Wong and Strangway (1981) assume the interfacial space charge layer to be infinitely thin. Trukhan (1962) was the first to consider a finite thickness and polarization in the double layer, and Trukhan's formula (equation [158] reduces to the Maxwell formula for $\kappa a >> 1$ (e.g., thin space charge layers relative to particle size).

Further development of the mixing formulas added the

effects of surface conduction around the particle and of polarization of the diffuse part of the double layer (see review in Dukhin, 1971, 1975; Dukhin and Shilov, 1972; Pethig, 1979; Schwarz, 1972; Chew and Sen, 1982). Arulanandan and Mitchell (1968) have found that the electrical properties of clay-water systems can only be reasonably explained by requiring these double-layer effects to be present.

One noteworthy aspect of the effective media theories, such as the Maxwell-Wagner effect, is that they do not produce electrical properties of magnitude greater than any component of the mixture. By allowing the double-layer effects in Trukhan and later theories, it is possible to predict how a mixture of dry clay with relative dielectric permittivity near 8 can be mixed with water of relative dielectric permittivity near 80 to produce a composite permittivity greater than 10^5 at low frequencies. At very high frequencies (10^9 Hz and higher), the double-layer generally cannot respond and the Bruggeman-Hanai formulas are adequate.

When mixing conductors and dielectrics, the Maxwell-Wagner effect is joined by the phenomenon called percolation. This is the phenomenon related to the minimum number of conducting branches required to make a connected path through an insulator. Shankland and Waff (1974) have an excellent review. (Shante and Kirkpatrick, 1973; Kirkpatrick, 1973, 1978; Brandt, 1975; Clerc et al., 1975; Coniglio, 1975;

Cusack, 1976; Bideau et al., 1976; Kesten, 1982; Deutscher et al., 1983) The largest problem with percolation theory is that it predicts minimum required bond connectivities for conduction in insulators that are not observed in real rocks. Recent fractal theories suggest the problem is rocks behave like 2.5 dimensional solids, not 3-dimensional solids.

Remarkably, there are two mixing formulas that are widely used which have no physical derivation as do the formulas above. These are both based upon geometric mean mixing and are widely found in thermal, magnetic, elastic, and electrical properties. For dielectrics, the formula is called Lichtenecker's formula (see [70] to [74] and Olhoeft, 1979) with the result that nearly all rocks have dry relative dielectric permittivities given by

$$K_m = 1.9^d$$

where d = dry bulk density in g/cm^3. For a series of materials,the formula is

$$K_m = K_1^{v_1} K_2^{v_2} K_3^{v_3} \ldots \qquad [176]$$

where v_i is the volume fraction of material with permittivity K_i and $\Sigma v_i = 1$.

For conductors, the most common formula is called Archie's Law, given by

$$\sigma_{rock} = \sigma_{fluid} \eta^m \qquad [177]$$

where η = porosity

and m = an empirical exponent varying generally between 1 and 2.

Shankland and Waff (1974) and Madden (1976) give arguments as to the value of the exponent, m. Brace et al. (1965) have experimentally demonstrated that m = 2 is a very good fit to the changing porosity of rock due to fracture closing under compression above 4 kBar. Keller and Frischknecht (1966) review the various Archie's Law expressions reported in the literature, finding the exponent to vary from m = 1.64 to 2.23 (see also Timur et al., 1972; Keller, 1982). Jackson et al.(1978) have shown that the shape of particles (and hence the shape of the pore structure) is the primary determinant in the value of m, with m = -1.20 for spherical particles and m = -1.85 for angular particles. Hermance (1979) concludes that Archie's Law is a reasonable model for partial melt (Schmeling, 1985), and it has been in use for many years as a technique to derive formation properties from well logs. Sen et al.(1981) have shown that [176] and [177] are limiting cases of [174].

Waxman and Smits (1968) extended Archie's Law to include surface conduction due to clays in shaly sands. Archie (1942) originally included the effect of partial water saturation with

$$\sigma_r = \sigma_w \eta^m S_w^n \qquad [178]$$

where σ_r = conductivity of rock containing the fluid

σ_w = conductivity of fluid in pores

S_w = fractional fluid saturation of pores

and n = empirical exponent (generally betwen 4 and 5).

Waxman and Smits modified this to

$$\sigma_r = \eta^m S_w^n \left(\sigma_w + \frac{BQ_v}{S_w}\right) \qquad [179]$$

where B = equivalent conductance of clay exchange cations

and Q_v = volume concentration of clay exchange cations.

This relationship has been the subject of extensive investigation, with recent papers and reviews by Patchett (1975), Hill et al (1979), Juhasz (1979), Worthington (1982, 1985), Binh (1983), White (1983), Dunning (1983), and others.

This modification adding surface conductance to Archie's Law also is required in many igneous rocks with very clean water (high resistivity) and in materials which undergo surficial alteration at high temperatures (see Figures 10 and 11, and Olhoeft, 1977; Ucok, 1979; Drury and Hyndman, 1979).

The mixing laws available in the literature were generally developed for limiting cases, such as infinitely thin charging layers, pure dielectrics in the absence of conductors, pure conductors in the absence of dielectrics, or small concentrations of non-interacting particles. The frequency dependent behavior of clean silicates and of linear mineralized rocks have been modelled by Wong (1979), Wong and Strangway (1981), Sen et al. (1981), Sen (1981), and a few

others. In general, The Bruggeman-Hanai mixing formula works better than any other (especially in the recursive form of [175]). Sen et al (1981) have shown the relevance of this formula to rocks in general and how Archie's Law may be derived as a limiting case at very low frequencies. This and the other formulas described do not work however, when clays are present with high surface conduction, in nonlinear mineralized or altered systems, nor at high frequencies (above 10^7 Hz) when geometric scattering becomes important (e.g., when the wavelength of electromagnetic energy propagating through the medium becomes comparable to the scale of inhomogeneity in the medium and scale-invariance is violated; Cohen, 1981).

While the above formulas predict the value of electrical properties for a mixture of materials, it is also possible to predict the range of values for a mixture given different configurations of the components. In other words, the above formulas assume statistical homogeneity and isotropy. In many natural systems, the electrical properties are a result of preferred grain orientation or alignment (ore structure or other geometric anisotropy). The range can be predicted by using bounding formulas. Hashin and Schtrickman (1962) used a variational approach to show that there existed predictable upper and lower bounds to the properties of composite media. By using [173] or [174] and solving for K_m versus v as written, one bound is obtained. The other bound is obtained by solving the equation again with K_1 and K_2

reversed and substituting v for 1-v. For further discussions of bounding, see Landauer (1978), Milton (1980, 1984), Bergman (1978), 1980), Milton and McPhedran (1982), and Kohler and Papanicolaou (1982).

Wet Rocks Summary

In summary, the electrical properties of dry rocks are relatively simple, with the DC conductivity having a very low value ($<10^{-9}$ mho/m) in the absence of connected conductive minerals such as dendritic hematite, and having high frequency dielectric permitivities that may be described roughly by the physical mixing formula

$$K_\infty = 1.92^d.$$

Combined, these result in a complex electrical conductivity of the form

$$\sigma_T' + i\sigma_T'' = \sigma_{DC} + i\omega K_\infty \epsilon_o$$

slightly dependent on pressure, and strongly dependent upon temperature as discussed earlier.

Wet rocks have electrical properties that are considerably more complicated with a complex conductivity that is given by

$$\sigma_T' + i\sigma_T'' = \sigma_{DC}\{1 + m\, G(n,m,\omega\lambda)\} + i\omega K_\infty \epsilon_o \{1 + \xi\, K(\alpha,\omega\tau)\}$$

where the DC conductivity is a function

$$\sigma_{DC} = \eta^M S_w^N (\sigma_w + \sigma_s)$$

that is dependent upon the available volume for water to occupy (porosity) and how much is actually occupied (saturation), the surface conduction along pore walls, the electrical conductivity of the solution filling the pores, and the pressure and temperature dependence of these variables. The K_∞ given above must also be modified to include water filling the pores through the Bruggeman-Hanai formula [174, 175].

Further, at frequencies below about 10^9 Hz, the function $\zeta K(\alpha,\omega\tau)$ determines the frequency dependence due to dielectric relaxation mechanisms and the function $m\Theta(n,m,\omega\lambda)$ determines the frequency dependence due to Faradaic chemical reaction mechanisms. In a material like the clean sandstone shown in Figure 31, both ζ and m chargeabilities are zero with no dielectric or Faradaic relaxations.

In materials like Wy6-106, a sandstone with both reactive oxides, sulfides and clay minerals, shown in Figures 32 and 70 through 73, both Faradiac and dielectric relaxations may be present. The non-Faradaic terms (such as from clay cation exchange processes) are generally considered to be dielectric relaxations. More often than not, the Cole-Cole time constant distribution of [64] and [145] is used to describe the frequency dependence. The time constant of relaxation is

often controlled by the surface area involved in the water-rock interfacial polarization through the particle radius in theories of disseminated sulfides (Wong, 1979; Wong and Strangway, (1981), colloidal particles (Trukhin, 1961), and in pore structures (Rangarajan, 1969) in which the rate-limiting step is diffusion limited. In other systems (particularly cation exchange), the kinetics of the reactions may be the rate limiting step, determining the time constant of relaxation. The magnitude of the response is only understood for linear systems of conducting particles with assumptions as discussed earlier. However, these models do not adequately explain the dependence of the time constant upon volume fraction mineralization.

Nonlinearity appears in electrical properties at water-mineral interfaces (Olhoeft, 1979, 1985; Klein, 1980). However, nonlinearity also appears from cation exchange capacity in clay minerals and appears to be associated with the dielectric term. Nonlinear systems and insulating particles with high cation exchange capacity have no adequate models at this time. Few satisfactory models exist for nonlinear redox systems (Sluyters-Rehbach and Sluyters, 1970, 1984; Klein, 1980; Olhoeft, 1985).

There is a general ambiguity in deciding whether a particular relaxation process belongs in the Faradaic or dielectric portion of the model. If a broad enough frequency range is measured, both terms are separable in principle.

There is a general tendency for the Faradaic term to dominate below 10^3 Hz and phase angles less than $-\pi/4$, and the dielectric term to dominate above 10^5 Hz and phase angles between $-\pi/4$ and $\pi/2$.

Not reflected in the frequency dependence of electrical properties models are geometric scattering properties at high frequencies (above 10^7 Hz). These are scattering of the electromagntic energy due to the wavelength of the electromagnetic energy propagation being less than 3 times the size of the inhomogeneities or the scale of electrical properties variation (Watts and England, 1976; Rossiter, 1977; Ishimaru, 1978; Olhoeft et al, 1979). Such geometric scattering is observed in nature above 10^7 Hz and is particularly pronounced when clays are present. Such scattering appears as an increase in the imaginary part of K (increasing loss) and a decrease in the real part, with failure in all mixing laws (Cohen, 1981). Regular layering of the right periodicity has also been observed to produce geometric resonance that appears to enhance the real part of K (producing anomalously high apparent dielectric permittivity). Such scattering is rarely observed in the laboratory due to the size of samples that are typically measured.

The temperature dependence of most rocks appears mostly through the dependence of the electrical properties of water

on temperature as discussed earlier (and Olhoeft, 1981), with

$$\sigma_{DC} = \sigma_o e^{-E_o/kT}$$

and K_∞ relatively independent of temperature. The functions of K() and G() are both temperature dependent in their chargeabilities and time constants, with

$$\tau = \tau_o e^{+E_o/kT}$$

and similarly for λ. In some materials, the time constant distribution is independent of temperature and in others dependent upon temperature, causing the frequency spectra to change shape with temperature.

Pressure is only a significant parameter in most materials as it varies the porosity and hence the amount of water in the material. At low salinities, pressure is important in the electrical properties of water above the critical temperature for the solution.

Chemistry may be very important in determining which chemical reactions will occur. The pH and Eh of the pore water and the concentration of the solution will influence zeta potentials (and hence streaming and sedimentation potentials) and the occurrence of redox reactions. Concentrations of ions in solution will also affect solution

conductivity, dielectric permittivity, thickness of the electrical double layer, and a variety of other parameters. Rocks with low salinity water are more prone to have conductivity of the rock-water system dominated by surface conduction than volume conduction. Certain combinations of chemistry may result in time constant distributions controlled by diffusion processes while others will have time constant distributions conrolled by the kinetics of the chemical reaction paths. (For detailed discussions, see the electrochemical literature: Bockris and Reddy, 1970; Archer and Armstrong, 1980; Bard and Faulkner, 1980).

Texture may also be important in controlling frequency spectra. Very different electrical properties result from hematite in silicates depending on whether the hematite is finely disseminated as noninteracting particles, dendritic with connected conducting paths, massive, or interlaminated with ilmenite. Similar results hold for other sulfides and oxides. Different responses also result depending upon whether a clay lines a pore structure, bridges pores, or blocks and fills the pores. Isolated, occluded solution-filled porosity still alters the dielectric permittivity of the mixture even though the electrical conductivity is not altered, but connected solution-filled cracks are porosity that effects both permittivity and conductivity. Very fine, thin cracks tend to have higher proportionate surface conduction than large vugular pores

(and similarly for fine versus coarse particles).

The largest unsolved problems in the understanding of electrical properties of wet rocks involve variations with chemistry and texture, interacting particles, and geometric scattering. In particular, the electrical properties of clays, zeolites, and other surface-active materials need much more study, both experimentally and theoretically. Near DC the surface conductance is important, at intermediate frequencies the polarization and particle-interactions are important, and at high frequencies their contributions to geometric scattering are important.

Although clays, zeolites, colloidal humic materials, and organic materials are widespread in occurrence, very little about their electrical properties are understood. Of particular importance to oil exploration (Johns, 1979) and monitoring of enhanced oil recovery processes (Law and Kunze, 1966), mineral exploration, toxic waste disposal (Anderson et al., 1982), and a variety of agriculture purposes (Bailey and White, 1970; Burchill et al., 1981) are clay-organic interactions (Fripiat and Cruz-Cumplido, 1974; van Olphen, 1977; Theng, 1979; Yariv and Cross, 1979), which result in a wide variety of measurable electrical properties, but are not understood (Trasatti, 1980; Appleby, 1983; Olhoeft, 1984, 1985).